THE UNIVERSITY OF MICHIGAN

STUDIES IN RADAR CROSS SECTIONS XXVII

CALCULATED FAR FIELD PATTERNS FROM SLOT ARRAYS ON CONICAL SHAPES

R. E. Doll, R. F. Goodrich, R. E. Kleinman, A. L. Maffett,
C. E. Schensted and K. M. Siegel

Contracts AF-33(038)-28634 and AF-33(600)-36192
Hughes Aircraft Company Purchase Orders
L-265165-F47
4-500469-FC-47-D
4-526406-FC-89-3

February 1958

2713-1-F

Approved Keeve M. Siegel
Keeve M. Siegel
Project Supervisor

The University of Michigan
Engineering Research Institute
The Radiation Laboratory
Ann Arbor, Michigan

STUDIES IN RADAR CROSS SECTIONS

I "Scattering by a Prolate Spheroid", F. V. Schultz (UMM-42, March 1950), W-33(038)-ac-14222. UNCLASSIFIED.

II "The Zeros of the Associated Legendre Functions $P_n^m(\mu')$ of Non-Integral Degree", K. M. Siegel, D. M. Brown, H. E. Hunter, H. A. Alperin and C. W. Quillen (UMM-82, April 1951), W-33(038)-ac-14222. UNCLASSIFIED.

III "Scattering by a Cone", K. M. Siegel and H. A. Alperin (UMM-87, January 1952), AF-30(602)-9. UNCLASSIFIED.

IV "Comparison Between Theory and Experiment of the Cross Section of a Cone", K. M. Siegel, H. A. Alperin, J. W. Crispin, Jr., H. E. Hunter, R. E. Kleinman, W. C. Orthwein and C. E. Schensted (UMM-92, February 1953), AF-30(602)-9. UNCLASSIFIED.

V "An Examination of Bistatic Early Warning Radars", K. M. Siegel (UMM-98, August 1952), W-33(038)-ac-14222. SECRET.

VI "Cross Sections of Corner Reflectors and Other Multiple Scatterers at Microwave Frequencies", R. R. Bonkowski, C. R. Lubitz and C. E. Schensted (UMM-106, October 1953), AF-30(602)-9. SECRET - Unclassified when Appendix is removed.

VII "Summary of Radar Cross Section Studies Under Project Wizard", K. M. Siegel, J. W. Crispin, Jr., and R. E. Kleinman (UMM-108, November 1952), W-33(038)-ac-14222. SECRET.

VIII "Theoretical Cross Section as a Function of Separation Angle Between Transmitter and Receiver at Small Wavelengths", K. M. Siegel, H. A. Alperin, R. R. Bonkowski, J. W. Crispin, Jr., A. L. Maffett, C. E. Schensted and I. V. Schensted (UMM-115, October 1953), W-33(038)-ac-14222. UNCLASSIFIED.

IX "Electromagnetic Scattering by an Oblate Spheroid", L. M. Rauch (UMM-116, October 1953), AF-30(602)-9. UNCLASSIFIED.

X "Scattering of Electromagnetic Waves by Spheres", H. Weil, M. L. Barasch and T. A. Kaplan (2255-20-T, July 1956), AF-30(602)-1070. UNCLASSIFIED.

XI "The Numerical Determination of the Radar Cross Section of a Prolate Spheroid", K. M. Siegel, B. H. Gere, I. Marx and F. B. Sleator (UMM-126, December 1953), AF-30(602)-9. UNCLASSIFIED.

XII "Summary of Radar Cross Section Studies Under Project MIRO", K. M. Siegel, M. E. Anderson, R. R. Bonkowski and W. C. Orthwein (UMM-127, December 1953), AF-30(602)-9. SECRET.

XIII "Description of a Dynamic Measurement Program", K. M. Siegel and J. M. Wolf, (UMM-128, May 1954), W-33(038)-ac-14222. CONFIDENTIAL.

XIV "Radar Cross Section of a Ballistic Missile", K. M. Siegel, M. L. Barasch, J. W. Crispin, Jr., W. C. Orthwein, I. V. Schensted and H. Weil (UMM-134, September 1954), W-33(038)-ac-14222. SECRET.

XV "Radar Cross Sections of B-47 and B-52 Aircraft", C. E. Schensted, J. W. Crispin, and K. M. Siegel (2260-1-T, August 1954), AF-33(616)-2531. CONFIDENTIAL.

XVI "Microwave Reflection Characteristics of Buildings", H. Weil, R. R. Bonkowski, T. A. Kaplan and M. Leichter (2255-12-T, May 1955), AF-30(602)-1070. SECRET.

XVII Complete Scattering Matrices and Circular Polarization Cross Sections for the B-47 Aircraft at S-band", A. L. Maffett, M. L. Barasch, W. E. Burdick, R. F. Goodrich, W. C. Orthwein, C. E. Schensted and K. M. Siegel (2260-6-T, June 1955), AF-33(616)-2531. CONFIDENTIAL.

XVIII "Airborne Passive Measures and Countermeasures", K. M. Siegel, M. L. Barasch, J. W. Crispin, Jr., R. F. Goodrich, A. H. Halpin, A. L. Maffett, W. C. Orthwein, C. E. Schensted and C. J. Titus (2260-29-F, January 1956), AF-33(616)-2531. SECRET.

XIX "Radar Cross Section of a Ballistic Missile II", K. M. Siegel, M. L. Barasch, H. Brysk, J. W. Crispin, Jr., T. B. Curtz and T. A. Kaplan (2428-3-T, January 1956), AF-04(645)-33. SECRET.

XX "Radar Cross Section of Aircraft and Missiles", K. M. Siegel, W. E. Burdick, J. W. Crispin, Jr., and S. Chapman (WR-31-J, ONR-ACR-10, March 1956). SECRET.

XXI "Radar Cross Section of a Ballistic Missile III", K. M. Siegel, H. Brysk, J. W. Crispin, Jr., and R. E. Kleinman (2428-19-T, October 1956), AF-04(645)-33. SECRET.

XXII "Elementary Slot Radiators", R. F. Goodrich, A. L. Maffett, N. E. Reitlinger, C. E. Schensted and K. M. Siegel (2472-13-T, November 1956), AF-33(038)-28634, HAC PO L-265165-F47. UNCLASSIFIED.

XXIII "A Variational Solution tot the Problem of Scalar Scattering by a Prolate Spheroid", F. B. Sleator (2591-1-T, March 1957), AFCRC-TN-57-586, ASTIA Document No. 133631, AF-19(604)-1949. UNCLASSIFIED.

XXIV "Radar Cross Section of a Ballistic Missile IV", to be published. SECRET.

XXV "Diffraction by an Imperfectly Conducting Wedge", T. B. A. Senior (2591-2-T, October 1957), AFCRC-TN-57-791, ASTIA Document No. AD 133746, AF-19(604)-1949. UNCLASSIFIED.

XXVI "Fock Theory Applied to an Infinite Cone", R. F. Goodrich (2591-3-T, January 1958), AF-19(604)-1949. UNCLASSIFIED.

XXVII "Calculated Far Field Patterns from Slot Arrays on Conical Shapes", R. E. Doll, R. F. Goodrich, R. E. Kleinman, A. L. Maffett, C. E. Schensted and K. M. Siegel (2713-1-F, February 1958), AF-33(038)-28634, AF-33(600)-36192. UNCLASSIFIED.

PREFACE

This paper is the twenty-seventh in a series growing out of studies of radar cross sections at the Engineering Research Institute of The University of Michigan. The primary aims of this program are:

1. To show that radar cross sections can be determined analytically.

2. A. To determine means for computing the radiation patterns from antennas by approximate techniques which determine the pattern to the accuracy required in military problems but which do not require the unique determination of exact solutions.

   B. To determine means for computing the radar cross sections of various objects of military interest.

   (Since 2A and 2B are inter-related by the reciprocity theorem it is necessary to solve only one of these problems.)

3. To demonstrate that these theoretical cross sections and theoretically determined radiation patterns are in agreement with experimentally determined ones.

Intermediate objectives are:

1. A. To compute the exact theoretical cross sections of various simple bodies by solution of the appropriate boundary-value problems arising from electromagnetic theory.

   B. Compute the exact radiation patterns from infinitesimal solutions on the surface of simple shapes by the solution of appropriate boundary-value problems arising from electromagnetic theory.

   (Since 1A and 1B are inter-related by the reciprocity theorem it is necessary to solve only one of these problems.)

2. To examine the various approximations possible in this problem and to determine the limits of their validity and utility.

3. To find means of combining the simple-body solutions in order to determine the cross sections of composite bodies.

4. To tabulate various formulas and functions necessary to enable such computations to be done quickly for arbitrary objects.

5. To collect, summarize, and evaluate existing experimental data.

Titles of the papers already published or presently in process of publication are listed on the preceding pages.

The major portion of the effort in this report was performed for the Hughes Aircraft Company and under Air Force Contracts AF-33(038)-28634 and AF-33(600)-36192.

K. M. Siegel

TABLE OF CONTENTS

I

INTRODUCTION AND SUMMARY

This is the final report on Purchase Order Numbers L-265165-F47; 4-500469-FC-47-D; and 4-526406-FC-89-3 entered into between The University of Michigan and the Hughes Aircraft Company on Air Force Contracts AF-33(038)-28634 and AF-33(600)-36192. The ultimate purpose of this study is to replace radome-dish combinations (postulated but not yet researched and developed) with arrays of slots on the nose cone of a high speed vehicle. Such a replacement would eliminate the many problems associated with radomes, e.g., rain erosion, thermal stress, boresight error rate, and weight and balance problems.

Theoretically, it is always possible to duplicate a pattern produced by one type of antenna using another antenna of equal or larger surface area. For example, the pattern produced by a radome and parabolic dish combination can be duplicated by using any given covering surface as an antenna by correctly distributing the current on that surface. The required current distribution can be calculated by an application of Huygen's Principle. In particular, if the surface is chosen to be a semi-infinite cone, assume that the parabolic dish lies within the conical surface and compute the "dish field" on this surface; this field, then, if induced on a real cone, would reproduce the "dish pattern". Such a calculation serves two purposes: (1) it yields the precise current necessary to duplicate the parabolic-dish pattern, and (2) it yields results which serve as design criteria for arrays of slots, indicating a possible interim slot array design.

Such a computation is presented in Appendix C. The current distribution required varies as a function of the scan angle and the problems involved in attempting to instrument this distribution on a conical surface appear to be extremely difficult; however, since more promising methods are available, e.g., optimized slot arrays, a serious attempt at instrumentation is not warranted.

The value of most theoretical studies on either radiation or scattering problems is that the theoretical analysis very often has in it the seeds of better methods of design. Experiments can only determine the characteristics of existing designs. The approach used here was to:

1. Determine the theoretical means of computing the complete pattern of a single slot on a conical surface.

2. Determine the means of computing the pattern for any given array of slots using the methods of 1.

3. Determine optimization techniques for various design criteria.

4. Given a design configuration, to compute the pattern, e.g., the 65-slot array chosen by the Hughes Aircraft Company for analysis.

5. Apply the optimization techniques of 3, to the pattern of 4.

This report gives the results of 1 through 4.

The slot location is illustrated in Figure 1-1 which also indicates the coordinate system employed in the theoretical analysis of the 65-slot problem. Figures 1-2 through 1-5 contain comparisons of results obtained in the theoretical study with results obtained in the experimental program at the Hughes Aircraft Company.* The formulas employed

*See Appendix A (Section A.3) for a discussion of these comparisons, and additional experimental data obtained by HAC.

in the theoretical analysis of this 65-slot problem together with all of the theoretical results obtained are presented in Appendix A. This paper reports the first analysis which theoretically determines the pattern resulting from a many slot array on a conical surface.

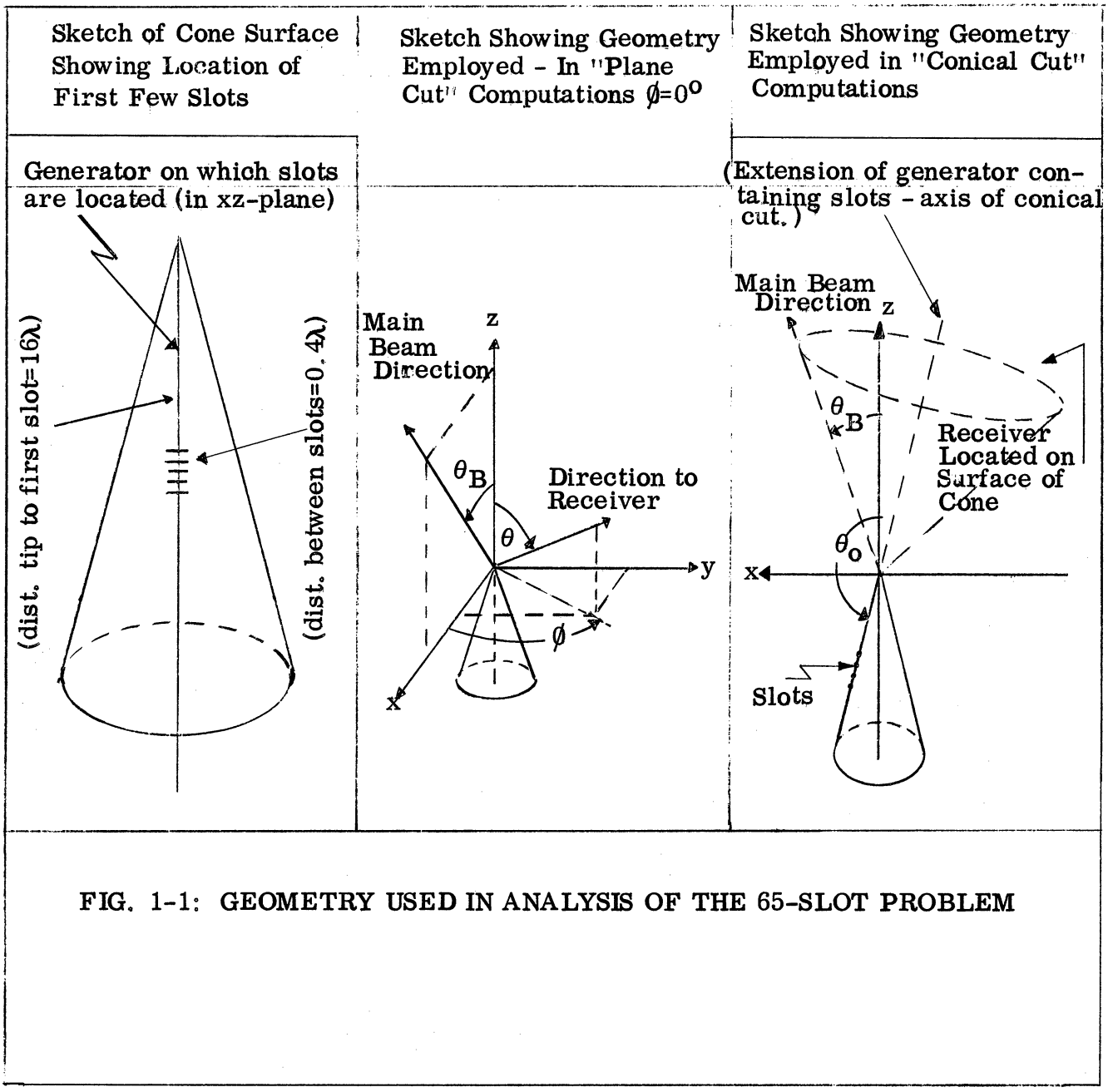

FIG. 1-1: GEOMETRY USED IN ANALYSIS OF THE 65-SLOT PROBLEM

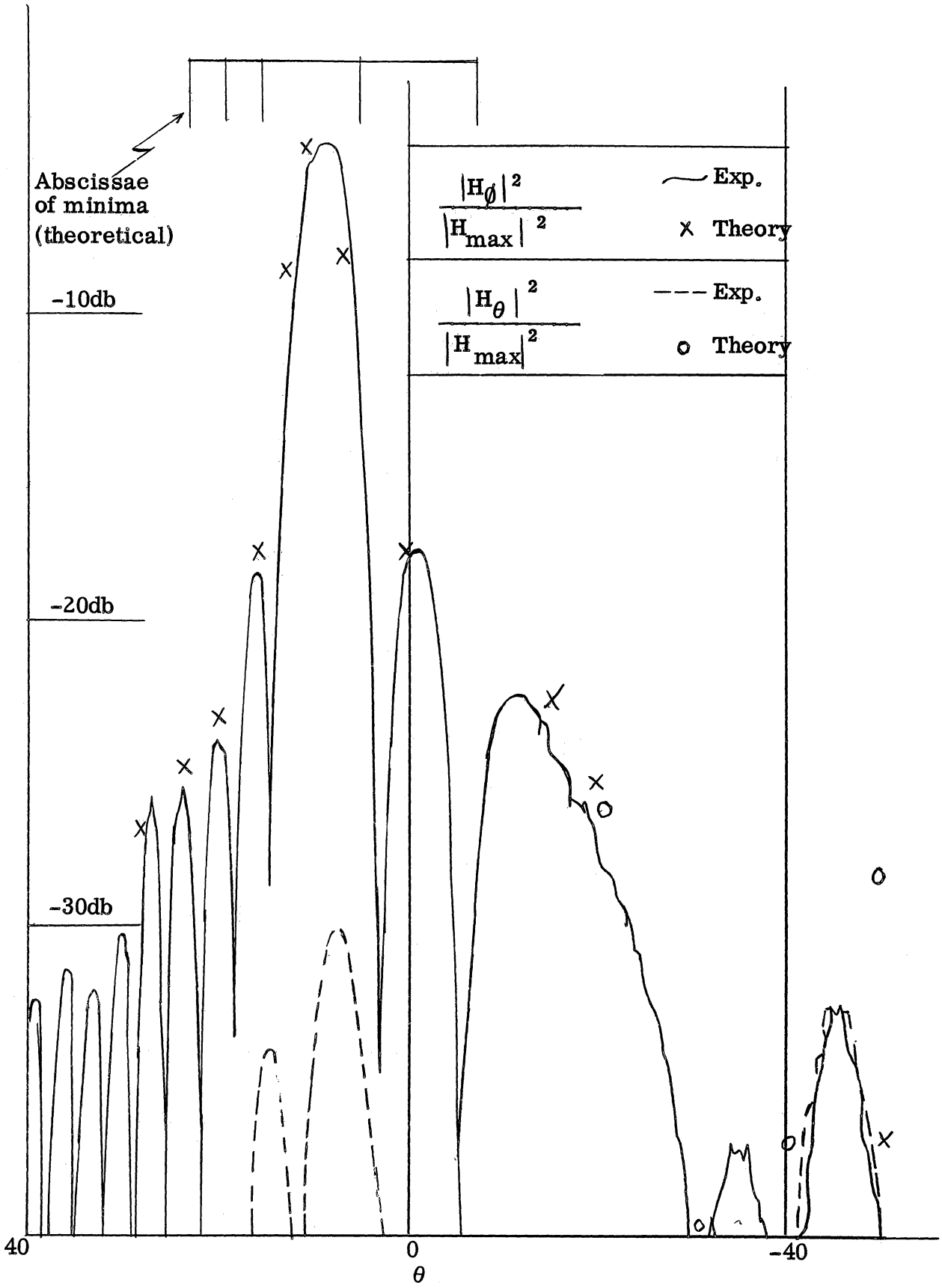

FIG. 1-2 COMPARISON BETWEEN THEORY AND EXPERIMENT FOR A PLANE CUT ($\theta_B = 10^o$, $\phi = 0^o$)

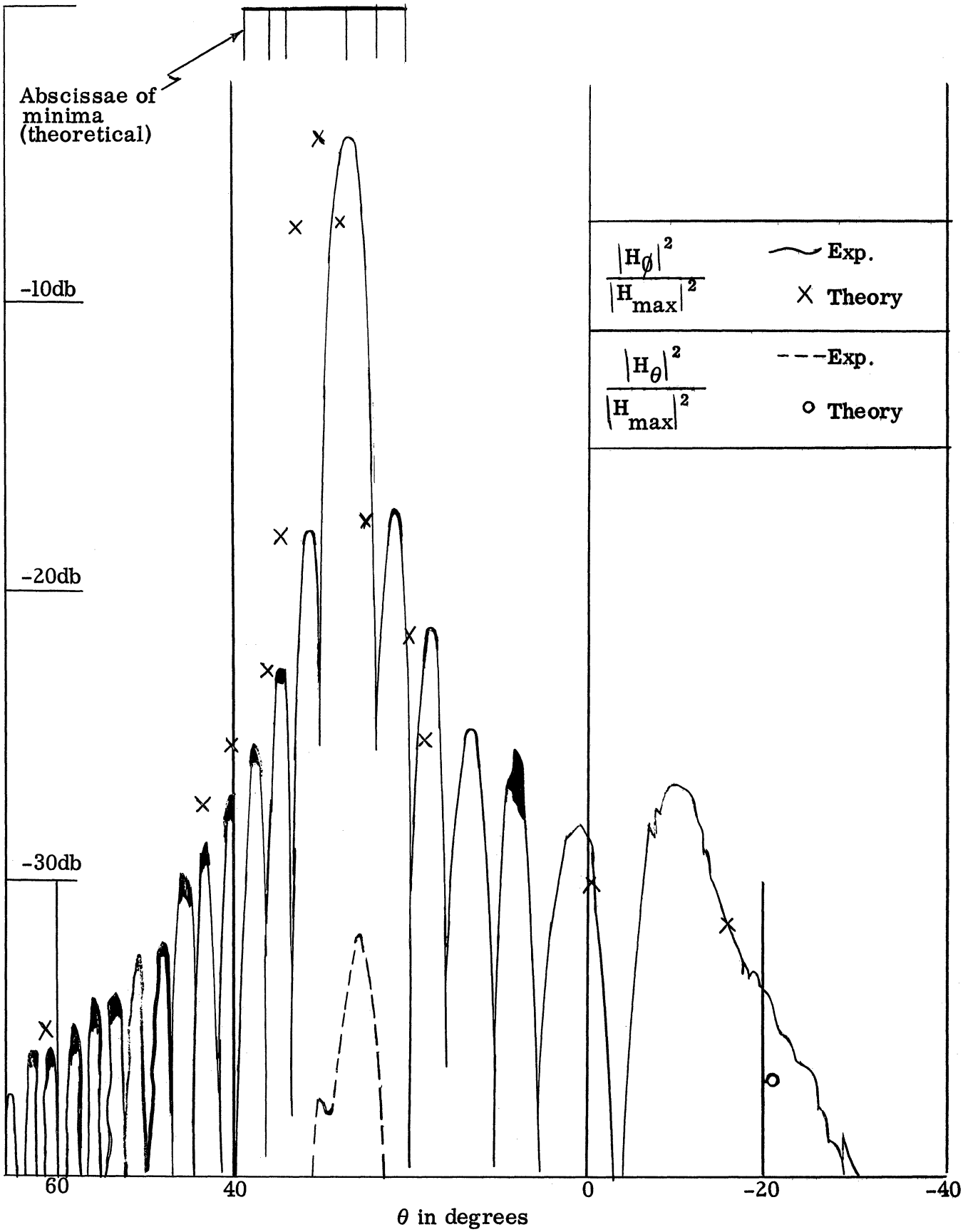

FIG. 1-3 COMPARISON BETWEEN THEORY AND EXPERIMENT FOR A PLANE CUT ($\theta_B = 30^o$, $\phi = 0^o$)

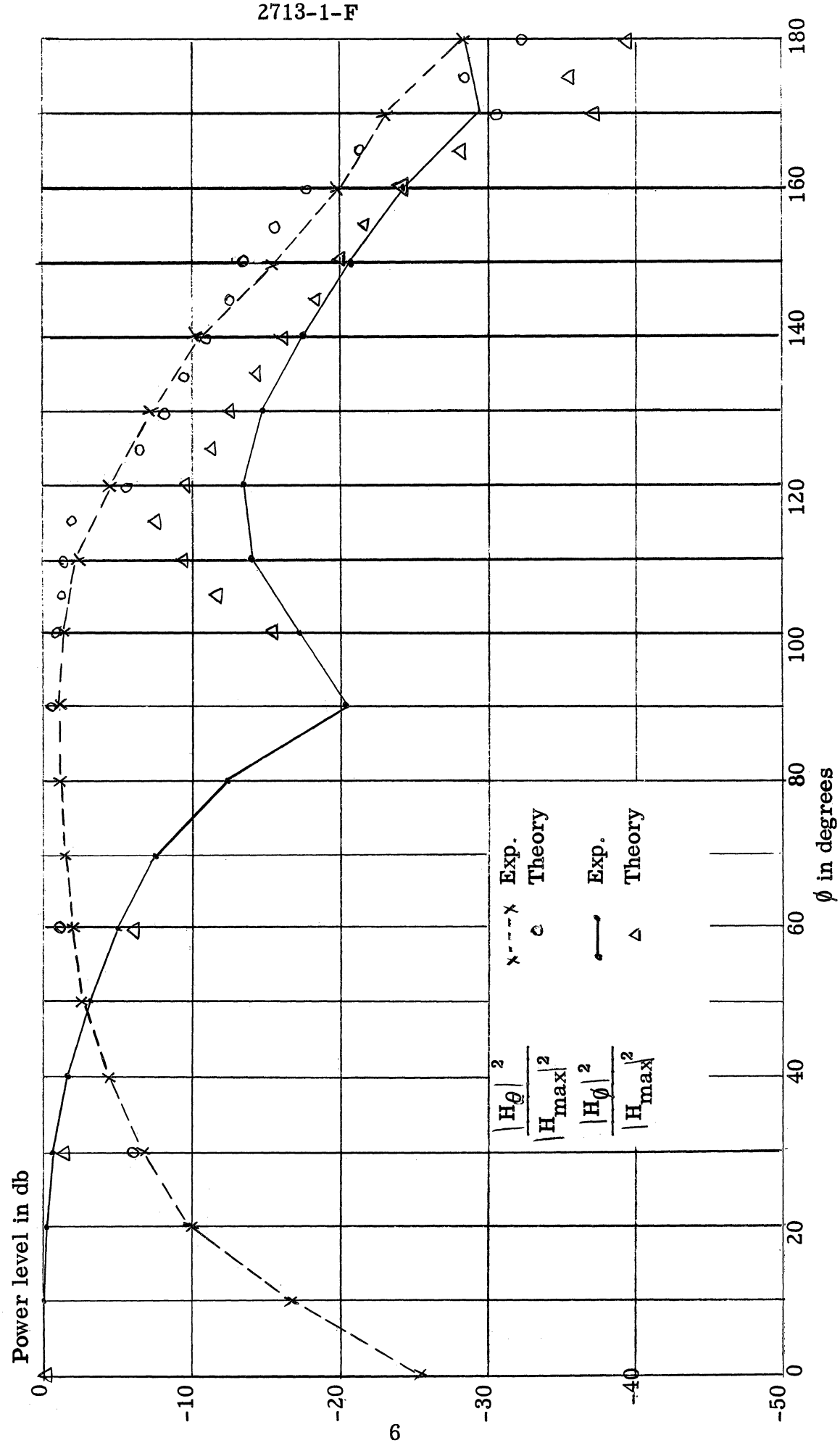

FIG. 1-4 COMPARISON BETWEEN THEORY AND EXPERIMENT FOR A CONICAL CUT ($\theta_B = 10^o$)

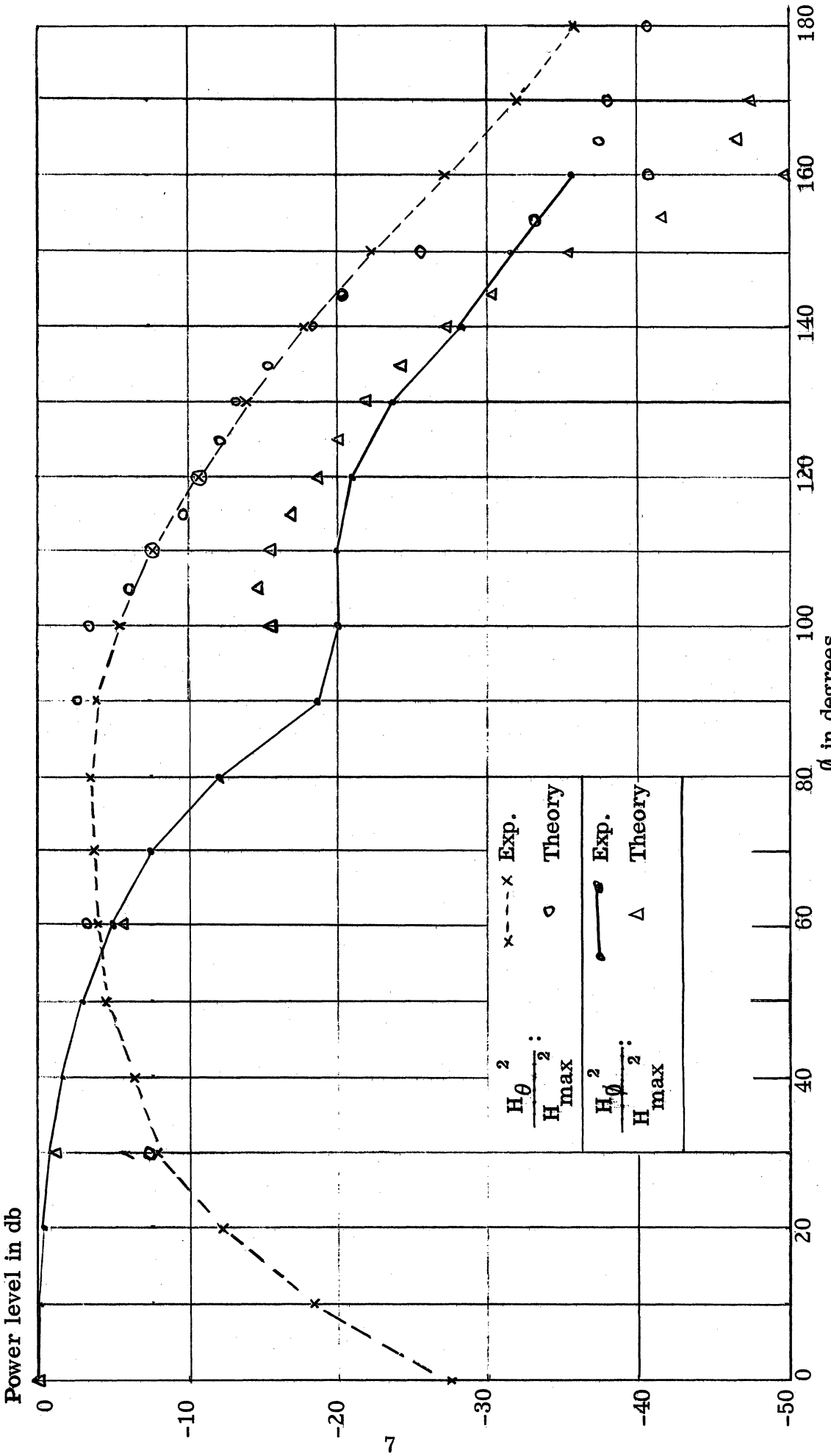

FIG. 1-5 COMPARISON BETWEEN THEORY AND EXPERIMENT FOR A CONICAL CUT
($\theta_B = 30°$)

In order to obtain theoretically the far field radiated in all directions, it is necessary to employ different methods of approximation to account for different contributions to the field. Geometric Optics suffices for main beam calculations. For the receiver not in the main beam, other techniques are required to describe both the effect of the cone's tip on the radiated field and the effect of energy which appears to have crept along the body before being radiated, since these effects predominate out of the line of sight of the array. Physical Optics was used to determine the tip effect while the method available to treat the creeping waves was that due to V. A. Fock (Ref. 1) and this application used analyses of N. A. Logan (Ref. 2), J. B. Keller (Ref. 3) and one of the authors (R. F. Goodrich). The generalized arguments for Fock's universal functions were obtained for application to a conical surface; this work was performed under another Air Force Contract (AF-19(604)-1949) and is discussed in Reference 4.

In the calculation reported on in Appendix A, the Fock technique was employed only when the slots were in the cone's shadow relative to the receiver, and Geometric Optics was used in the lit region. In addition, the tip effect was examined and found (for a 15^{o} half angle cone with the first slot 16 wavelengths from the tip) to be of a lower order of magnitude than the other contributions to the field. These three methods for the analysis of a single slot on a cone are discussed in Section II and the regions of their applicability in the 65-slot problem are indicated graphically in Figure 1-6.

As mentioned above, although a pattern obtained from a single analysis such as the 65-slot program is, in and of itself, of extreme interest, the seeds of improvement

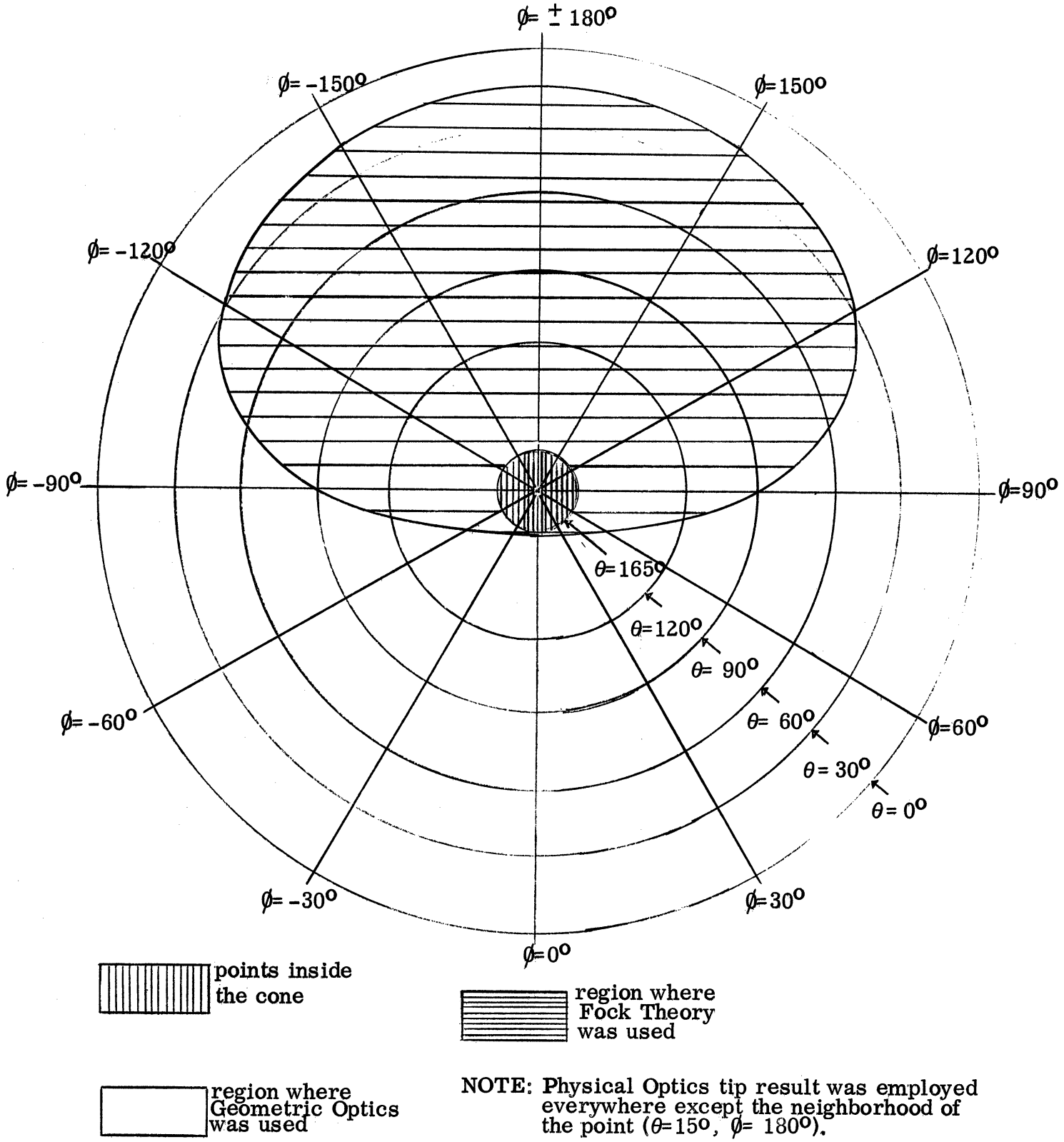

FIG. 1-6 PLANAR REPRESENTATION OF (FAR ZONE) RECEIVER POSITIONS

contained in the analysis are of even greater importance. That is, for many arrays of practical interest it is possible to find a method of predicting how to alter the array to produce a better pattern for a given purpose from the given (or computed) pattern until we have reached a satisfactory practical solution to many particular radiation problems. There are several methods of optimization possible and these are associated with the particular problems present in a given system. Various systems might require as criteria:

1. that a maximum amount of energy be in the main beam for a given amount of power put into the system,
2. that there be a maximum gain for a fixed amount of input power,
3. that the ratio of main beam power to side lobe level be a maximum,
4. that there be a certain spread of power in many side lobes as compared with the admissable power in a few side lobes, etc.

In a given application the criteria which are used will depend upon the specific system requirements. Rather than consider a specific system we have selected two more general criteria for analysis here. We feel that the results obtained are highly important contributions to the optimization problem and that these optimization methods should be applied to slot array computations. The first of these deals with obtaining a low side lobe level for a given maximum beam power; this method of optimization is discussed in Section III. The second method utilizes a special purpose analog computor which we feel

may yield the excitation for the maximum gain possible in surface arrays. This second optimization procedure is discussed in Section IV.

Thus, in summary, we have established the fact that radiation patterns from slots on cones can be computed, we know what current distributions are required to duplicate radome-dish patterns, and we have methods which give every indication of leading to patterns which will be an improvement over the radome-dish type. One would expect this on theoretical grounds since utilizing the entire surface of a cone as an antenna increases the area available over a radome-dish combination (thus obtaining a larger effective aperture) and also because the bias errors due to the radome would be withdrawn from the system.

Although the results reported here represent a definite breakthrough for the surface antenna problem, considerably more work is required before this program can be considered to be complete. For example, the optimization methods should be explored more fully and applied to particular cases of interest, e.g., the 65 slots on a cone generator. Further basic research is required on the nature of the radiated field in the vicinity of the transition region (that region of space which separates the "geometric optics region" from the "Fock theory region"). It is our belief that the amplitude is a slowly varying function in this transition region although the phase is a rapidly varying function. However, this belief is based upon physical principles and should be substantiated by basic mathematical analysis. In addition to the consideration of optimization from the viewpoint of a particular array, considerable attention should be given to

optimization on the basis of a variable array; such an approach (if successful) would lead to a method of optimization which would be applicable to almost any system regardless of what basic input parameter philosophy was inherent in that system.

In considering the optimization procedures, it is necessary to keep sight of the final applications. Indeed, the optimization goal is, given a certain antenna requirement, to reduce to a minimum the complexity, value, and number of the input parameters. As an illustration, it has been shown that point by point control of the field on the entire surface will permit the reproduction of a dish pattern but at the cost of a greatly complicated excitation mechanism. On the other hand, a series of linear arrays of the kind considered in this report may be quite sufficient for a given application at a much reduced cost in the complexity of the input mechanism. An understanding of this approach to optimization needs to be an aim of future study.

Under University of Michigan Purchase Order No. 154216 (under the prime Contract No. AF-33(038)-28634) the University of Illinois investigated the problem of establishing a criterion for approximating a continuous source distribution by a discrete source distribution for line sources under various conditions of excitation. A further investigation considered the approximation of the radiation pattern of an electric dipole in free space by a distribution of dipoles on the surface of a perfectly conducting sphere. This work is reported in Reference 5.

Under subcontract to The University of Michigan (University of Michigan Purchase Order Numbers 154700, 239327 and E-500183) the Polytechnic Institute of Brooklyn carried out studies concerned with the computation of the radiation patterns from leaky wave and surface wave ring sources distributed over a finite area on a perfectly conducting semi-infinite cone. The theoretical formulas for the far radiated fields (including geometric optics and diffraction effects) were obtained by integration over the assumed source distribution of the ring source Green's functions. Explicit results for various source polarizations were obtained for two types of variation of the source distributed over a finite distance along the radial dimension of the cone. In order to gain a better understanding of the radiation from sources distributed on a cone, the simpler problem of radiation from sources on a semi-infinite wedge was also investigated as a preliminary. The results of these and related investigations carried out at the Polytechnic Institute of Brooklyn under these purchase orders are reported in References 6, 7, 8, 9 and 10.

The authors wish to acknowledge the assistance of the following members of the Radiation Laboratory during the computational phase of the study: H. E. Hunter, S. E. Stone, D. Way, D. M. Raybin, M. Plonus, T. Hon, L. S. Gregory, T. B. Curtz, J. W. Crispin, Jr., K. Najita and N. E. Reitlinger.

II

INFINITESIMAL SLOTS

2.1 Introduction

We wish to find an expression for the far field radiated by a transverse infinitesimal slot located on the surface of a cone at a large distance (in wavelengths) from the tip of the cone. The infinitesimal slot can be considered as a magnetic dipole. To find its far field we make use of the Reciprocity Theorem (see Section 2.6). This theorem requires us then to find the field induced on the cone (at the point where we wish to locate the slot) by a magnetic dipole. The dipole is arbitrarily oriented at an arbitrary point in space but has to be located far from both the cone tip and the point where the slot is to be placed.

If the dipole is located sufficiently far from the cone, the wavefronts of the dipole field near the cone are essentially plane. Hence, we approximate the field incident upon the cone by the field of a plane wave, whose magnitude is carefully adjusted so that the dipole nature of the incident field is retained. Thus our problem becomes one of determining the fields induced on the cone surface by a plane wave incident from an arbitrary direction.

We treat this field induced on the cone surface as a quantity having two dominant contributions. One of these contributions arises from energy which either impinges directly upon a neighborhood of the point where the slot is to be placed or travels to this point along a geodesic from the shadow boundary. We call the former part of this

contribution the "geometric optics" term and the latter the "creeping wave" term. The other of these contributions consists of energy which is scattered by the tip of the cone to the point where the slot is to be located. We call this the "tip" term. In the succeeding sections we present the methods by which these two contributions are obtained and the procedures for using them to describe the far field radiated by an infinitesimal slot on a cone. The "geometric optics" term is given implicitly in Section 2.4 and discussed more fully in Reference 16.

2.2 Notation

We adhere to the following notation throughout this section. Let r, θ, ϕ be the usual spherical coordinates describing a field point in the radiation problem, a source point in the reciprocal problem. Primed, these variables designate a field point in the reciprocal problem; double-primed, they refer to points on the cone $\theta'' = \alpha$, $\alpha < \pi/2$.

We specify that all electromagnetic fields have a time dependence given by e^{-ikct} where c is the velocity of light and $k = 2\pi/\lambda$, λ designating wavelength. The unit vector $\hat{p}$ designates the magnetic field direction for a plane wave and is called polarization by us.

2.3 Fock Theory

We obtain the creeping wave contribution to the field on the surface of a cone due to an incident plane wave by suitably extending an analysis due to V. A. Fock (Ref. 1).

We can consider the Fock formulation as a modification of geometric optics

based on a local analysis of the field in the region of the shadow boundary. In particular, Fock defines two universal scalar functions, F and G, whose argument ξ is a function of distance measured from the shadow boundary. The polarization of the incident radiation determines the linear vector combination of the Fock functions which is approximately proportional to the field induced on the scatterer.

The creeping wave term, i.e., the magnetic field $\vec{H}_c$ evaluated on the surface at a point ξ which is a function of distance into the shadow region along a geodesic, can be given in terms of the unit vectors $\hat{\theta}''$, $\hat{T}$, and $\hat{\theta}'' \times \hat{T}$ as

$$\frac{\vec{H}_c(\xi)}{H_o} = \left\{\hat{p} \cdot \hat{\theta}''\Big|_{\text{shadow}}\right\} F(\xi)\hat{T} + \left\{\hat{p} \cdot \hat{\theta}'' \times \hat{T}\Big|_{\text{shadow}}\right\} G(\xi)\hat{\theta}'' \times \hat{T} \qquad (2.3.1)$$

where $\hat{T}$ is the tangent to the geodesic, $\hat{\theta}''$ is the normal to the surface, $\hat{p}$ is the polarization of the incident plane wave, and $F(\xi)$ and $G(\xi)$ are Fock's functions. It is important to note that in this expression for $\vec{H}_c$, $\hat{p} \cdot \hat{\theta}''$ and $\hat{p} \cdot \hat{\theta}'' \times \hat{T}$ are evaluated at that point on the shadow boundary where the creeping wave is launched, while $F(\xi)\hat{T}$ and $G(\xi)\hat{\theta}'' \times \hat{T}$ are evaluated at the point of interest in the shadow region, i.e., at the point where the slot is to be placed.

We now need to determine the geodesics on a cone, the shadow boundary for a given incidence of a plane wave, and curvature along a geodesic (to find Fock's argument ξ).

We find the equation of a geodesic on the cone $\theta'' = \alpha$ to be

$$r'' = a \sin\psi \sec\left[(|\phi''| - \phi_s'') \sin\alpha \pm \frac{\pi}{2} - \psi \right] = \frac{a \sin\psi}{\sin\left[\psi - (|\phi''| - \phi_s'') \sin\alpha\right]} \qquad (2.3.2)$$

where

$$\phi_s'' = \arccos \frac{\tan\alpha}{\tan\theta}, \quad 0 \leq \phi_s'' \leq \pi, \quad \alpha \leq \theta \leq \pi - \alpha, \qquad (2.3.3)$$

gives the equation of the generator forming the shadow boundary (for incidence in the xz-plane); where

$$\psi = \arccos\left(-\frac{\cos\theta}{\cos\alpha}\right), \qquad 0 \leq \psi \leq \pi, \qquad (2.3.4)$$

is the angle the incident direction forms with the shadow boundary; and where a is the distance from cone tip to point where slot is to be located. The curvature K along a geodesic is given by

$$K = \frac{a^2 \cos\alpha \sin^2\psi}{r''^3 \sin\alpha} \qquad (2.3.5)$$

Finally, ξ, the argument of the Fock functions for the creeping wave term, is

$$\xi = \left(\frac{k a \sin\psi}{2 \tan^2\alpha}\right)^{1/3} (|\phi''| - \phi_s'') \sin\alpha \quad . \qquad (2.3.6)$$

2.4. Tip-scattering

We use the expression "Physical Optics field" to denote the scattered far field, $\vec{H}_s$, obtained by using Geometric Optics (i.e., the magnetic field on the surface is given by twice the tangential component of the incident magnetic field in the lit region and zero in the shadow) in the Kirchhoff-Huygens integral representation for a scattered field.

$\vec{H}_s$ is, for a plane wave of magnitude H_o incident from an arbitrary direction,

$$\vec{H}_s \cong \frac{H_o\, ike^{ikr'}}{2\pi r'}\, \vec{g}, \quad \vec{g}=(\hat{r}'\cdot\hat{p})\vec{f}-(\hat{r}'\cdot\vec{f})\,\hat{p} \tag{2.4.1}$$

where

$$\vec{f} = \int_S \hat{n} e^{-ik\vec{r}''\cdot(\hat{r}+\hat{r}')}\, dS \ . \tag{2.4.2}$$

S is the portion of the cone surface illuminated by the plane wave and $\hat{n}$ is the outward normal to the cone. Equation (2.4.2) may be written

$$\vec{f} = \int_0^{\infty} \int_A^B (\cos\alpha\cos\phi''\hat{i}_x+\cos\alpha\sin\phi''\hat{i}_y-\sin\alpha\hat{i}_z)e^{-ikr''M}\, r''\sin\alpha\, d\phi''dr''. \tag{2.4.3}$$

A and B are generator shadow boundaries cast on the cone by the incident plane wave; they are

$$A=\phi-\arccos\left(\frac{\tan\alpha}{\tan\theta}\right), \qquad B=\phi+\arccos\left(\frac{\tan\alpha}{\tan\theta}\right),$$

when no shadow exists, i.e., the cone is entirely illuminated or $\theta > \pi-\alpha$, $A=\phi-\pi$ and $B=\phi+\pi$. The quantity M is given by

$$M = q + b\cos\phi'' + c\sin\phi''$$

where

$$q = \cos\alpha\,(\cos\theta' + \cos\theta),$$

$$b = \sin\alpha\,(\cos\phi'\sin\theta' + \sin\theta\cos\phi),$$

$$c = \sin\alpha\,(\sin\phi'\sin\theta' + \sin\phi\sin\theta).$$

The r'' integration is accomplished by an Abelian limit argument (Ref. 11), yielding for $\vec{f}$

$$\vec{f} \cong -\frac{\sin\alpha}{k^2} \int_A^B \frac{d\phi''}{M^2} (\cos\alpha \cos\phi'' \hat{i}_x + \cos\alpha \sin\phi'' \hat{i}_y - \sin\alpha \hat{i}_z) \; ; \qquad (2.4.4)$$

this integration can be expressed in finite terms (Ref. 12);

$$\vec{f} \cong -\frac{\sin\alpha}{k^2} \left\{ \cos\alpha \left[\frac{c+q\sin\phi''}{MQ} - 2bQ^{-3/2} \arctan \frac{(q-b)\tan(\phi''/2)+c}{\sqrt{Q}} \right] \hat{i}_x \right.$$

$$- \cos\alpha \left[\frac{b+q\cos\phi''}{MQ} + 2cQ^{-3/2} \arctan \frac{(q-b)\tan(\phi''/2)+c}{\sqrt{Q}} \right] \hat{i}_y$$

$$\left. - \sin\alpha \left[\frac{c\cos\phi'' - b\sin\phi''}{MQ} + 2qQ^{-3/2} \arctan \frac{(q-b)\tan(\phi''/2)+c}{\sqrt{Q}} \right] \hat{i}_z \right\} \Bigg|_A^B ,$$

where

$$Q = q^2 - b^2 - c^2 \; .$$

Care must be taken with the value of the arctangent to note where its value has moved from one Riemann surface to the next as the value of ϕ'' moves from A to B.

The field $\vec{H}_s$ given by Equation (2.4.1) is called the tip-scattered field because in the Abelian evaluation of the integral for $\vec{f}$ (Eqn. 2.4.4) the major contribution, for M bounded away from zero, is obtained from a neighborhood of the point $r''=0$, i.e., the tip of the cone. The cases for which $M=0$ for all values of ϕ'' in Equation (2.4.4), correspond to forward scattering situations and these cases are dealt with by Geometric Optics. The cases for which $M=0$ at only one value of $|\phi''|$

in the region of integration either correspond to specular reflection where again Geometric Optics is used or require a re-examination of the Physical Optics approximation. Although the integral in (2.4.4) does not exist in this last case we know how to correctly handle this situation. In Appendix B we make a closer examination of the Physical Optics integral (Eqn. 2.4.1) for this case and find that the evaluation given above can be formally extended to include it. Since the major contribution to the Physical Optics integral, when it exists, comes from a neighborhood of the cone tip we now require only that the field point be far from this neighborhood. In this way we obtain a representation of the tip-scattered contribution to the field on the cone surface far from the tip.

There are substantial indications that the Physical Optics field closely approximates the exact field scattered by a cone. For example, the Physical Optics method produces, for large and small angle cones, a result for the nose-on monostatic radar cross section which is in excellent agreement with the result produced by an exact expansion of the cross section in powers of the cone angle(Refs. 13,14). In addition, the rigorous bistatic radar cross section for an electromagnetic plane wave incident along the cone axis agrees well with the Physical Optics result (Ref. 14). We know also that it has exactly the right wavelength dependence.

2.5. Plane Waves versus Dipoles

In the previous sections we dealt with an incident plane wave. The field of the plane wave on the cone surface is given by

$$\vec{H}_i = \hat{p}\, H_o\, e^{-ik\hat{r}\cdot\vec{r}''} \quad . \tag{2.5.1}$$

Since we are really interested in an incident field due to a magnetic dipole far from the cone, we relate these fields as follows:

Let a magnetic dipole with orientation $\hat{m}$, such that $\hat{m} \cdot \hat{r}$ vanishes, be located at the point (r, θ, ϕ). Then its far field is

$$\frac{C\, e^{ikR}}{R} \hat{R} \times (\hat{R} \times \hat{m}),$$

where C is the dipole strength coefficient and R is the distance from the point (r, θ, ϕ) to the point of observation (r', θ', ϕ'),

$$R = \left[r^2 + r'^2 - 2\vec{r} \cdot \vec{r}'\right]^{1/2},$$
$$\cong r - \hat{r} \cdot \vec{r}' \quad \text{for } r \gg r',$$

and

$$\hat{R} = \nabla R.$$

For large r, $\hat{R}$ may be replaced by $-\hat{r}$. Since the dipole is far from the cone its field at the cone surface is given approximately by

$$\vec{H}_i = -\hat{m}\, C \frac{e^{ik(r - \hat{r} \cdot \vec{r}'')}}{r} . \qquad (2.5.2)$$

Thus we see from Equations (2.5.1) and (2.5.2) that, at the cone surface, we may replace the incident field of a plane wave by the incident field of a dipole placed at a very large but finite distance from the cone simply by placing $\hat{p} = -\hat{m}$ and

$$H_o = C \frac{e^{ikr}}{r} .$$

2.6 The Reciprocity Theorem

We now present the Reciprocity Theorem in a form which, with the results of the previous sections, will enable us to obtain the far field radiated by an infinitesimal slot

on a cone.

The Lorentz Reciprocity Theorem may be stated in the form

$$\int \vec{H}_1 \cdot \vec{M}_2 \, dV = \int \vec{H}_2 \cdot \vec{M}_1 \, dV$$

where $\vec{H}_1(\vec{H}_2)$ is the field due to the magnetization $\vec{M}_1(\vec{M}_2)$ and the integration is over all space. If $\vec{M}_{1,2}$ are of the form $\hat{m}_{1,2}\,\delta(\vec{r}-\vec{r}_{1,2})$, that is, point sources, then we find

$$\vec{H}_1(\vec{r}_2) \cdot \hat{m}_2 = \vec{H}_2(\vec{r}_1) \cdot \hat{m}_1 \quad . \tag{2.6.1}$$

Let $\hat{m}_2$ designate the direction of some specifically oriented dipole located by the vector $\vec{r}_2$. We wish to determine its field $\vec{H}_2$ at some far point $\vec{r}_1$. Suppose

$$\vec{H}_2(\vec{r}_1) = A_1(\vec{r}_1)\hat{u}_1 + A_2(\vec{r}_1)\hat{v}_1,$$

where $\hat{u}_1 \cdot \hat{v}_1 = 0$. Let $\hat{u}_1$ and $\hat{v}_1$ designate in turn the orientation of $\hat{m}_1$ of a dipole located by $\vec{r}_1$. Its field at $\vec{r}_2$ is in turn $\vec{H}_1(\vec{r}_2, \hat{u}_1)$ and $\vec{H}_1(\vec{r}_2, \hat{v}_1)$.

It follows from (2.6.1) that

$$\vec{H}_1(\vec{r}_2, \hat{u}_1) \cdot \hat{m}_2 = \left[A_1(\vec{r}_1)\hat{u}_1 + A_2(\vec{r}_1)\hat{v}_1\right] \cdot \hat{u}_1,$$

from which

$$\left[\vec{H}_1(\vec{r}_2, \hat{u}_1) \cdot \hat{m}_2\right] = A_1(\vec{r}_1) \quad . \tag{2.6.2}$$

Similarly, from (2.6.1)

$$\vec{H}_1(\vec{r}_2, \hat{v}_1) \cdot \hat{m}_2 = \left[A_1(\vec{r}_1)\hat{u}_1 + A_2(\vec{r}_1)\hat{v}_1\right] \cdot \hat{v}_1 \quad ,$$

from which

$$\left[\vec{H}_1(\vec{r}_2, \hat{v}_1) \cdot \hat{m}_2\right] = A_2(\vec{r}_1) \quad . \tag{2.6.3}$$

Therefore

$$\vec{H}_2(\vec{r}_1) = \left[\vec{H}_1(\vec{r}_2, \hat{u}_1) \cdot \hat{m}_2\right] \hat{u}_1 + \left[\vec{H}_1(\vec{r}_2, \hat{v}_1) \cdot \hat{m}_2\right] \hat{v}_1 \quad . \tag{2.6.4}$$

Equation (2.6.4) gives the radiated far field of a slot on the surface of a cone if we let

$\vec{r}_1 \to \vec{r}$, $\vec{r}_2 \to \vec{r}''$, $\hat{m}_2 \to$ direction of slot, $\hat{u}_1, \hat{v}_1 \to$ successive values for polarization, $\hat{p}$; $\vec{H}_1 \to \vec{H}_s + \vec{H}_c$, and $\vec{H}_2 \to \vec{H}$.

2.7 The Far Field Radiated by an Infinitesimal Slot

The final part of the preceding section explains exactly how to employ the Reciprocity Theorem to obtain a radiated far field due to an infinitesimal slot on a cone.

In Section 2.3 we have, without loss of generality, restricted the direction of incidence to lie in the xz-plane. We may treat the results of Section 2.4 in a similar fashion, again without loss of generality.

Now employing the results of Section 2.6 we may express the radiated far field at a point $(r, \theta, 0)$ due to an infinitesimal slot located at (a, α, ϕ'') in the direction ϕ'' on the cone as

$$\vec{H} = \left\{ \left[\vec{H}_c(\hat{p}_1) + \vec{H}_s(\hat{p}_1) \right] \cdot \hat{\phi}'' \right\} \hat{p}_1 + \left\{ \left[\vec{H}_c(\hat{p}_2) + \vec{H}_s(\hat{p}_2) \right] \cdot \hat{\phi}'' \right\} \hat{p}_2 ,$$

where the results of Section 2.5 must be used to define the quantity H_o appearing in expressions for $\vec{H}_c$ and $\vec{H}_s$ given by Equations (2.3.1) and (2.4.1), respectively. Note that $\vec{H}_c$, for a point in the lit region, is given by geometric optics.

If the slot has a small but finite length, L, then the expression for the radiated far field obtained above can be adjusted so as to include the length and voltage, V_o, across the slot. As long as a radiating magnetic dipole is equivalent to a slot in a plane we can relate the dipole strength coefficient, C, of Section 2.5 with the voltage

across the slot as follows

$$C = \frac{ik\, V_o L}{4\pi}$$

(see Section A. 1. 3, p. 68 of Reference 15).

It is significant to note that the term "Geometric Optics field" is a misnomer when applied to radiated fields obtained via reciprocity from scattered "Geometric Optics fields", since such radiated fields are no longer wavelength independent.

III

A THEORY OF LOW SIDE LOBE ANTENNA ARRAYS

In the problem which will be considered in this Section it is assumed that there are a number of current distributions for the array which can be excited independently, and for each of which the radiated field is known. We might assume that the array consists of a number of elements which can be separately excited, and that the field radiated when any one of these elements is excited is known. For example, we have shown in Section 2 how to find the radiated field of an infinitesimal slot on a cone. The problem we set for ourselves is that of determining the excitation coefficients for an array in such a way as to minimize the side lobe level (compared to the main beam) for a beam of a fixed width.

To restate the above symbolically let the currents I_n give the radiated fields, F_n. We now want to determine coefficients A_n which are related to the current, $I = \sum A_n I_n$, and field, $F = \sum A_n F_n$, in such a way that the largest value taken on by the ratio $\left| \frac{F(\theta, \phi)}{F(0, 0)} \right|$ in a given region, **R**, which excludes a neighborhood of the point $\theta = 0, \phi = 0$ is as small as possible (θ and ϕ are the polar angles of the field point).

We will consider a series of less ambitious problems which will finally lead us to the desired problem. Rather than minimizing the largest value taken on by $\left| \frac{F(\theta, \phi)}{F(0, 0)} \right|$ for all points θ, ϕ in **R** we will minimize the largest value taken on by $\left| \frac{F(\theta, \phi)}{F(0, 0)} \right|$ at a set of points θ_i, ϕ_i in **R**. We will eventually let the number of points cover **R** densely so as to solve the original problem. Throughout the discussion we will not insist on any more mathematical rigor than is necessary to put forward a convincing argument for the methods used.

As a matter of notation let

$$F_n(\theta_i, \phi_i) = F_{in}$$

$$F_n(0, 0) = F_{on} \quad .$$

Then we seek the values of $A_1, A_2, \ldots, A_N$ which will give

$$\underset{A_1, A_2, \ldots, A_N}{\text{Min}} \quad \underset{i}{\text{Max}} \quad \left| \frac{\sum_n A_n F_{in}}{\sum_n A_n F_{on}} \right| \quad , \tag{3.1}$$

that is we seek the values of $A_1, A_2, \ldots, A_N$ which will minimize the largest value taken on by $\left| \frac{\sum A_n F_{in}}{\sum A_n F_{on}} \right|$. Let M be the number of values taken on by i (excluding zero). First of all assume $M < N$. Then we can make $\sum A_n F_{in} = 0$ for all $i \neq 0$ while $\sum A_n F_{on} \neq 0$. This disposes of this case which will not be of interest hereafter.

Next consider the case $M = N$. This case, as it will turn out, is fundamental to the rest of the analysis. We are assuming that the matrix F_{in} is non-singular which will ordinarily be the case. For simplicity we now let

$$B_i = \sum_n F_{in} A_n \quad . \tag{3.2}$$

We can solve for the A_n in the form

$$A_n = \sum_i (F^{-1})_{ni} B_i \quad . \tag{3.3}$$

Thus we have

$$\sum_n F_{on} A_n = \sum_n \sum_i F_{on} (F^{-1})_{ni} B_i = \sum_i G_i B_i \tag{3.4}$$

where

$$G_i = \sum_n F_{on} (F^{-1})_{ni} \quad .$$

Now our problem is to determine the values of $B_1, B_2, \ldots, B_N$ which will give

$$\underset{B_1, B_2, \ldots, B_N}{\text{Min}} \quad \underset{i}{\text{Max}} \left| \frac{B_i}{\sum G_j B_j} \right| . \tag{3.5}$$

It is clear that the B's are not unique to the extent that we can make the replacement $B_i \rightarrow \lambda B_i$ without affecting the value of $\underset{i}{\text{Max}} \left| \frac{B_i}{\sum G_j B_j} \right|$. We will make use of this later to simplify the form of the problem. Let us now assume that all of the B's except B_1 have the correct value (or rather a correct value in view of the non-uniqueness). We will now proceed to evaluate B_1 in terms of the other B's.

First we note that

$$\underset{i}{\text{Max}} \left| \frac{B_i}{\sum G_j B_j} \right| = \underset{i}{\text{Max}} \left| \frac{B_i}{\sum \frac{G_j}{G_1} B_j} \right| \frac{1}{|G_1|}$$

$$= \frac{1}{|G_1|} \underset{i}{\text{Max}} \left| \frac{B_i}{\sum \frac{G_j}{G_1} B_j} \right| , \tag{3.6}$$

Next we make use of the non-uniqueness to replace B_j by $B_j e^{i\alpha}$ (α real) where α is chosen so as to make $\sum_{j \neq 1} \frac{G_j}{G_1} B_j$ a positive real number, γ. Finally we let $x = -B_1$. Now what we seek is

$$\underset{x}{\text{Min}} \quad \text{Max} \left\{ \underset{i \neq 1}{\text{Max}} \left| \frac{B_i}{\gamma - x} \right| , \left| \frac{x}{\gamma - x} \right| \right\} . \tag{3.7}$$

Let i_M be a value of i (other than 1) for which $\left| \frac{B_i}{\gamma - x} \right|$ takes on its maximum value. Thus we want

$$\underset{x}{\text{Min}} \quad \text{Max} \left\{ \left| \frac{B_{i_M}}{\gamma - x} \right| , \left| \frac{x}{\gamma - x} \right| \right\} . \tag{3.8}$$

Figure 3-1 is a contour plot of $\text{Max}\left\{\left|\frac{B_i M}{\gamma - x}\right| , \left|\frac{x}{\gamma - x}\right|\right\}$ in the x-plane for $B_{i_M} = \gamma/2$. The contour lines are for the indicated side lobe levels. The dotted circle divides the region $|B_{i_M}| > |x|$ from the region $|B_{i_M}| < |x|$. It is clear that the minimum occurs for $x = -|B_{i_M}|$. From this we see that $|B_1| = |B_{i_M}|$. Since we could equally well have chosen any of the other B's in place of B_1 we see that the minimum occurs when all of the B's are equal in magnitude. Due to the non-uniqueness we can take the B's to all be equal to one in magnitude. Then (3.5) can be written

$$\underset{\substack{B_1, B_2, \ldots, B_N \\ |B_1| = |B_2| = \ldots = |B_N| = 1}}{\text{Max}} \left| \sum G_j B_j \right| . \tag{3.9}$$

But $\left|\sum G_j B_j\right| \leq \sum |G_j B_j| = \sum |G_j|$ ($|B_j| = 1$), so that it is clear that the maximum will be attained for $B_j = \frac{|G_j|}{G_j}$. Thus we have

$$\underset{B_1, B_2, \ldots, B_n}{\text{Min}} \ \underset{i}{\text{Max}} \left| \frac{B_i}{\sum G_j B_j} \right| = \frac{1}{\sum |G_j|} \tag{3.10}$$

is attained for

$$B_j = \frac{|G_j|}{G_j} . \tag{3.11}$$

To get the corresponding values of the A's we use (3.3). This completes the solution of the problem M = N.

Next we consider the case $\infty > M > N$. Suppose we had a correct set of A_n. Now order the M quantities $\left|\frac{\sum A_n F_{in}}{\sum A_n F_{on}}\right|$ starting with the largest and ending with the smallest. Pick out the first N of these.

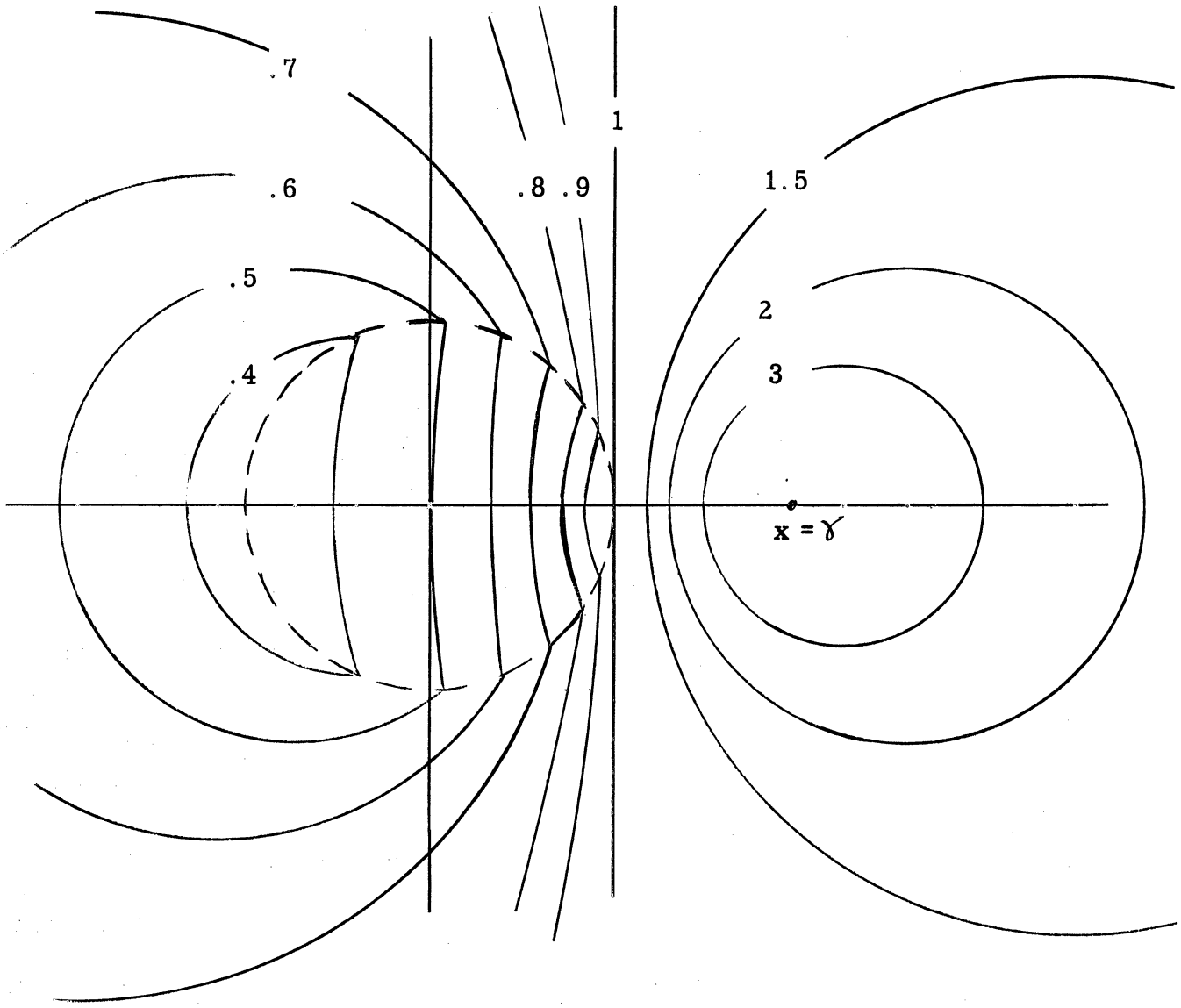

FIG. 3-1: CONTOUR PLOT OF MAX $\left\{\left|\frac{B_{i_M}}{\gamma - x}\right| , \left|\frac{x}{\gamma - x}\right|\right\}$

IN THE COMPLEX x-PLANE FOR THE CASE OF $B_{i_M} = \gamma/2$.

Suppose, in the first instance, that the N quantities are not all equal for the solution when all M are involved. Then we can make a small change in the A's in such a way as to decrease the largest of the N quantities while, if the change in the A's is small enough, none of the other M - N values will be larger than the largest of the N values. Thus the N values are equal.

Next suppose that the N chosen quantities are larger than the next largest of the M. Then unless the N A's have the values they would have if the remaining M - N quantities were ignored, we can again make small changes in the A's which will reduce the N quantities uniformly while keeping any of the remaining M - N all smaller than the chosen N.

Thus we see in this case (when the N largest quantities are larger than the remaining M - N if the A's have been correctly chosen to solve the problem) that we need to consider only N of the M quantities in order to arrive at the correct solution. The question is, which N of the M quantities must we deal with. We will now answer this question. We assert that we must choose the N quantities which yield the largest value of $\frac{1}{\sum |G_j|}$ (note that the G_j depend on which N of the M quantities are chosen). To establish this assertion we show a contradiction in the converse assumption. Let us assume, then, that the solution is obtained for a choice which does not lead to the maximum value of $\frac{1}{\sum |G_j|}$. Now let us consider the N quantities which lead to the largest value of $\frac{1}{\sum |G_j|}$. We know that not all of these N quantities can be made smaller than the largest $\frac{1}{\sum |G_j|}$ and thus the assumption that none of them are larger than one of the smaller $\frac{1}{\sum |G_j|}$ is false. This establishes the assertion.

We are thus led to the following method of attacking our original problem. First we start with N arbitrary points. We then vary these points so as to maximize the value of $\frac{1}{\sum|G_j|}$. We would then hope that the A's which correspond to the N points which maximize $\frac{1}{\sum|G_j|}$ would solve the problem. We can easily test to see if they do solve our problem by computing the field resulting from this choice of the A's. If the side-lobe level is nowhere greater than it is at the N chosen points we have solved our problem since the side-lobe level cannot be made any lower at the N points. However, if the side-lobe level is higher at some other point then we have not solved our problem.

Now it turns out that in some cases the above method works, and in some cases it does not. We can get some insight into the question of how frequently we can expect the method to work by considering the following analogous problem (it is, in fact, a special case of our general problem but we will not bother to make the exact connection). Suppose that we have a number of points in the complex plane, z_n, and that we wish to find a point z such that $\underset{n}{\text{Max}} \left| z - z_n \right|$ is made as small as possible. A method of attacking this problem which is exactly analogous to the method described above is the following. Find the pair or points, z_n and z_m, from the given set which maximize $\left|z_m - z_n\right|$ (this is analogous to maximizing $\frac{1}{\sum|G_j|}$). Then let $z = (z_m + z_n)/2$. This value of z will sometimes solve the problem, and sometimes not. It depends on whether the rest of the points in the set lie inside the circle having z as a center and $\left|z_m - z_n\right|/2$ as a radius. In the figure below (Figure 3-2) we show some sets of points for which the method would work, and some for which it would not work.

Among the cases where this method does work is the design of a broadside linear array where the results of this method coincide with those of the Dolph-Chebychev method. We can certainly expect the method to work also in cases which do not differ too radically from this one, as well as in some of the cases which do differ radically. It is expected that future study will yield methods which work in all cases.

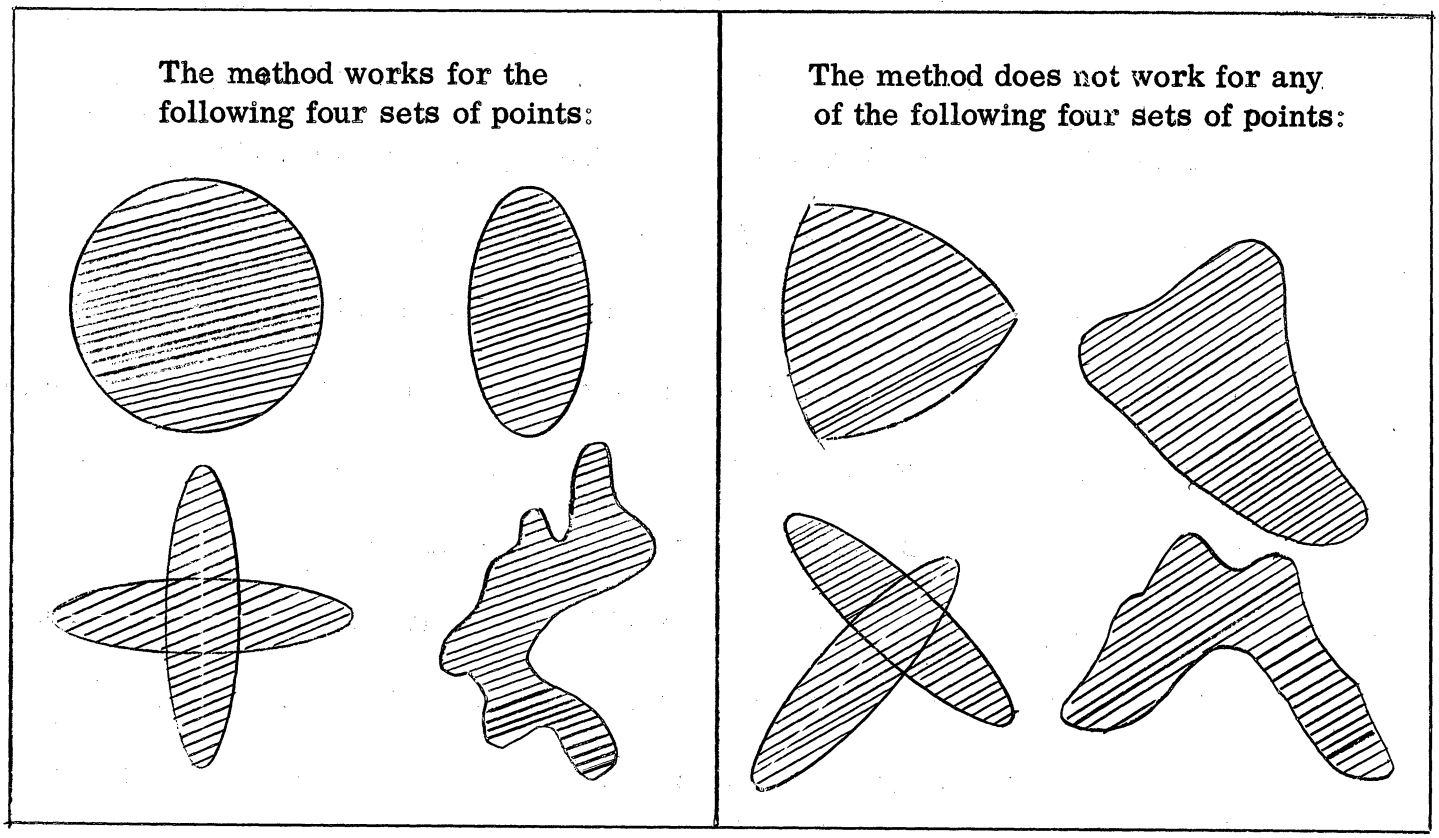

FIG. 3-2: THE PROBLEM OF MINIMIZING $\underset{n}{\text{MAX}} \left|z - z_n\right|$ - EXAMPLES OF SETS OF POINTS FOR WHICH METHOD WORKS AND SETS OF POINTS FOR WHICH METHOD DOES NOT WORK

In order to give an idea of how this method goes we will now consider a very simple numerical example. We will take the case of a linear broadside array of four isotropic elements where the ratios of the currents in the elements is to be chosen so as to produce a low side-lobe level. This problem can also be treated by standard methods so that we have a standard of comparison.

Let the inter-element spacing be $\lambda/2$. We will consider the case where there are only four elements which we take to be located at

$$x = y = 0 \; ; \; z = \pm \lambda/4 \, , \, \pm 3\lambda/4 \; . \tag{3.12}$$

The radiated field in the direction (θ, ϕ) is given by

$$E = \frac{e^{ikr}}{r} \; F = A_{-2} \; \frac{\exp\left[ik(r + \frac{3\lambda}{4}\cos\theta)\right]}{r} + A_{-1} \; \frac{\exp\left[ik(r + \frac{\lambda}{4}\cos\theta)\right]}{r} \tag{3.13}$$

$$+ A_1 \; \frac{\exp\left[ik(r - \frac{\lambda}{4}\cos\theta)\right]}{r} + A_2 \; \frac{\exp\left[ik(r - \frac{3\lambda}{4}\cos\theta)\right]}{r} \; .$$

Let us first of all consider a standard design of such an array. In the Dolph-Chebychev design we would have $A_1 = A_{-1}$, $A_2 = A_{-2}$, A_1 and A_2 real. In this case we get

$$F = 2A_1 \cos\left(\frac{\pi}{2}\cos\theta\right) + 2A_2 \cos\left(\frac{3\pi}{2}\cos\theta\right) \; . \tag{3.14}$$

Now the field broadside $(\theta = \pi/2)$ is $F_o = 2(A_1 + A_2)$. There will be sidelobes symmetrically situated relative to $\theta = \pi/2$ which are located by the condition $\frac{\partial F}{\partial \cos\theta} = 0$ or

$$-\pi A_1 \sin\left(\frac{\pi}{2}\cos\theta\right) - 3\pi A_2 \sin\left(\frac{3\pi}{2}\cos\theta\right) = 0 \; . \tag{3.15}$$

Making use of the relation $\sin 3x = \sin x\,(3-4\sin^2 x)$ we put (3.15) in the form

$$A_1+9A_2 = 12A_2 \sin^2\left(\frac{\pi}{2}\cos\theta\right)$$

$$\sin\left(\frac{\pi}{2}\cos\theta\right) = \sqrt{\frac{A_1+9A_2}{12A_2}}\,. \tag{3.16}$$

Using this value of (θ) in (3.14) we get

$$F = 2A_1\sqrt{\frac{3A_2-A_1}{12A_2}} + 2A_2\sqrt{\frac{3A_2-A_1}{12A_2}}\left\{1 - \frac{A_1+9A_2}{3A_2}\right\} = -\frac{2}{3}\,\frac{(3A_2-A_1)^{3/2}}{\sqrt{3A_2}} \tag{3.17}$$

The value of θ for which the main beam has decreased to the value given by (3.17) is also of interest. It is given by

$$2A_1\cos\left(\frac{\pi}{2}\cos\theta\right)+2A_2\cos\left(\frac{3\pi}{2}\cos\theta\right) = \frac{2(3A_2-A_1)^{3/2}}{3\sqrt{3A_2}}$$

or

$$\cos\left(\frac{\pi}{2}\cos\theta\right) = \sqrt{\frac{3A_2-A_1}{3A_2}}\,. \tag{3.18}$$

Figure 3-3 gives θ as given by Equations (3.18) and (3.16) as a function of A_1/A_2 while Figure 3-4 gives the side-lobe level in db down from the main dobe as a function of A_1/A_2.

The results given above from Equation (3.14) on are essentially taken from Dolph's "A Current Distribution for Broadside Arrays which Optimizes the Relationship Between Beam Width and Side-Lobe Level". With these results available for comparison we are prepared to treat the same problem with the method discussed previously.

FIG. 3-3

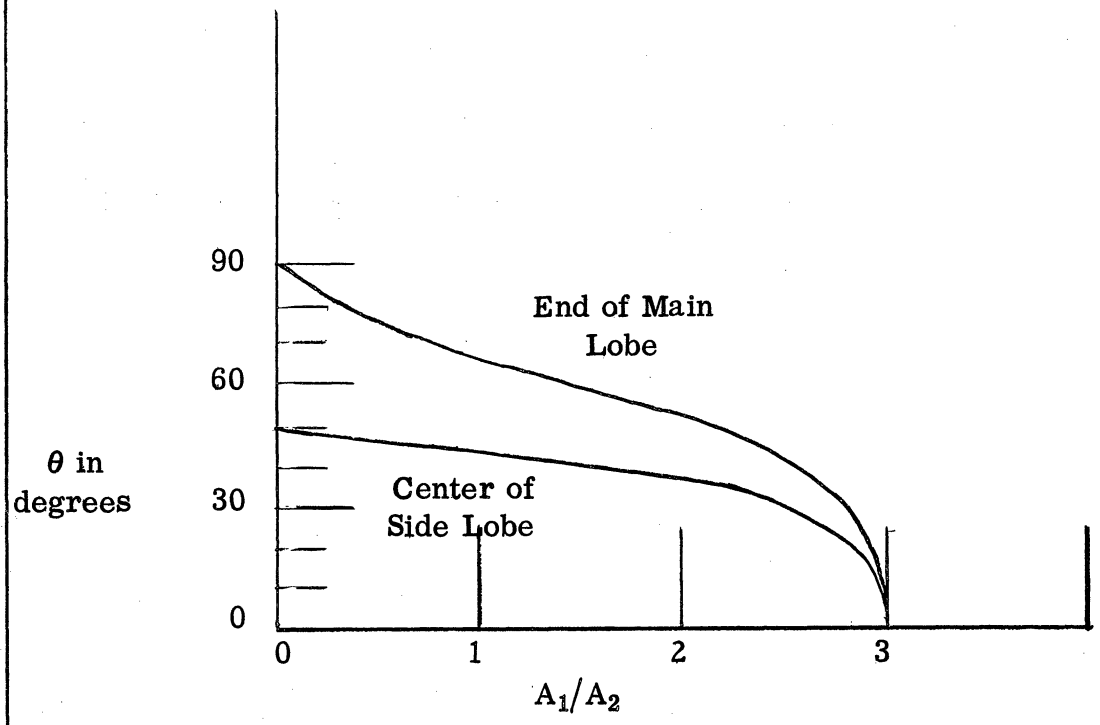
θ in degrees
90
60
30
0
End of Main Lobe
Center of Side Lobe
0
1
2
3
A1/A2

FIG. 3-4

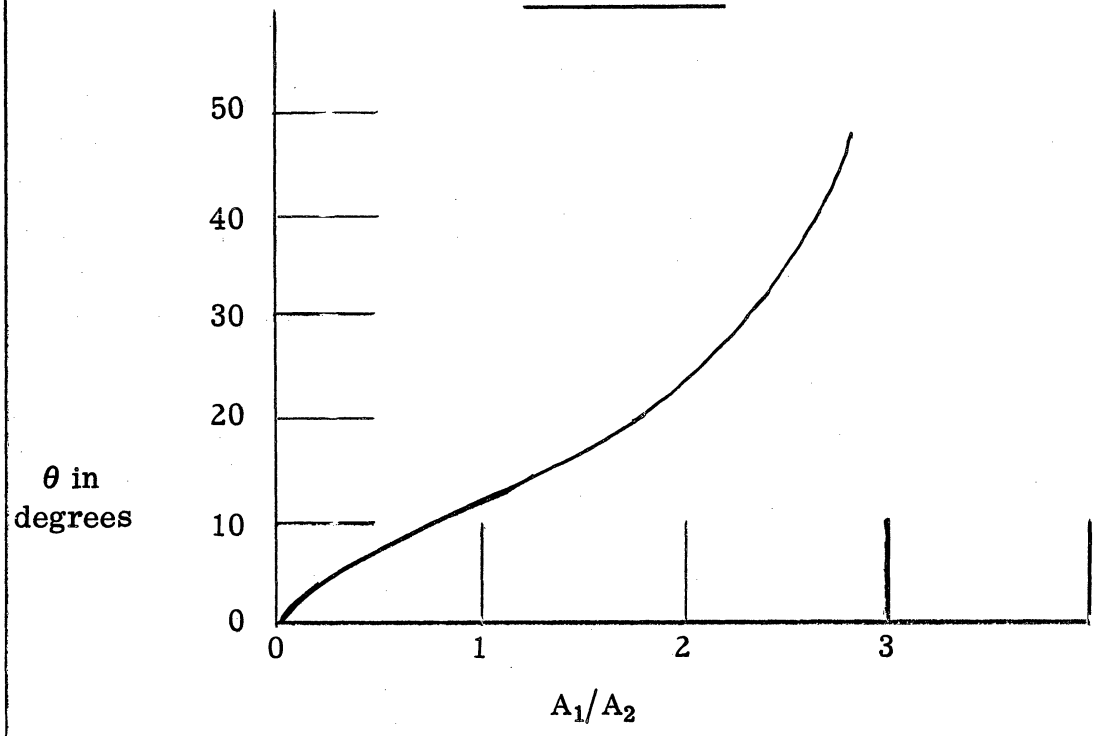
θ in degrees
50
40
30
20
10
0
0
1
2
3
A1/A2

If we take the main lobe to be constrained to $60^\circ \leq \theta \leq 120^\circ$, then (3.18) and (3.17) show that the side lobes will be about 17 DB down from the main lobe. The relationship between the currents is $A_1 = \frac{3}{2} A_2$.

In our method if we were to take the θ_i to be symmetrically placed about $\theta = 90^\circ$, we would obtain symmetric current distributions automatically. We will avoid this by taking the initial values of θ_i to be

$$\begin{aligned} \theta_1 &= 0^\circ \\ \theta_2 &= 60^\circ \\ \theta_3 &= 120^\circ \\ \theta_4 &= 120^\circ + \epsilon \ , \end{aligned} \tag{3.19}$$

where by $120^\circ + \epsilon$ we mean to take the limit as $\epsilon \to 0$. Using (3.13) and (3.19) we find

$$\sum G_n B_n = \sum A_n F_{on} = A_{-2} + A_{-1} + A_1 + A_2 \tag{3.20}$$

$$B_1 = \sum A_n F_{1n} = -i A_{-2} + i A_{-1} - i A_1 + i A_2$$

$$B_2 = \sum A_n F_{2n} = \frac{-1+i}{\sqrt{2}} A_{-2} + \frac{1-i}{\sqrt{2}} A_{-1} + \frac{1-i}{\sqrt{2}} A_1 + \frac{-1-i}{\sqrt{2}} A_2$$

$$B_3 = \sum A_n F_{3n} = \frac{-1-i}{\sqrt{2}} A_{-2} + \frac{1-i}{\sqrt{2}} A_{-1} + \frac{1+i}{\sqrt{2}} A_1 + \frac{-1+i}{\sqrt{2}} A_2$$

$$B_4 = \sum A_n F_{4n} \approx \frac{-1-i}{\sqrt{2}} A_{-2} + \frac{1-i}{\sqrt{2}} A_{-1} + \frac{1+i}{\sqrt{2}} A_1 + \frac{-1+i}{\sqrt{2}} A_2$$

$$+ \epsilon \left[\frac{3\pi\sqrt{3}}{4\sqrt{2}} (-1+i) A_{-2} + \frac{\pi\sqrt{3}}{4\sqrt{2}} (-1-i) A_{-1} + \frac{\pi\sqrt{3}}{4\sqrt{2}} (-1+i) A_1 + \frac{3\pi\sqrt{3}}{4\sqrt{2}} (-1 \right.$$

Rather than solve for the A's in terms of the B's for the special values given by (3.19) we will find it more profitable to carry through the work for general θ_i.

In the general case

$$\begin{aligned}
&\exp\left[\frac{3\pi i}{2}x_1\right]A_{-2}+\exp\left[\frac{\pi i}{2}x_1\right]A_{-1}+\exp\left[-\frac{\pi i}{2}x_1\right]A_1+\exp\left[-\frac{3\pi i}{2}x_1\right]A_2=B_1\\
&\exp\left[\frac{3\pi i}{2}x_2\right]A_{-2}+\exp\left[\frac{\pi i}{2}x_2\right]A_{-1}+\exp\left[-\frac{\pi i}{2}x_2\right]A_1+\exp\left[-\frac{3\pi i}{2}x_2\right]A_2=B_2\\
&\exp\left[\frac{3\pi i}{2}x_3\right]A_{-2}+\exp\left[\frac{\pi i}{2}x_3\right]A_{-1}+\exp\left[-\frac{\pi i}{2}x_3\right]A_1+\exp\left[-\frac{3\pi i}{2}x_3\right]A_2=B_3\\
&\exp\left[\frac{3\pi i}{2}x_4\right]A_{-2}+\exp\left[\frac{\pi i}{2}x_4\right]A_{-1}+\exp\left[-\frac{\pi i}{2}x_4\right]A_1+\exp\left[-\frac{3\pi i}{2}x_4\right]A_2=B_4\ ,
\end{aligned} \tag{3.21}$$

where $x_i = \cos\theta_i$.

The solution to the set of Equations (3.21) is

$$\begin{aligned}
A_{-2} &= \frac{\exp\left[\frac{3\pi i}{2}x_1\right]B_1}{(e^{\pi i x_1}-e^{\pi i x_2})(e^{\pi i x_1}-e^{\pi i x_3})(e^{\pi i x_1}-e^{\pi i x_4})}+\cdots\\
A_{-1} &= \frac{\exp\left[\frac{3\pi i}{2}x_1\right](e^{\pi i x_2}+e^{\pi i x_3}+e^{\pi i x_4})B_1}{(e^{\pi i x_1}-e^{\pi i x_2})(e^{\pi i x_1}-e^{\pi i x_3})(e^{\pi i x_1}-e^{\pi i x_4})}+\cdots\\
A_1 &= \frac{\exp\left[\frac{3\pi i}{2}x_1\right](e^{\pi i(x_2+x_3)}+e^{\pi i(x_2+x_4)}+e^{\pi i(x_3+x_4)})B_1}{(e^{\pi i x_1}-e^{\pi i x_2})(e^{\pi i x_1}-e^{\pi i x_3})(e^{\pi i x_1}-e^{\pi i x_4})}+\cdots\\
A_2 &= \frac{-\exp\left[\frac{3\pi i}{2}x_1\right]e^{\pi i x(x_2+x_3+x_4)}B_1}{(e^{\pi i x_1}-e^{\pi i x_2})(e^{\pi i x_1}-e^{\pi i x_3})(e^{\pi i x_1}-e^{\pi i x_4})}+\cdots\ ,
\end{aligned} \tag{3.22}$$

where the dots indicate similar terms involving B_1, B_2, B_3, B_4 .

From (3.20) and (3.22) we find

$$G_1 = \frac{(1 - e^{\pi i x_2})(1 - e^{\pi i x_3})(1 - e^{\pi i x_4}) \exp\left[\frac{3\pi i}{2} x_1\right]}{(e^{\pi i x_1} - e^{\pi i x_2})(e^{\pi i x_1} - e^{\pi i x_3})(e^{\pi i x_1} - e^{\pi i x_4})}, \tag{3.23}$$

with similar expressions for G_2, G_3, G_4. Since we take $B_i = \frac{|G_i|}{G_i}$ we have

$$\begin{aligned}
\sum G_n B_n &= \sum |G_n| \\
&= \left| \frac{\sin \frac{\pi x_2}{2} \sin \frac{\pi x_3}{2} \sin \frac{\pi x_4}{2}}{\sin \frac{\pi(x_1 - x_2)}{2} \sin \frac{\pi(x_3 - x_1)}{2} \sin \frac{\pi(x_4 - x_1)}{2}} \right| \\
&+ \left| \frac{\sin \frac{\pi x_1}{2} \sin \frac{\pi x_3}{2} \sin \frac{\pi x_4}{2}}{\sin \frac{\pi(x_1 - x_2)}{2} \sin \frac{\pi(x_3 - x_2)}{2} \sin \frac{\pi(x_4 - x_2)}{2}} \right| \\
&+ \left| \frac{\sin \frac{\pi x_1}{2} \sin \frac{\pi x_2}{2} \sin \frac{\pi x_4}{2}}{\sin \frac{\pi(x_1 - x_3)}{2} \sin \frac{\pi(x_2 - x_3)}{2} \sin \frac{\pi(x_4 - x_3)}{2}} \right| \\
&+ \left| \frac{\sin \frac{\pi x_1}{2} \sin \frac{\pi x_2}{2} \sin \frac{\pi x_3}{2}}{\sin \frac{\pi(x_1 - x_4)}{2} \sin \frac{\pi(x_2 - x_4)}{2} \sin \frac{\pi(x_3 - x_4)}{2}} \right| .
\end{aligned} \tag{3.24}$$

In order to restrict the beam in the desired way, we must keep $x_2 = 1/2$, $x_3 = -1/2$.

Thus (3.24) becomes

$$\sum |G_n| = \left| \frac{\sin \frac{\pi x_4}{2}}{\cos \pi x_1 \sin \frac{\pi(x_4 - x_1)}{2}} \right| + \left| \frac{\sin \frac{\pi x_1}{2} \sin \frac{\pi x_4}{2}}{\sqrt{2} \sin\left(\frac{\pi x_1}{2} - \frac{\pi}{4}\right) \sin\left(\frac{\pi x_4}{2} - \frac{\pi}{4}\right)} \right| + \left| \frac{\sin \frac{\pi x_1}{2} \sin \frac{\pi x_4}{2}}{\sqrt{2} \sin\left(\frac{\pi x_1}{2} + \frac{\pi}{4}\right) \sin\left(\frac{\pi x_4}{2} + \frac{\pi}{4}\right)} \right| + \left| \frac{\sin \frac{\pi x_1}{2}}{\cos \pi x_4 \sin \frac{\pi(x_1 - x_4)}{2}} \right| . \tag{3.25}$$

What we now seek is a minimum of (3.25) with respect to x_1 and x_4 ($|x_1|, |x_4| > 1/2$). It is clear that it will be simpler to vary x_4, then x_1, then x_4 again, etc. rather than computing the gradient of (3.25) and varying x_1 and x_4 along the gradient. Thus, instead of (3.19) we have initially

$$\begin{aligned} x_1 &= 1 \\ x_2 &= 1/2 \\ x_3 &= -1/2 \end{aligned} \tag{3.26}$$

where x_4 is to be chosen to minimize (3.25), which becomes due to (3.26)

$$\sum |G_n| = \left| \tan \frac{\pi x_4}{2} \right| + \frac{\sqrt{2}}{\left| 1 - \cot \frac{\pi x_4}{2} \right|} + \frac{\sqrt{2}}{\left| 1 + \cot \frac{\pi x_4}{2} \right|} + \frac{1}{\left| \cos \frac{\pi x_4}{2} \cos \pi x_4 \right|} . \tag{3.27}$$

It is clear that (3.27) is unchanged if we replace x_4 by $-x_4$. Thus we will take $-1 \leq x_4 \leq -1/2$. With this restriction we are able to remove the absolute value signs in (3.27) obtaining

$$\sum |G_n| = -\tan \frac{\pi x_4}{2} + \frac{\sqrt{2}}{1 - \cot \frac{\pi x_4}{2}} + \frac{\sqrt{2}}{1 + \cot \frac{\pi x_4}{2}} - \frac{1}{\cos \frac{\pi x_4}{2} \cos \pi x_4} \tag{3.28}$$

$$= \sqrt{\frac{1 - \cos \pi x_4}{1 + \cos \pi x_4}} + \sqrt{2} \frac{\cos \pi x_4 - 1}{\cos \pi x_4} - \frac{\sqrt{2}}{\cos \pi x_4 \sqrt{1 + \cos \pi x_4}} .$$

Figure 3-5 shows the variation of $\sum|G_n|$ with x_4 for $x_1 = 1$. The minimum occurs approximately at $x_4 = -0.73$. The value of $\sum|G_n|$ at the minimum is approximately 9.43 (19.5 DB). Since the predicted side lobe level is appreciably below that actually obtainable, the true side lobe level is probably a few DB higher than the ultimate limit. Thus we

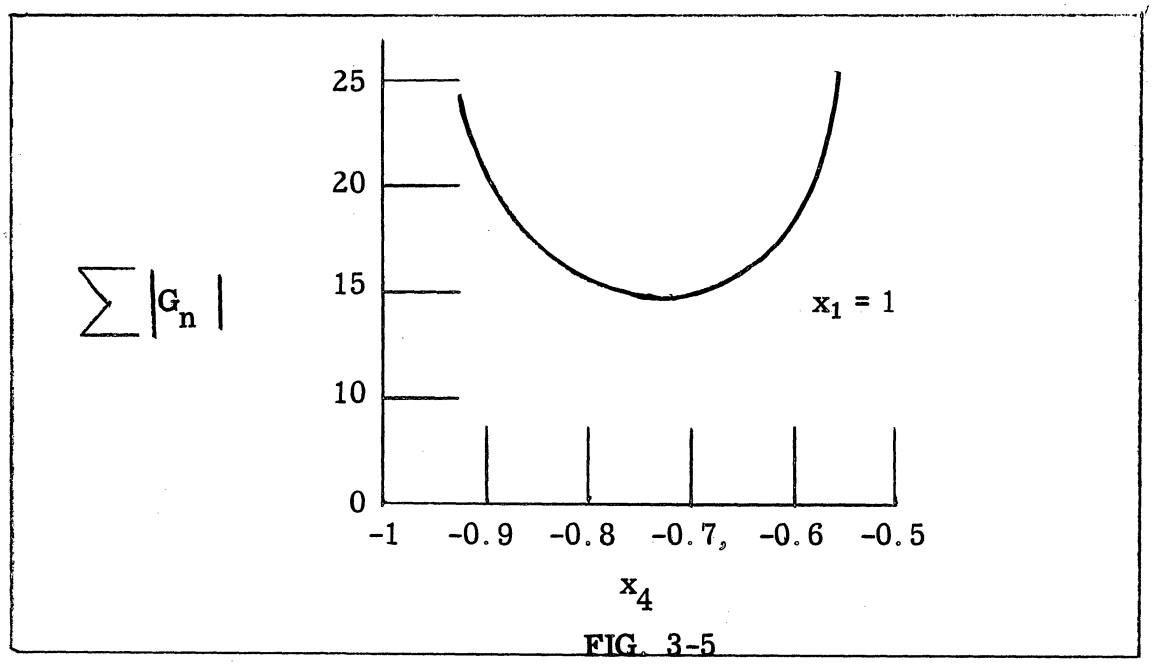

FIG. 3-5

will postpone the calculation of the corresponding current distribution until we have gone through at least one more step. For this step we take

$$x_2 = 1/2$$
$$x_3 = -1/2 \qquad (3.29)$$
$$x_4 = -0.73 \ ,$$

and choose x_1, so as to minimize (3.25).

Using (3.25) in (3.29) we obtain

$$\sum |G_n| = \left| \frac{\sin 65.7^\circ}{\cos \pi x_1 \sin (65.7^\circ + \frac{\pi x_1}{2})} \right| + \left| \frac{\sin \frac{\pi x_1}{2} \sin 65.7^\circ}{\sqrt{2} \sin (\frac{\pi x_1}{2} - 45^\circ) \sin 69.3^\circ} \right|$$

$$+ \left| \frac{\sin \frac{\pi x_1}{2} \sin 65.7^\circ}{\sqrt{2} \sin (\frac{\pi x_1}{2} + 45^\circ) \sin 20.7^\circ} \right| + \left| \frac{\sin \frac{\pi x_1}{2}}{\cos 48.6^\circ \sin (\frac{\pi x_1}{2} + 65.7^\circ)} \right| \qquad (3.30)$$

$$\sim \frac{.9114}{\left| \cos \pi x_1 \sin (\frac{\pi x_1}{2} + 65.7^\circ) \right|} + .689 \left| \frac{\sin \frac{\pi x_1}{2}}{\sin (\frac{\pi x_1}{2} - 45^\circ)} \right|$$

$$+ 1.824 \left| \frac{\sin \frac{\pi x_1}{2}}{\sin (\frac{\pi x_1}{2} + 45^\circ)} \right| + 1.512 \left| \frac{\sin \frac{\pi x_1}{2}}{\sin (\frac{\pi x_1}{2} + 65.7^\circ)} \right| .$$

Figure 3-6 shows the variation of $\sum |G_n|$ with x_1 in the allowable region $|x_1| > 1/2$ for $x_4 = -0.73$. The minimum occurs approximately at $x_1 = .775$. The

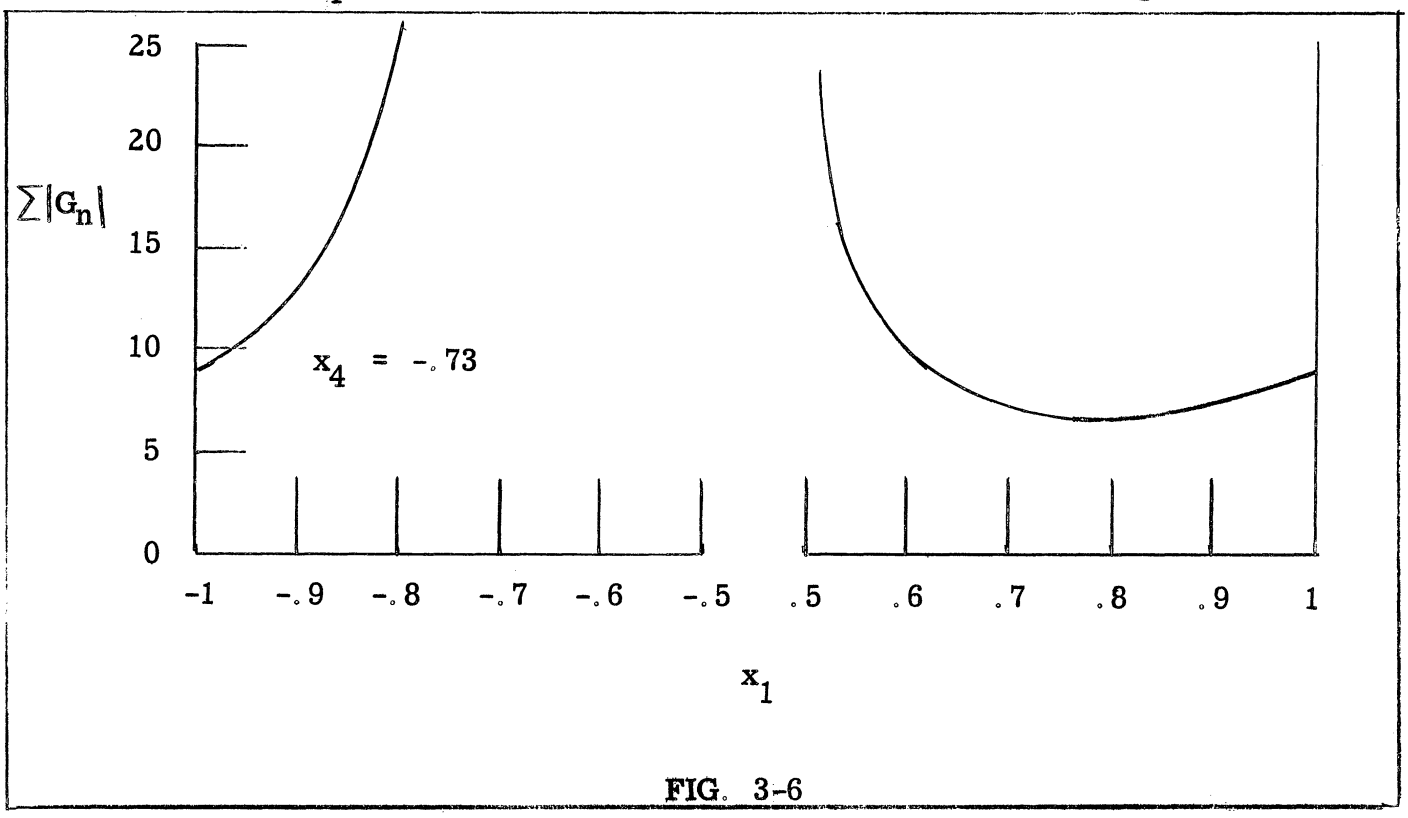

FIG. 3-6

value of $\sum|G_n|$ at the minimum is approximately 7.17 (17.1 DB). Since the predicted side lobe level is now only slightly below that actually obtainable, we can expect the true side lobe level to be only slightly above that actually obtainable. Thus we will compute the actual pattern with

$$\begin{aligned} x_1 &= .775 \\ x_2 &= .5 \\ x_3 &= -.5 \\ x_4 &= -.73 \end{aligned} \tag{3.31}$$

We have

$$\begin{aligned} G_1 &= -1.707 \\ G_2 &= 1.553 \\ G_3 &= 1.896 \\ G_4 &= -2.037 \end{aligned} \tag{3.32}$$

Since $B_i = \dfrac{|G_i|}{G_i}$ we have $B_1 = B_4 = -1$, $B_2 = B_3 = 1$. For simplicity in computing the A's it is convenient to rewrite (3.22) in the form

$$A_{-2} = \frac{\exp\left[\frac{\pi i}{2}(1-x_2-x_3-x_4)\right] B_1}{8 \sin\frac{\pi(x_1-x_2)}{2} \sin\frac{\pi(x_1-x_3)}{2} \sin\frac{\pi(x_1-x_4)}{2}} + \ldots = A_2^*$$

$$A_{-1} = \frac{\exp\left[\frac{\pi i}{2}(-1+x_2-x_3-x_4)\right] + \exp\left[\frac{\pi i}{2}(-1-x_2+x_3-x_4)\right] + \exp\left[\frac{\pi i}{2}(-1-x_2-x_3+x_4)\right]}{8 \sin\frac{\pi(x_1-x_2)}{2} \sin\frac{\pi(x_1-x_3)}{2} \sin\frac{\pi(x_1-x_4)}{2}} B_1 + \ldots = A_1^*$$

$$A_1 = \frac{\exp\left[\frac{\pi i}{2}(1-x_2+x_3+x_4)\right] + \exp\left[\frac{\pi i}{2}(1+x_2-x_3+x_4)\right] + \exp\left[\frac{\pi i}{2}(1+x_2+x_3-x_4)\right]}{8 \sin\frac{\pi(x_1-x_2)}{2} \sin\frac{\pi(x_1-x_3)}{2} \sin\frac{\pi(x_1-x_4)}{2}} B_1 + \ldots$$

$$A_2 = \frac{\exp\left[\frac{\pi i}{2}(-1+x_2+x_3+x_4)\right] B_1}{8 \sin\frac{\pi(x_1-x_2)}{2} \sin\frac{\pi(x_1-x_3)}{2} \sin\frac{\pi(x_1-x_4)}{2}} + \ldots \quad , \tag{3.33}$$

where the fact that $A_{-j} = A_j^*$ follows from the fact that the B's are all real.

The general expression for F is

$$F = A_{-2} \exp\left[\frac{3\pi i}{2} x\right] + A_{-1} \exp\left[\frac{\pi i}{2} x\right] + A_1 \exp\left[-\frac{\pi i}{2} x\right] + A_2 \exp\left[-\frac{3\pi i}{2} x\right]. \tag{3.34}$$

Using the values of the A's given by (3.33) we obtain

$$F = \frac{\sin\frac{\pi(x-x_2)}{2} \sin\frac{\pi(x-x_3)}{2} \sin\frac{\pi(x-x_4)}{2}}{\sin\frac{\pi(x_1-x_2)}{2} \sin\frac{\pi(x_1-x_3)}{2} \sin\frac{\pi(x_1-x_4)}{2}} B_1 + \ldots \tag{3.35}$$

Figure 3-7 shows the pattern finally obtained after two steps. Figure 3-8 shows the optimum (Dolph-Chebychev) pattern. Figure 3-9 shows the pattern obtained by the above method after only the first step. Upon comparing the patterns of Figures 3-7 and 3-8 we see that the pattern obtained after two steps cannot be differentiated, graphically, from the optimum pattern.

In closing, a word is in order about the use of the above method when the fields due to the individual elements are only approximately known. In this case we go ahead with the design procedure as outlined above using the approximate patterns of the elements. We test the result experimentally. In general the side-lobes will not actually be as small as indicated by the design theory. We then use the array and its experimentally determined pattern as one element in an array, with the other elements corresponding to elements in the original array. We then apply the design procedure to these elements. Since we are now only making a small correction to the first design we can expect to get an array whose theoretically predicted pattern agrees well with the experimentally determined one. If necessary, the procedure may be repeated.

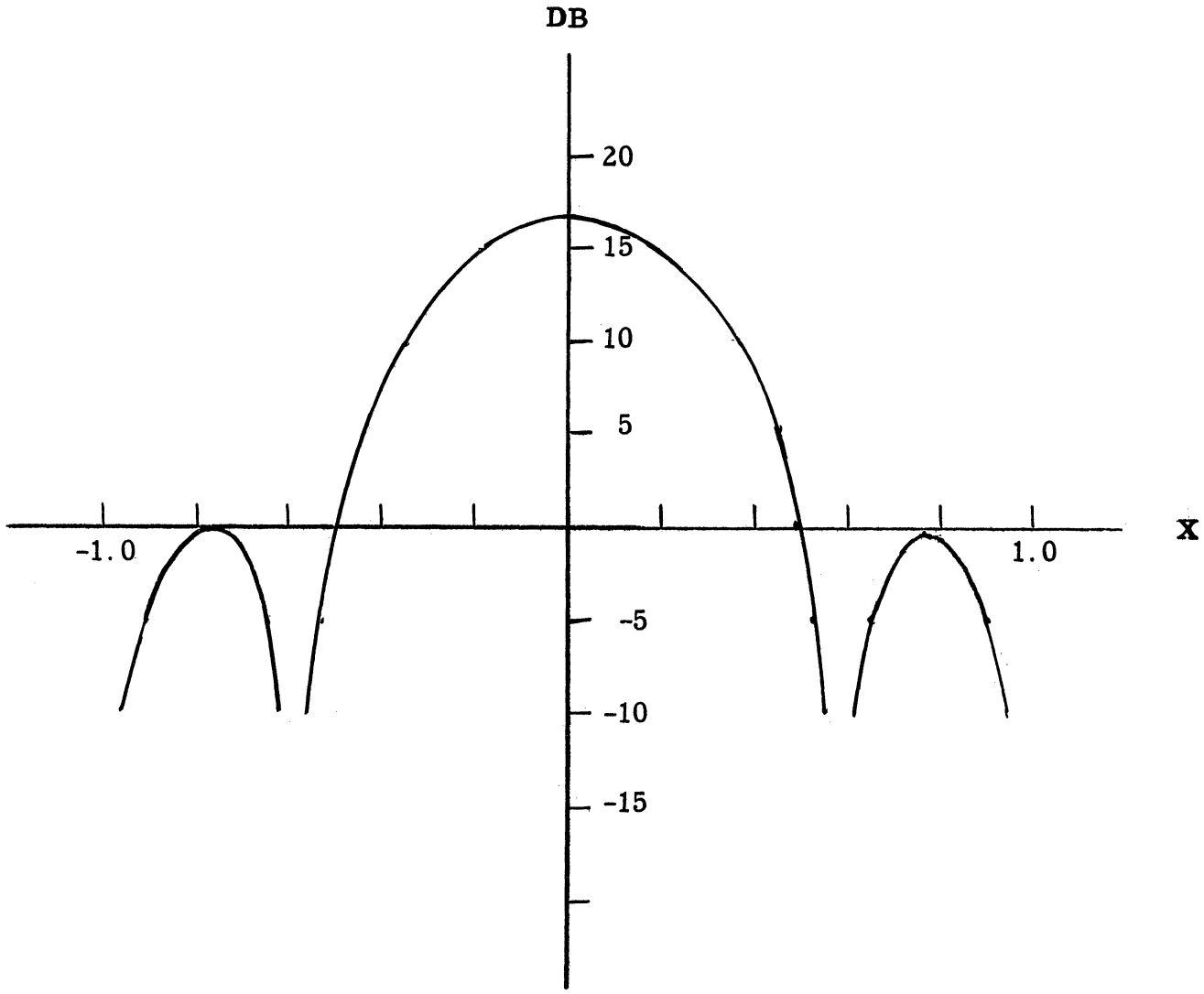

FIG. 3-7: ILLUSTRATIVE EXAMPLE - PATTERN OBTAINED UPON THE COMPLETION OF TWO STEPS

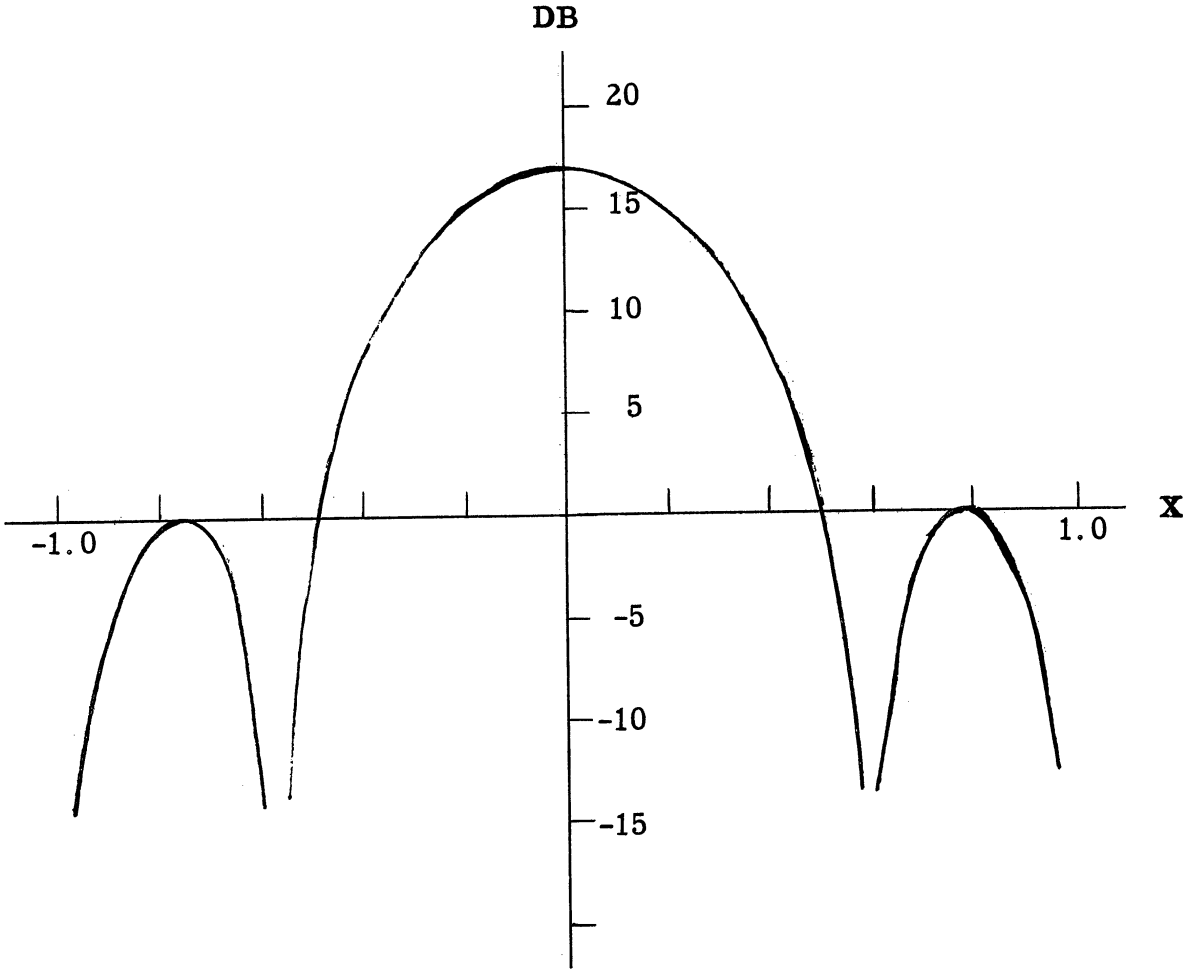

FIG. 3-8: ILLUSTRATIVE EXAMPLE -

OPTIMUM (DOLPH-CHEBYCHEV) PATTERN

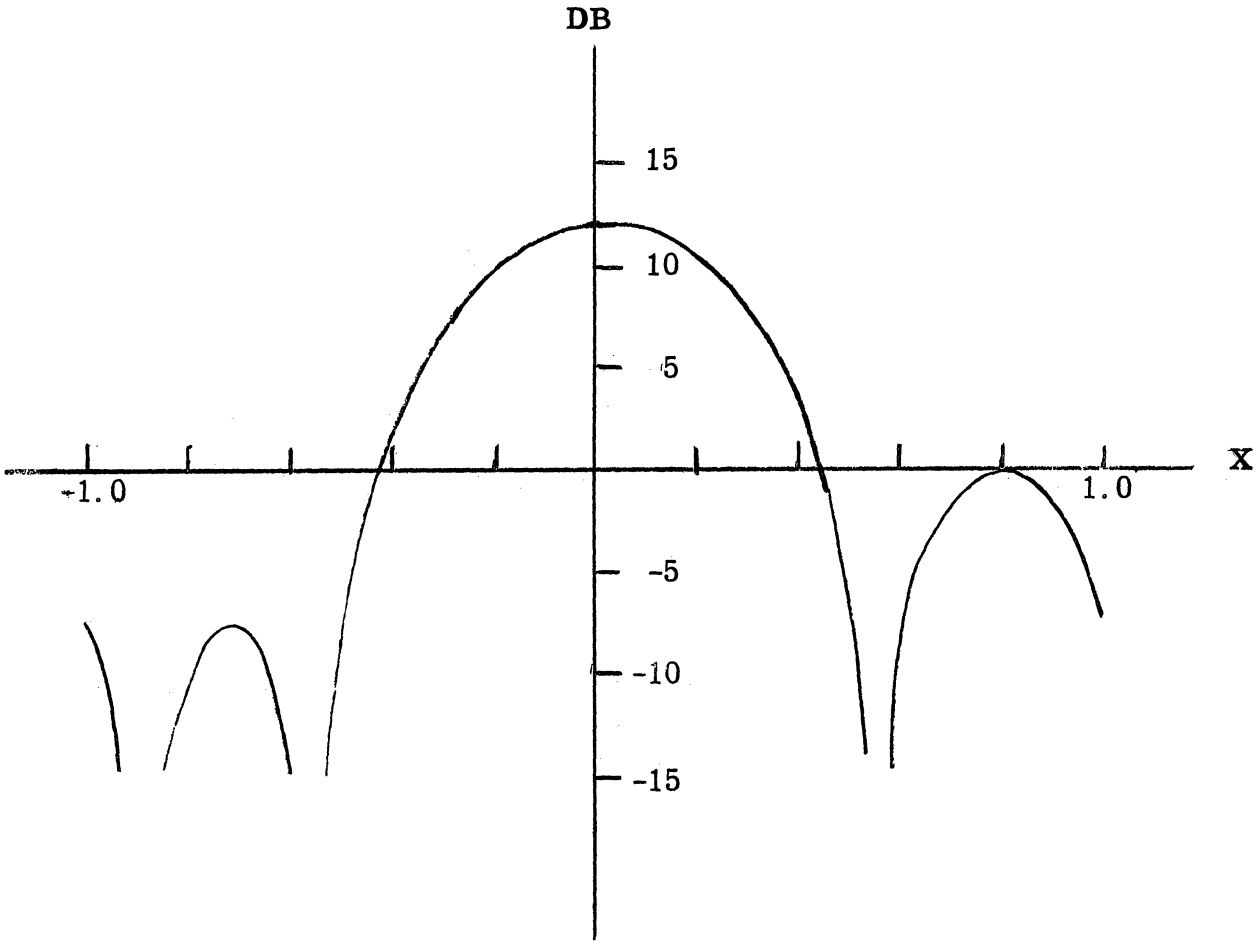

FIG. 3-9: ILLUSTRATIVE EXAMPLE - PATTERN OBTAINED UPON THE COMPLETION OF THE FIRST STEP

IV

A THEORY OF MAXIMUM GAIN ANTENNA ARRAYS

To give a broad base to the method of design of surface antennas we now shall consider a general approach.

We let $\vec{m}(s)$ be a magnetic dipole distribution on a perfectly conducting surface S. The radiation pattern arising from such a configuration is given by

$$R(\hat{k}) = \int_S \vec{H}(\hat{k}, s) \cdot \vec{m}(s)\, dS, \tag{4.1}$$

where $\vec{H}$ can be taken as the field induced on S at s by an incident plane wave of direction $\hat{k}$ and unit amplitude. In briefer notation we put

$$R = H \circ m . \tag{4.2}$$

The properties of this transformation will be our present concern.

The antenna synthesis problem is that of determining the inverse, i.e. given a radiation pattern R we need to find

$$m = H^{-1} \circ R , \tag{4.3}$$

This is very difficult for most surfaces S so we seek to characterize some general properties of the transformation. What we have accomplished is no more than some conjectures based on analogy with the better understood case of a line source.

The principle properties we need to know are (1) how to maximize the gain and (2) how to control the side-lobe levels. We consider these for a line source. In this relatively simple example the radiation pattern is given by

$$R = \int_{-a}^{a} e^{i\xi z} f(\xi)\, d\xi \tag{4.4}$$

where the length of the source is $2a$, f is the excitation and $z = \frac{2\pi}{\lambda} \cos\theta$. If we take $a >> \lambda$ we see that (4.4) approximates a Fourier transform. Hence the gain is maximized for f = constant and the side lobes are reduced for f approximating a Gaussian.

By use of our knowledge of Fourier transforms we can characterize the transformation from the excitation f to the radiation pattern R in such a way as to enable us to modify the pattern without any detailed treatment of the inverse transformation. Ultimately we wish to find such a technique for our general surface S.

Up to now we have considered only the first problem; that of obtaining the maximum gain configuration. Our progress is yet only a conjecture. By analogy with the long line source we presume that for large surfaces, i.e. the characteristic dimensions much larger than a wave length, the maximum gain configuration results from an excitation which is just the complex conjugate of the field induced on the surface by a plane wave incident from the main beam direction. As an illustration we give the case of a circumferential slot on a large circular cylinder confining our attention to the principal plane. By reciprocity the radiation pattern at an angle ϕ due to a source at ϕ' on the surface is given by the field induced at ϕ' by a plane wave incident in the direction ϕ. Let this be denoted by $k(\phi, \phi')$; then, for an excitation $f(\phi)$ we have the radiation pattern

$$R(\phi) = \int k(\phi, \phi')\, f(\phi')\, d\phi' \tag{4.5}$$

or

$$R(\phi) = K \circ f(\phi)$$

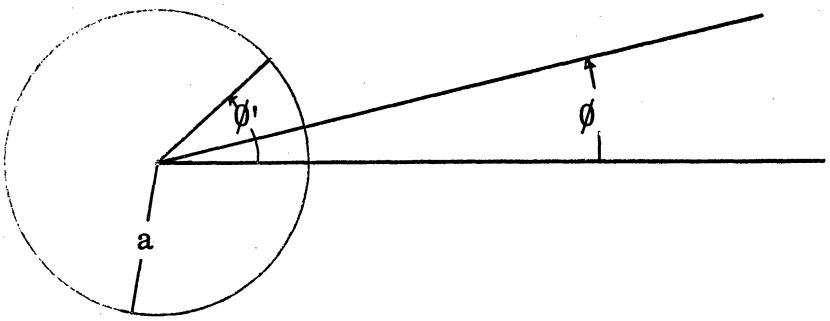

The problem is to determine the excitation f such that the side-lobe levels meet the requirements of a particular application, i.e. if the main beam is in the direction $\phi = 0$ and the side lobes are required to be down A db, we have for the set $\{\phi_n\}$, which are solutions of

$$\frac{\partial R(\phi)}{\partial \phi} = 0, \quad \phi_n \neq 0,$$

that

$$\min_n 10 \log \left[\frac{R(0)}{R(\phi_n)} \right]^2 \geq A . \tag{4.6}$$

In our example we can express (4.6) in terms of the Fourier coefficients of the functions R, k, f,

$$R_n = k_n f_n \tag{4.7}$$

where we use the fact that

$$k(\phi, \phi') = \sum e^{in(\phi-\phi')} k_n .$$

So the inversion of the operator K results in

$$f(\phi) = \sum e^{in\phi} \frac{R_n}{k_n} , \tag{4.8}$$

a relatively simple result.

We are interested primarily in the more difficult cases in which S is not such a simple shape. We wish, however, to approach the more difficult problem in terms of the simpler one; so instead of solving (4.8) we will look for a method of choosing f which can be used in the more general cases.

In our example, if we choose the main beam to be in the direction $\phi = 0$ we know that we control the side-lobe levels by tapering the excitation, i.e. $f(\phi)$ should decrease as $|\phi|$ increases in order to decrease the side lobes as compared, say, with those resulting from a uniform excitation, f = const. A readily available tapered excitation is just the complex conjugate of the field induced by a plane wave

$$f(\phi) = \overline{k(\phi, 0)} \tag{4.9}$$

where we take the complex conjugate in order that the phase be such that the radiation pattern be maximized for this case. This gives

$$\mathbf{R}(\phi) = \mathbf{K} \circ \mathbf{K}' \circ \delta(\phi) , \tag{4.10}$$

where $\delta(\phi)$ is the Dirac delta.

This has been computed (Fig. 4-1) in the case ka = 10 where a is the radius of the cylinder and $k = 2\pi/\lambda$, λ is the wavelength. This gives a side-lobe level of approximately 18 db.

If such an excitation were to be used the origin of it suggests a novel means of producing this excitation. Since the excitation is, in fact, the complex conjugate of the field induced on the surface by a plane wave, we can then devise an analog device in which we model the antenna surface, illuminate it by a plane wave, and use the measured surface

FIG. 4-1 RADIATION PATTERN FOR A CIRCULAR CYLINDER WITH A CIRCUMFERENTIAL SLOT EXCITATION (ka = 10)

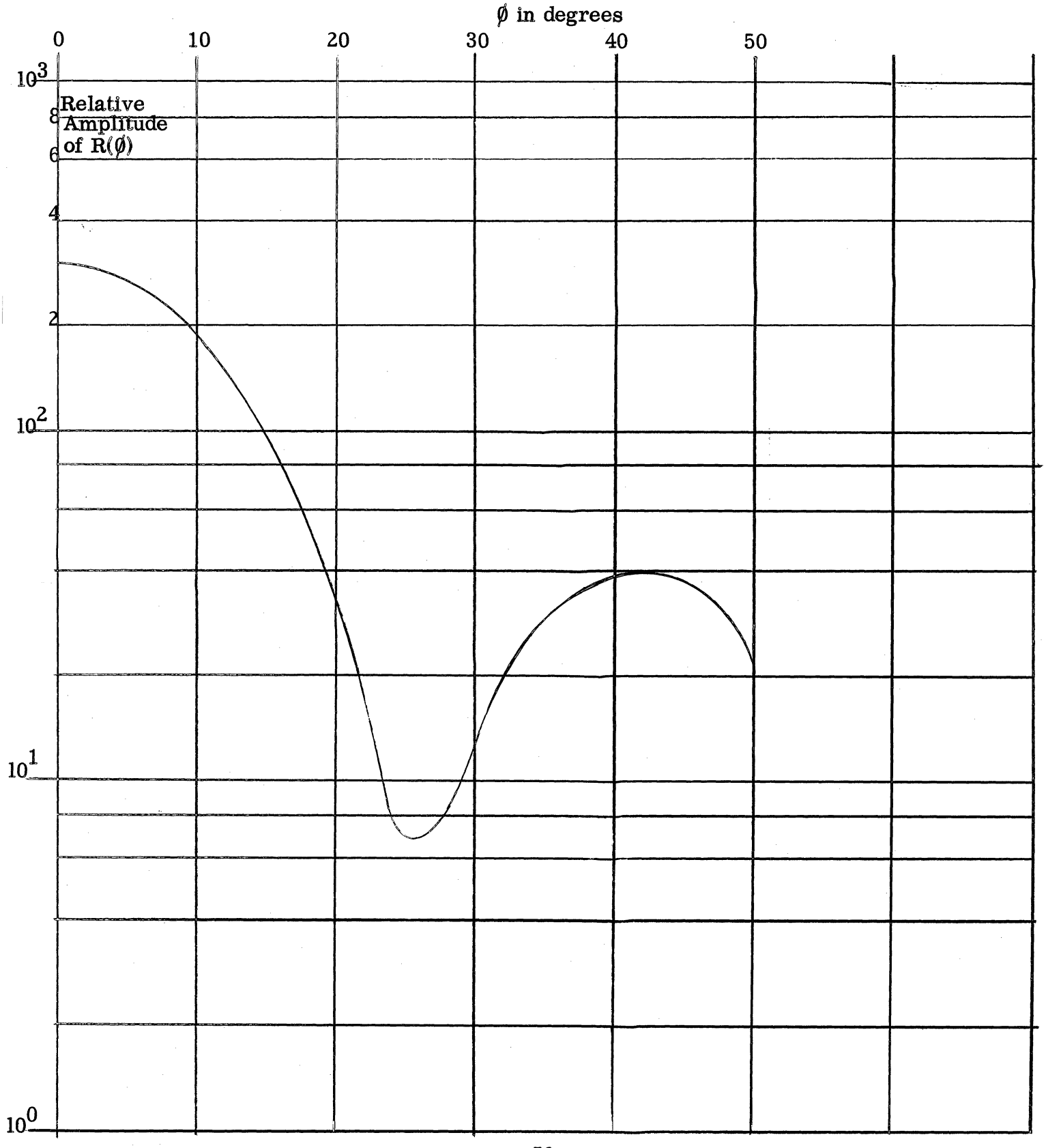

field after an appropriate phase change of 180^{o} as the input of the excitation on the actual antenna surface. Alternatively, the measurements could be made in the laboratory and recorded on tape to be used in some sort of digital computer to control the excitation.

Since the above scheme uses an approximation to a continuous distribution, we must solve two additional problems. The first is to discover the density of slot radiators necessary for a sufficiently close approximation; the second is the method of exciting these elementary radiators. It may be that the second problem is too difficult; i.e. if we need control over each of the elements the scheme may not be useful for the type of antenna we finally wish to construct. To this point little effort has been spent on this problem.

APPENDIX A

THE 65-SLOT PROBLEM - THE METHOD OF COMPUTATION AND THE RESULTS OBTAINED

A.1 The Method of Computation

In this Appendix we present the formulas employed in the 65-slot problem together with a discussion of the method of computation and the results obtained. The single slot expressions needed for such calculations have been discussed in Section II (these single slot expressions also appear as Equations (4.2.4), (4.2.5), and (4.2.11) for Geometric Optics, Fock Theory, and Physical Optics respectively in Reference 16.

In the expressions for the 65-slot calculations given in this Appendix the polarization, $\hat{p}$, will denote directions of the magnetic field with $\hat{p}_1 = \theta$ and $\hat{p}_2 = \phi$. The following parameter values are fixed throughout:

θ_B = (main beam direction) = 70^o, 50^o, 30^o, 10^o .

θ_o = 165^o, denotes cone surface

d_o = (distance from tip of cone to first slot = 16λ.

d_j = (distance from tip of cone to $j^{\underline{th}}$ slot), $j = 0, 1, 2, \ldots, 64$.

$d = d_{j+1} - d_j$ = (distance between slots) = 0.4λ.

In performing the calculations for the 65-slot problem, each of the 65 values of $\vec{H}$ determined according to the methods of Geometric Optics, Physical Optics, or Fock Theory (corresponding to $j = 0, 1, 2, \ldots, 64$) are multiplied by the corresponding phase factor, $\exp(ikd_j(\theta_B - \theta_o))$, and the resulting 65 expressions summed.

We now turn our attention to the formulas employed in the 65-slot computations; the derivations of these expressions have been discussed in Section II.

A.1.1. The Geometric Optics Formulas

In determining the magnitudes of the Geometric Optics contributions in the 65-slot problem we employed the following formulas.

For a single slot

$$\frac{\vec{H}_{GO}}{C\,\frac{e^{ikr}}{r}} = 2\, e^{-ikd_o D}\,(\cos\theta \sin\phi\ \hat{p}_1 + \cos\phi\ \hat{p}_2),$$

where d_o = distance from tip to slot,

$$D = \cos\theta \cos\theta_o + \sin\theta \sin\theta_o \cos\phi, \text{ and}$$

$$2C = ikV_o\, L/2\pi\ ,$$

with V_o = the voltage across the slot and L = the length of the slot.

In the general case of N slots with d_j = distance from tip to the $j^{\underline{th}}$ slot

$$\frac{\vec{H}_{GO}}{C\,\frac{e^{ikr}}{r}} = 2\,(\cos\theta \sin\phi\ \hat{p}_1 + \cos\phi\ \hat{p}_2) \sum_{j=1}^{N} \exp\left[ikd_j\,(-D + \cos(\theta_B - \theta_o))\right] .$$

This becomes, for 65 slots,

$$\frac{\vec{H}_{GO}}{C\,\frac{e^{ikr}}{r}} = 2\,(\cos\theta \sin\phi\ \hat{p}_1 + \cos\phi\ \hat{p}_2)\ \frac{\sin(65(0.4\pi x))}{\sin(0.4\pi x)}\ e^{-57.6\pi i x}\ ,$$

where $x = D - \cos(\theta_B - \theta_o)$.

A.1.2. The Physical Optics Formulas

In determining the magnitudes of the Physical Optics contributions in the 65-slot problem we employed for the entire set of 65 slots

$$\frac{\vec{H}}{C\,\frac{e^{ikr}}{r}} = \frac{iT}{4\pi^2}\Big\{ \Big[-f_x \sin\theta \cos\theta_o \sin\phi + f_y(-\cos\theta \sin\theta_o + \sin\theta \cos\theta_o \cos\phi) - f_z \cos\theta \cos\theta_o \sin\phi \Big] \hat{p}_1 - \Big[f_x \sin\theta_o + f_z \cos\theta_o \cos\phi \Big] \hat{p}_2 \Big\} \; *$$

where $T = \lambda \sum_{j=0}^{64} (1/d_j) \exp\left[ikd_j + ikd_j \cos(\theta_B - \theta_o)\right]$,

$$d_j = d_o + jd \;,$$

$$f_x = \sin\theta_o \cos\theta_o \left[\frac{2c^2 \sin x - 2q \sin x (q + b\cos x)}{(q + b\cos x)^2 - c^2 \sin^2 x)\, Q} + 2bA \right] \;,$$

$$f_y = \sin\theta_o \cos\theta_o \left[\frac{-2bc \sin x - 2qc \sin x \cos x}{((q + b\cos x)^2 - c^2 \sin^2 x)\, Q} + 2cA \right] \;,$$

$$f_z = \sin^2\theta_o \left[\frac{-2c^2 \sin x \cos x - 2b \sin x (q + b\cos x)}{(q + b\cos x)^2 - c^2 \sin^2 x)\, Q} + 2qA \right] \;,$$

and

$$A = Q^{-3/2} \arctan\left[Q^{1/2} \sin x / (q\cos x + b) \right] \;,$$

$$Q = q^2 - b^2 - c^2 \;,$$

$$q = \cos\theta_o (\cos\theta_o + \cos\theta) \;,$$

---

* In the one slot case the expression is the same except that the factor $iT/4\pi^2$ is replaced by the factor $\frac{i\lambda e^{ikd_o}}{4\pi^2 d_o}$ with d_o being the distance from the tip to the slot.

$$b = \sin\theta_o (\cos\phi \sin\theta_o + \sin\theta) \ ,$$

$$c = \sin\phi \sin^2\theta_o \ , \text{ and}$$

$$x = \arccos\left(\frac{\tan\theta_o}{\tan\theta}\right)$$

The values of T corresponding to the four values of θ_B studied are

$$T = 0.11193 + 0.34491\ i \quad \text{for } \theta_B = 10^o,$$

$$= 0.0273 + 0.112\ i \quad \text{for } \theta_B = 30^o,$$

$$= 0.0211 + 0.0209\ i \quad \text{for } \theta_B = 50^o, \text{ and}$$

$$= 0.0276 + 0.0265\ i \quad \text{for } \theta_B = 70^o \ .$$

The C appearing in the above expression is defined in the same manner as in the Geometric Optics expressions.

A.1.3 Fock Theory Expressions

To determine the contribution for each of the 65 slots as determined by Fock Theory we use the following expressions:

$$\frac{\vec{H}\cdot\hat{p}}{C\frac{e^{ikr}}{r}} =$$

$$\left[\sum_{n=0}^{*} e^{iA_n}\left\{c_1 g(\xi_n)\sin\left[(2n\pi+\phi-\phi_s)\sin\theta_o+\pi/2-\psi\right]\right.\right.$$

$$\left. + (ic_2/m_n) f(\xi_n)\cos\left[(2n\pi+\phi-\phi_s)\sin\theta_o+\pi/2-\psi\right]\right.$$

$$+\sum_{n=1}^{*} e^{iA_n'}\left\{c_1 g(\xi_n')\sin\left[(2n\pi-\phi-\phi_s)\sin\theta_o+\pi/2-\psi\right]\right.$$

$$\left.\left. + (ic_2/m_n') f(\xi_n')\cos\left[(2n\pi-\phi-\phi_s)\sin\theta_o+\pi/2-\psi\right]\right]$$

where $\cos \phi_s = (\tan \theta_o)/(\tan \theta)$; $\cos \psi = -\cos \theta/\cos \theta_o$; $\phi > \phi_s$; $k = 2\pi/\lambda$,

$$A_n(a_n, \phi) = -ka_n (\sin \theta_o \sin \theta \cos \phi_s + \cos \theta_o \cos \theta) + \frac{kd_j \sin\left[(2n\pi + \phi - \phi_s) \sin \theta_o\right]}{\sin \psi} ,$$

$$A_n' = A_n (a_n', -\phi) ,$$

$$a_n (\phi) = \frac{d_j \cos\left[(2n\pi + \phi - \phi_s) \sin \theta_o + \pi/2 - \psi\right]}{\sin \psi}$$

$$a_n' = a_n (-\phi) ,$$

d_j = distance from tip to $j^{\underline{th}}$ slot,

* = sums cut off when argument of the cosine reaches $\pi/2$,

$$m_n (a_n) = \left\{ \frac{kd_j^3}{2a_n^2} \frac{|\tan \theta_o|}{\sin^2 \psi} \right\}^{1/3} ,$$

$$m_n' = m_n (a_n') ,$$

$$\xi_n (a_n, \phi) = \left\{ \frac{ka_n \sin \psi}{2 \tan^2 \theta_o} \right\}^{1/3} (2n\pi + \phi - \phi_s) \sin \theta_o ,$$

$$\xi_n' = \xi_n (a_n', -\phi) , \text{ and}$$

$2C = ikV_oL/2\pi$ where V_o = the voltage across the slot and L is the length of the slot.

For $\hat{p} = \hat{p}_2$, $c_1 = -\sin \theta_o/\sin \theta$,

$c_2 = \cos \theta_o \sin \phi_s$, and

for $\hat{p} = \hat{p}_1$, $c_1 = -\cos \theta_o \sin \phi_s$,

$c_2 = -\sin \theta_o/\sin \theta$.

The expressions f( ) and g( ) are the Fock functions which are tabulated (Ref. 17).

In the conical cut computations, described more fully in A.3, $\hat{p}$ was taken in 5^o intervals from $\phi = \phi_s$ to $\phi = 175^o$ and the corresponding θ value was determined from the following

$$\cos\theta = \frac{\cos(\theta_o - \theta_B)\cos\theta_o + \sin\theta_o \cos\phi \sqrt{\cos^2\theta_o + \sin^2\theta_o \cos^2\phi - \cos^2(\theta_o - \theta_B)}}{\cos^2\theta_o + \sin^2\theta_o \cos^2\phi}$$

In the limiting case of $\phi = \phi_s$ we have (on the conical cut)

$$\cos\phi_s = \frac{\sin\theta_o \cos(\theta_o - \theta_B)}{\sqrt{1 - \cos^2\theta_o \cos^2(\theta_o - \theta_B)}} .$$

Upon multiplying each of the single slot expressions by the corresponding phase factor $\exp(ikdj(\theta_B - \theta_o))$ and summing, we obtain an expression of the form

$$\sum_{j=0}^{N} F(j)\, e^{i\alpha j} .$$

Approximating the function $F(j)$ by $F(0)\left(\frac{F(N)}{F(0)}\right)^{j/N}$ we obtain

$$\sum_{j=0}^{N} F(j)\, e^{i\alpha j} \approx F(0) \left\{ \frac{1 - e^{i\alpha(N+1)} \left[F(N)/F(0)\right]^{\frac{N+1}{N}}}{1 - e^{i\alpha} \left[F(N)/F(0)\right]^{\frac{1}{N}}} \right\} .$$

This approximate summation method was employed for all four cases (i.e. for $\theta_B = 10^o, 30^o, 50^o$, and 70^o); the actual sum was obtained only for the $\theta_B = 70^o$ case. A comparison of the sums obtained in the $\theta_B = 70^o$ case indicated a maximum difference of about 20 per cent between the actual sum and the result obtained using the approximate summation method described above. The nature of this approximate summation process is such as to lead one to expect the greatest accuracy in the middle of the interval between the shadow boundary and $\phi = 180^o$.

A.2 Beam Direction

The relative maximum in θ for a given ϕ and main beam direction θ_B is given, in the illuminated region, by the cone

$$\sin\theta_B \sin\theta \cos\phi + \cos\theta_B \cos\theta = \cos(\theta_o - \theta_B)$$

about the slot array as axis, while in the shadow region, the locus of the relative maximum departs from the conical surface and is given parametrically by

$$\theta_B + \alpha = \psi - (\phi - \phi_S)\sin\alpha \ ,$$

$$\cos\psi = \frac{\cos\theta}{\cos\alpha} \ ,$$

$$\cos\phi_S = -\frac{\tan\alpha}{\tan\theta} \ , \text{ and}$$

$$\alpha = \pi - \theta_o \ .$$

Plots of the beam direction for $\theta_B = 10^o, 30^o, 50^o, 70^o$ are included here in Figure A.2-1, showing θ as a function of $|\phi|$. Although the locus of the relative maximum in θ is continued until it reaches the cone surface, $\theta = 165^o$, the field is dominated by that arising at the other shadow boundary when $\phi > 180^o$. The relative maximum in θ coincides with the conical cut out to about $\phi \approx 135^o$; this is also shown in Figure A.2-1.

FIG. A.2-1 THE RELATIVE MAXIMUM IN θ FOR A GIVEN ϕ AND MAIN BEAM DIRECTION θ_B

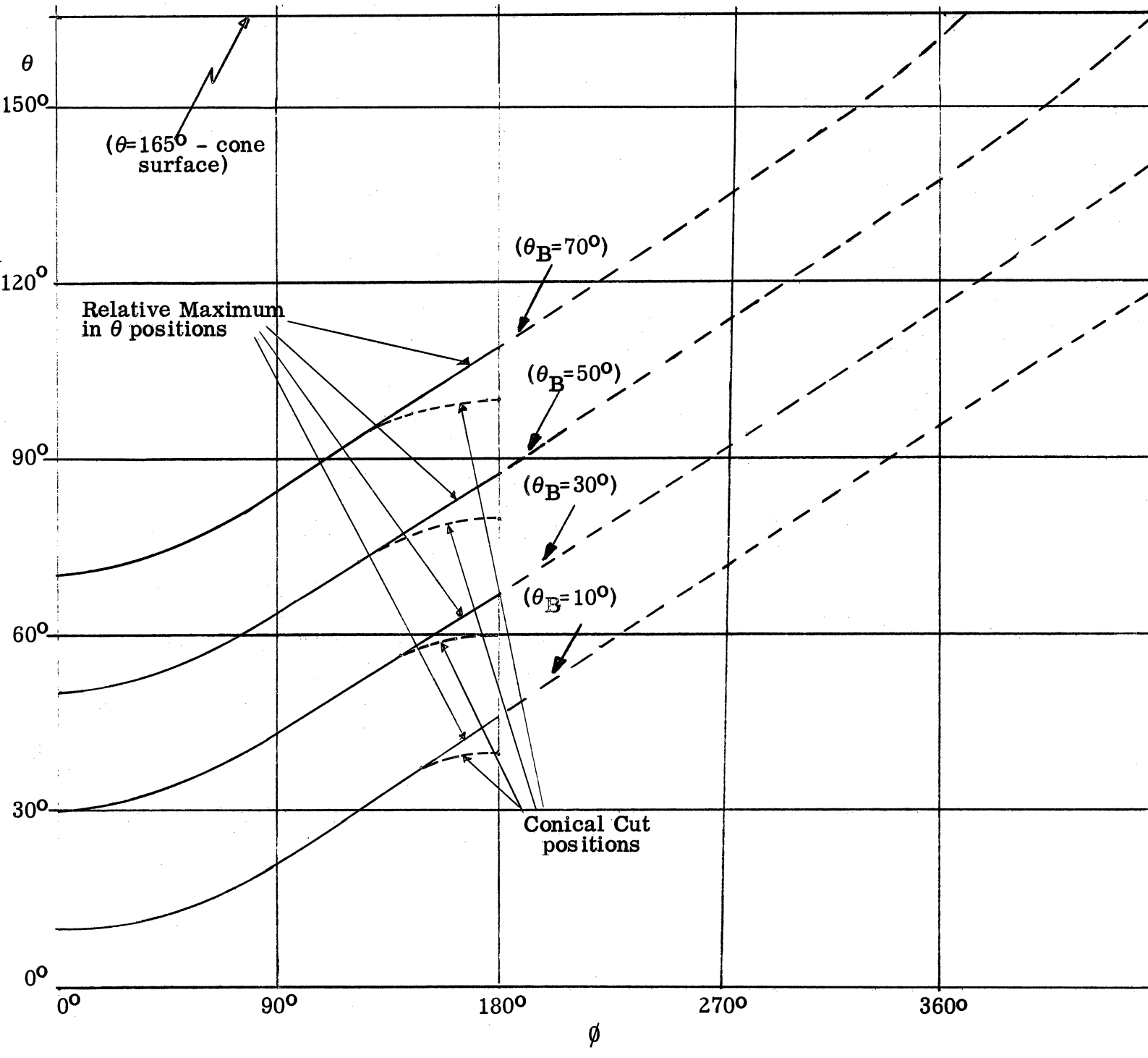

A.3 Results of the 65-Slot Computations

As pointed out at the beginning of this Appendix and in Section I computations were performed for four different beam directions,

$$\theta_B = 10^o, 30^o, 50^o, \text{ and } 70^o,$$

for the 65 slots located on a generator of a cone of half-angle 15^o. For each beam angle computations were performed on two "cuts":

(1) a conical cut for which the receiver is restricted to lie on a conical surface whose axis is the extension of the generator containing the slots and which has a half-angle equal to $15^o + \theta_B$, and

(2) a plane cut for which the receiver is restricted to lie in the plane of the generator containing the slots and the axis of the 15^o cone.

These two geometries are displayed in Figure 1-1 of Section I.

Values of $|H_\theta|^2$ and $|H_\phi|^2$ were computed at appropriate intervals in ϕ (or θ) using Geometric Optics, Physical Optics, and Fock Theory in their regions of applicability. The space regions of the applicability of these three methods is shown graphically in Figure 1-6 in Section I.

The results were obtained in db below the Geometric Optics maximum and are tabulated in Tables A.3.1 through A.3.4. Only the Geometric Optics and Fock Theory results are given in these tables; it was found that the Physical Optics results were negligible.* Graphical presentations of these Physical Optics results are given in

* As will be noted by an examination of Tables A.3.1 through A.3.4, only values less than 60 were recorded; that is, a value which was more than 60 db down from the Geometric Optics maximum was not included in the final summary.

Figure A.3-1 for the conical cut cases and a brief examination of the data contained in Figure A.3-1 indicates that the Physical Optics contribution is negligible in comparison with the "Fock Theory" contributions in the shadow region.

In the lit region where the Geometric Optics results were used, only the relative maxima were computed except in the vicinity of the main beam.

At the time of the writing of this report experimental results were available for the two beam directions $\theta_B = 10^o$ and $\theta_B = 30^o$. The theoretical results of Tables A.3.1 and A.3.2 are compared with the experimental data in Figures 1-2 through 1-5 in Section I. The theoretical data is superimposed upon copies of the actual patterns obtained from the Hughes Aircraft Company. For the plane cuts the experimental data was not normalized and thus the peak value (which would be 0 db) appears on the experimental curves as approximately -4.5 db. Thus, in making the comparisons between theory and experiment, the theoretical data has been normalized to the experimental peak value; i.e. each theoretical value, x, is plotted in Figures 1-2 and 1-3 as the quantity, -(x + 4.5). The slight angular variation between the theoretical and experimental patterns which can be observed in Figures 1-2 and 1-3 is due to a slight missalignment in the experimental tests (in fact, the main beam direction in the 30^o-experimental-test was actually 29^o); no attempt has been made to normalize angularly the results in the plane cut.

On the "conical cut", this normalization is partially accomplished since the comparison between theory and experiment shown in Figures 1-4 and 1-5 is actually a comparison between theoretical values for receiver positions on the conical cut while the experimental values are for "relative maxima in θ" positions. Examination of Figure A.2-1

indicates that such a comparison loses validity only near $\phi = 180^{o}$. Also, since the summation technique employed to obtain the Fock results was expected to be least accurate near $\phi = 180^{o}$, we expect the greatest deviation between theory and experiment in Figures 1-4 and 1-5 to occur near $\phi = 180^{o}$. *

This program of experimentation and theoretical calculation was set up primarily as a feasibility study and thus one would not expect "extreme" precision in the results. We feel that the excellent agreement between theory and experiment displayed in the comparisons of Section I definitely establishes that radiation patterns for slot arrays on conical surfaces can be theoretically determined.

* During the final editing stage, the experimental data for $\theta_B=50^{o}$ became available. These results are compared with the theoretical estimates in Figures A.3-2 and A.3-3. For this case in addition to the slight angular misalignment, it was found necessary to locate the slots in a manner slightly different from that used in the $\theta_B=60^{o}$ and $\theta_B=30^{o}$ cases; that is, the slots were tilted a few degrees from the transverse position. This slight tilt in the positioning of the slots could be expected to lead to larger differences between theory and experiment due to the polarization effects and thus the relatively poor agreement between theory and experiment for the H_ϕ case shown in Figure A.3-3 is not unexpected.

TABLE A. 3. 1
Results Obtained for $\theta_B = 10^o$

Conical Cut				Plane Cut			
ϕ^o	θ^o	$\lvert H_\theta \rvert^2$ *	$\lvert H_\phi \rvert^2$ *	ϕ^o	θ^o	$\lvert H_\theta \rvert^2$ *	$\lvert H_\phi \rvert^2$ *
0	10.	>60	0	0	150	>60 **	33. 3
30	10. 5	6. 2	1. 2	0	135	>60	34. 3
60	14	1. 5	6. 0	0	120	>60	35. 4
90	20. 3	. 6	>60	0	105	>60	36. 1
100	23. 1	. 9	15. 2	0	90	>60	36. 2
105	24. 6	1. 1	11. 7	0	75	>60	35. 4
110	26. 1	1. 5	9. 3	0	60	>60	33. 5
15	27. 7	1. 9	7. 6	0	45	>60	30. 0
120	29. 2	5. 8	9. 6	0	28	>60	22. 5
125	30. 7	6. 6	11. 1	0	24	>60	20. 8
130	32. 2	7. 8	12. 6	0	22. 5	>60	>60
135	33. 5	9. 1	14. 3	0	21	>60	17. 9
140	34. 8	10. 7	16. 2	0	19	>60	>60
145	36	12. 5	18. 3	0	17	>60	13. 5
150	37	13. 9	20. 2	0	15	>60	>60
155	37. 9	15. 6	22. 0	0	12. 5	>60	4. 0
160	38. 6	17. 8	24. 4	0	10	>60	0
165	39. 2	21. 4	28. 2	0	7	>60	4. 0
170	39. 7	30. 3	37. 1	0	4	>60	>60
175	39. 9	28. 7	35. 8	0	0	>60	13. 5
180	40	32. 3	39. 1	180	8	>60	>60
				180	16	>60	17. 9
				180	20	22. 2	20. 9
				180	30	34. 9	39. 0
				180	40	32. 3	39. 1
				180	50	23. 9	32. 6
				180	60	47. 5	57. 1
				180	70	55. 1	>60
				180	80	59. 2	>60

* Measured in db down from the Geometrics Optics Maximum
** Geometric Optics result only

TABLE A.3.2
Results Obtained for $\theta_B = 30^o$

Conical Cut				Plane Cut			
ϕ^o	θ^o	$\lvert H_\theta \rvert^2$ *	$\lvert H_\phi \rvert^2$ *	ϕ^o	θ^o	$\lvert H_\theta \rvert^2$ *	$\lvert H_\phi \rvert^2$ *
0	30	>60	0	0	150	>60 **	35
30	31.4	7.4	1.2	0	135	>60	35.6
60	35.8	3.1	6.0	0	120	>60	36.1
90	42.9	2.7	>60	0	105	>60	36.3
100	45.7	3.2	15.2	0	90	>60	35.6
105	47	6.2	14.4	0	75	>60	34.1
110	48.4	7.9	15.6	0	60	>60	30.7
115	49.8	9.2	17	0	43	>60	22.5
120	51.1	10.6	18.6	0	40	>60	20.8
125	52.4	12.2	20.4	0	38.5	>60	>60
130	53.6	13.9	22	0	37	>60	17.9
135	54.7	15.9	24.5	0	36	>60	>60
140	55.8	18.3	27.6	0	35	>60	13.5
145	56.7	21.4	30.4	0	33	>60	>60
150	57.6	25.8	35.1	0	31.5	>60	4
155	58.3	32.2	41.7	0	30	>60	0
160	58.9	41.1	50.1	0	28.5	>60	4
165	59.4	37.4	46.9	0	27	>60	>60
170	59.7	38.1	47.8	0	25	>60	13.5
175	59.9	>60	>60	0	23	>60	>60
180	60	40.9	50.7	0	21	>60	17.9
				0	19.5	>60	>60
				0	18	>60	20.9
				0	0	>60	26
				180	15	>60	27.3
				180	20	32.3	31.0
				180	30	38.4	42.7
				180	40	41.8	48.6
				180	50	40.9	49.6
				180	60	40.9	50.7
				180	70	33.5	44.2
				180	80	55.4	>60

* Measured in db down from the Geometric Optics Maximum

** Geometric Optics result only

TABLE A.3.3
Results Obtained for $\theta_B = 50^o$

Conical Cut				Plane Cut			
ϕ^o	θ^o	$\lvert H_\theta \rvert^2$ *	$\lvert H_\phi \rvert^2$ *	ϕ^o	θ^o	$\lvert H_\theta \rvert^2$ *	$\lvert H_\phi \rvert^2$ *
0	50	>60	0	0	150	>60 **	36.1
30	51.6	11.4	1.2	0	135	>60	36.3
60	56.6	6.4	6	0	120	>60	36.1
90	64	7.2	>60	0	105	>60	35.5
100	66.7	12.2	18.7	0	90	>60	33.9
105	68.1	13	19.8	0	75	>60	30.3
110	69.4	14.4	21.6	0	61	>60	22.5
115	70.7	16.1	23.6	0	58	>60	20.8
120	71.9	17.8	25.7	0	57	>60	>60
125	73.1	19.9	28.1	0	56	>60	17.9
130	74.2	22.1	31.6	0	55	>60	>60
135	75.3	27.4	36.5	0	54	>60	13.5
140	76.2	28.5	38.7	0	53	>60	>60
145	77.1	35.6	39.1	0	51.5	>60	4
150	77.8	46.4	55.3	0	50	>60	0
155	78.5	>60	>60	0	49	>60	4
160	79	>60	>60	0	48	>60	>60
165	79.5	52.4	>60	0	46	>60	13.5
170	79.8	52	>60	0	45	>60	>60
175	79.9	58.5	>60	0	44	>60	17.9
180	80	51.3	>60	0	42.5	>60	>60
				0	41	>60	20.8
				0	30	>60	26.9
				0	15	>60	30.7
				0	0	>60	32.1
				180	15	>60	32.7
				180	20	54.8	58.8
				180	30	52.3	46.5
				180	40	46.6	53.3
				180	50	56.7	>60
				180	60	51.4	>60
				180	70	52.9	>60
				180	80	51.3	>60

* Measured in db down from the Geometric Optics Maximum

** Geometric Optics result only

TABLE A.3.4
Results Obtained for $\theta_B = 70^o$

Conical Cut				Plane Cut			
ϕ^o	θ^o	$\lvert H_\theta \rvert^2$ *	$\lvert H_\phi \rvert^2$ *	ϕ^o	θ^o	$\lvert H_\theta \rvert^2$ *	$\lvert H_\phi \rvert^2$ *
0	70	>60	0	0	150	>60 **	36
30	71.9	16.2	1.2	0	135	>60	35.6
60	77.2	14.4	6	0	120	>60	34.7
90	84.8	20.9	>60	0	105	>60	32.8
95	86.2	24.7	19.7	0	90	>60	28.6
100	87.5	26.8	22.6	0	80.5	>60	22.5
105	88.8	28.8	25.8	0	78	>60	20.8
110	90.1	30.7	29	0	77	>60	>60
115	91.3	32.6	32.5	0	76	>60	17.9
120	92.5	34.5	36.2	0	74.5	>60	>60
125	93.6	36.5	39.9	0	73	>60	13.5
130	94.7	39.3	44.6	0	72	>60	>60
135	95.6	43.4	50.2	0	71	>60	4
140	96.5	51.3	58.4	0	70	>60	0
145	97.3	58.5	>60	0	69	>60	4
150	98	53.1	>60	0	68	>60	>60
155	98.6	58.9	>60	0	67	>60	13.5
160	99.1	>60	>60	0	66	>60	>60
165	99.5	>60	>60	0	65	>60	17.9
170	99.8	>60	>60	0	64	>60	>60
175	99.9	>60	>60	0	62.5	>60	20.8
				0	45	>60	30.2
				0	30	>60	33.2
				0	15	>60	34.7
				0	0	>60	35.3
				180	15	>60	35.5
				180	20	42.3	41
				180	30	44.8	49.1
				180	40	49.3	56.2
				180	50	53.7	>60
				180	60	56.3	>60
				180	70	58.3	>60
				180	80	>60	>60

* Measured in db down from the Geometric Optics Maximum

** Geometric Optics result only

FIG. A.3-1: PHYSICAL OPTICS RESULTS OBTAINED FOR THE CONICAL CUTS $\left(\frac{|H_{PO}|^2}{|H_{GO(max)}|^2} \text{ IN DB} \right)$

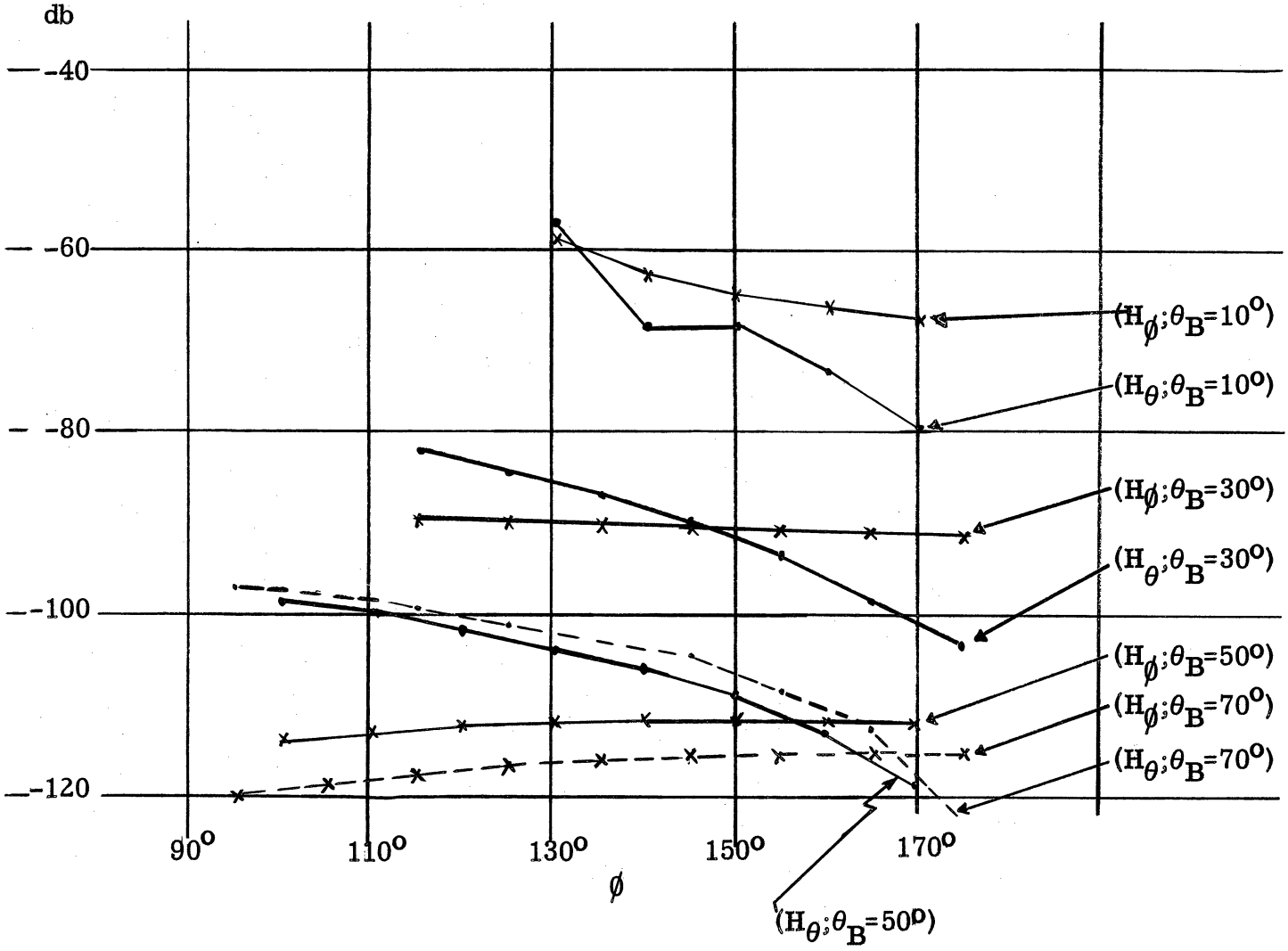

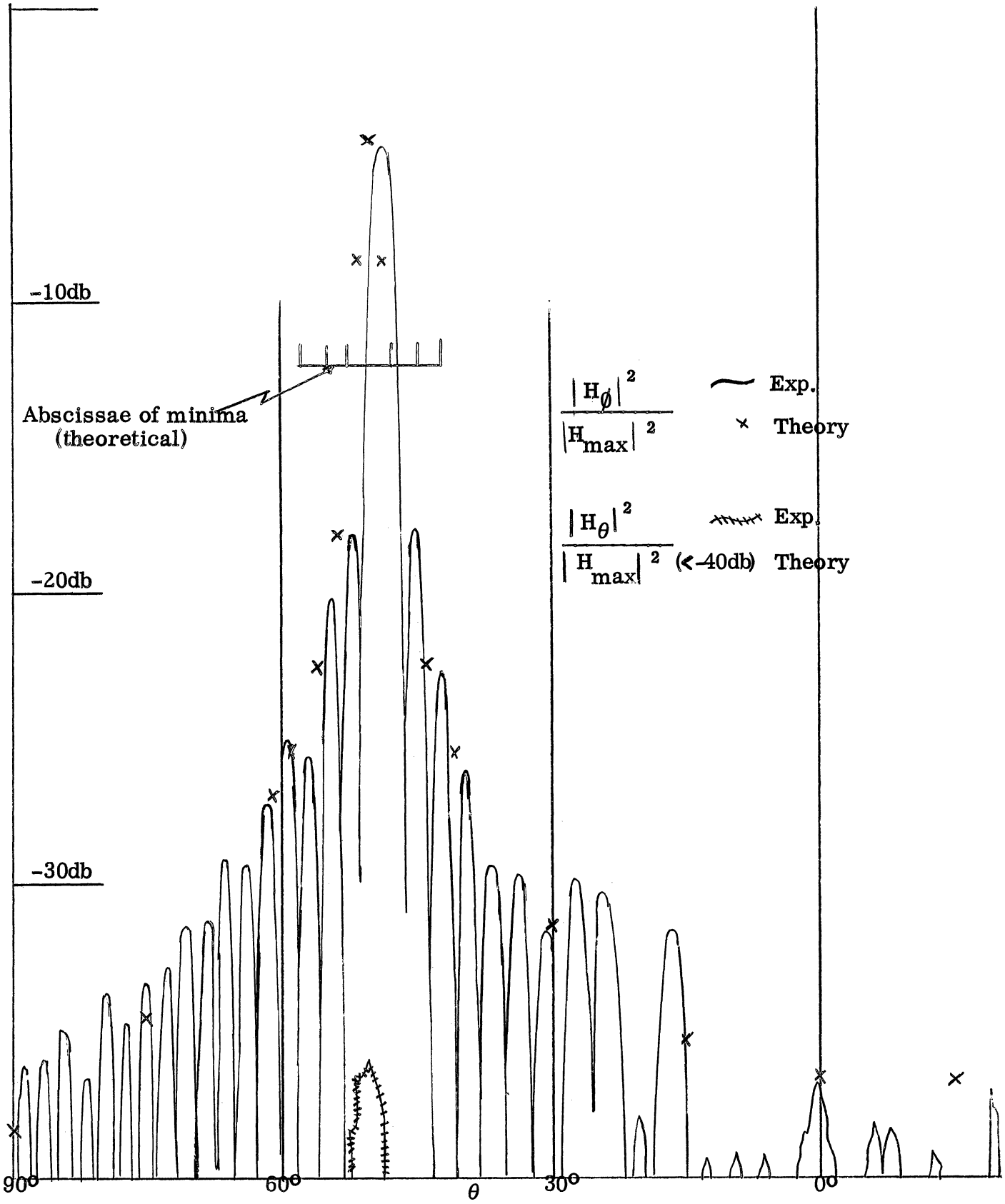

FIG. A. 3-2: COMPARISON BETWEEN THEORY AND EXPERIMENT FOR A PLANE CUT ($\theta_B = 50^\circ$, $\phi = 0^\circ$)

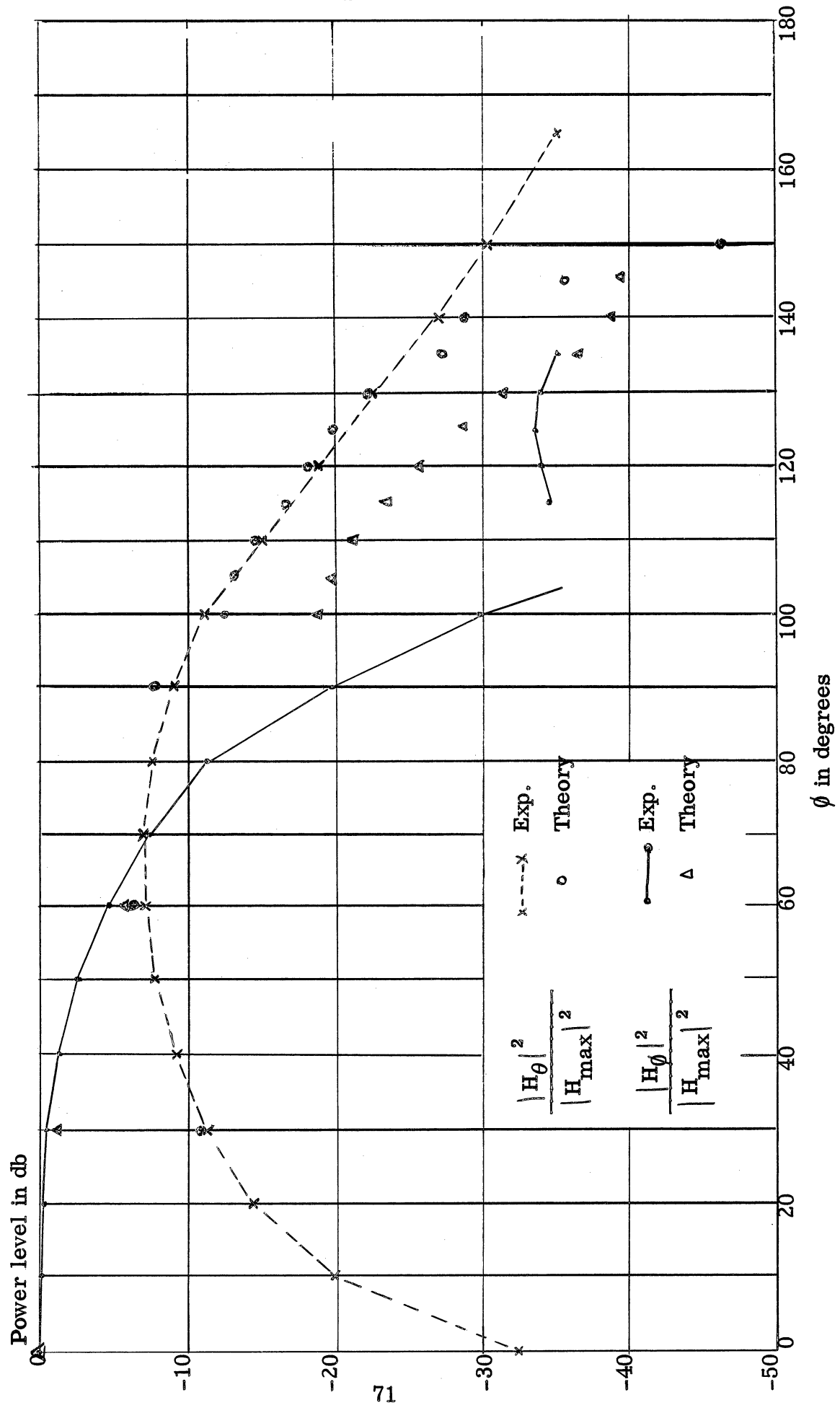

FIG. A.3-3: COMPARISON BETWEEN THEORY AND EXPERIMENT FOR A CONICAL CUT ($\theta_B=50^o$)

(see footnote on page 64)

APPENDIX B

A FURTHER ANALYSIS OF TIP SCATTERING

It will be recalled that in Section 2.4 we obtained an expression for the field scattered by the tip of a cone. It was noted at that time that the approximation which was employed gave rise in some cases to divergent integrals.

In this Appendix we shall examine these cases more closely. We start with the Kirchhoff expression for the scattered magnetic field

$$\vec{H}_s = \frac{1}{4\pi} \int_S (\hat{n} \times \vec{H}) \times \nabla \frac{e^{ikR}}{R} \, dS, \tag{B.1}$$

where

$\hat{n}$ is the unit outward normal ,

R is the distance from the integration point (x'', y'', z'') to the field point (x', y', z') ,

$k = \frac{2\pi}{\lambda}$,

S is the entire surface area, and time dependence e^{-iwt} has been assumed.

Our problem concerns a plane wave incident on a conical surface. The incident field at any point (x', y', z') is given by

$$H_i = \hat{p} H_o e^{-ik\hat{r} \cdot \vec{r}'},$$

where

$\hat{p}$ is the unit vector in the polarization direction,

$\hat{r}$ is a unit vector toward transmitter,

$\vec{r}'$ position vector for field point.

Points on the surface will be denoted by $\vec{r}''$. ($\hat{}$ will denote unit vectors while $\rightarrow$ will denote vectors of arbitrary magnitude).

As before, we employ the Physical Optics approximation, i.e. (1) the magnetic field on the surface is taken to be

$$\vec{H} = 2 H_o e^{-ik\hat{r}\cdot\vec{r}''} \vec{p}_t$$

where $\vec{p}_t$ is the tangential component of $\hat{p}$ and (2) S is the illuminated area.

Thus, we may rewrite B.1, remembering that $\hat{n} \times \hat{p} \equiv \hat{n} \times \vec{p}_t$, as follows

$$\vec{H}_s = \frac{H_o}{2\pi} \int_{\substack{\text{illuminated} \\ \text{area}}} \left[(\hat{n} \times \hat{p}) \times \nabla \frac{e^{ikR}}{R} \right] e^{-ik\hat{r}\cdot\vec{r}''} \, dS \, . \qquad \text{(B.2)}$$

However, $\nabla \frac{e^{ikR}}{R} = \left[\frac{-e^{ikR}}{R^2} + ik\frac{e^{ikR}}{R} \right] \nabla R$

$$= \left[\frac{-e^{ikR}}{R^2} + ik\frac{e^{ikR}}{R} \right] \hat{R}$$

$$= \left[\frac{-e^{ikR}}{R^2} + ik\frac{e^{ikR}}{R} \right] \frac{(\vec{r}' - \vec{r}'')}{|\vec{r}' - \vec{r}''|}$$

and

$$(\hat{n} \times \hat{p}) \times (\vec{r}' - \vec{r}'') = \left[(\vec{r}' - \vec{r}'')\cdot\hat{n}\right]\hat{p} - \left[(\vec{r}' - \vec{r}'')\cdot\hat{p}\right]\hat{n} \, ,$$

hence, (B.2) becomes

$$\vec{H}_s = \frac{H_o}{2\pi} \int_{\substack{\text{illuminated} \\ \text{area}}} \frac{\left[(\vec{r}' - \vec{r}'')\cdot\hat{n}\right]\hat{p} - \left[(\vec{r}' - \vec{r}'')\cdot\hat{p}\right]\hat{n}}{|\vec{r}' - \vec{r}''|} \left(-\frac{e^{ikR}}{R^2} + ik\frac{e^{ikR}}{R} \right) e^{-ik\hat{r}\cdot\vec{r}''} \, dS. \qquad \text{(B.3)}$$

The usual far zone assumptions are:

$$\text{(1)}\quad \frac{\vec{r}' - \vec{r}''}{|\vec{r}' - \vec{r}''|} \sim \hat{r}',$$

$$\text{(2)}\quad -\frac{1}{R^2} + \frac{ik}{R} \sim \frac{ik}{R}\quad , \tag{B. 4}$$

$$\text{(3)}\quad R \sim \begin{cases} r' & \text{when evaluating magnitude} \\ r' - \hat{r}' \cdot \vec{r}'' & \text{when evaluating phase} \end{cases}$$

Utilizing Equations (B. 4) in (B. 3) we obtain

$$\vec{H}_s = \frac{H_o}{2\pi} \int_{\substack{\text{illuminated} \\ \text{area}}} \left[(\hat{r}' \cdot \hat{n})\,\hat{p} - (\hat{r}' \cdot \hat{p})\hat{n}\right] \frac{ike}{r'}^{ik(r' - \hat{r}' \cdot \vec{r}'')} e^{-ik\hat{r} \cdot \vec{r}''}\, dS\ . \tag{B. 5}$$

Let us re-examine our far zone assumption B. 4 (3), retaining the next higher order terms. That is,

$$\begin{aligned} R &= \sqrt{r'^2 + r''^2 - 2\vec{r}' \cdot \vec{r}''} \\ &= r' \sqrt{1 + \frac{r''^2}{r'^2} - \frac{2\vec{r}' \cdot \vec{r}''}{r'^2}} \\ &= r' \left[1 + \frac{1}{2}\left(\frac{r''^2}{r'^2} - \frac{2\vec{r}' \cdot \vec{r}''}{r'^2}\right) - \frac{1}{8}\left(\frac{r''^2}{r'^2} \quad \frac{2\vec{r}' \cdot \vec{r}''}{r'^2}\right)^2 + \cdots\right] \\ &= r' \left[1 - \frac{\vec{r}' \cdot \vec{r}''}{r'} + \frac{r''^2}{2r'^2} - \frac{1}{2}\frac{(\hat{r}' \cdot \vec{r}'')^2}{r'^2} + O\left(\frac{1}{r'^3}\right)\right] \\ &\sim r' - \hat{r}' \cdot \vec{r}'' + \frac{r''^2 - (\hat{r}' \cdot \vec{r}'')^2}{2r'}\quad . \end{aligned} \tag{B. 6}$$

Now we rewrite (B. 5) using (B. 6),

$$\vec{H}_S = \frac{H_o\, ike^{ikr'}}{2\pi r'} \int_{\substack{\text{illuminated}\\ \text{area}}} \left[(\hat{r}'\cdot\hat{n})\,\hat{p} - (\hat{r}'\cdot\hat{p})\,\hat{n}\right] \exp\left[i k\left(-\vec{r}''\cdot(\hat{r}'+\hat{r}) + \frac{r'^2 - (\hat{r}'\cdot\vec{r}'')^2}{2r'}\right)\right] dS . \tag{B. 7}$$

Equation (B. 5) gave rise, in Section II, to the integral

$$\vec{f} = \int_{\substack{\text{illuminated}\\ \text{area}}} \hat{n}\, e^{-ik\vec{r}''\cdot(\hat{r}'+\hat{r})}\; r''\sin\alpha\, dr''\, d\phi''$$

which proved troublesome for values of ϕ'' such that $\vec{r}''\cdot(\hat{r}'+\hat{r}) = 0$. It is true that, as written, $\vec{f}$ diverges if there is a ϕ'' in the range of integration for which $\vec{r}''\cdot(\hat{r}'+\hat{r}) = 0$. If at the same point (x'', y'', z'') we also have $\hat{n}\times(\hat{r}'+\hat{r}) = 0$, then of course, we have a specular reflection situation and we would use Geometric Optics to describe the scattered field. However, let us assume that there is such a ϕ'', say ϕ''_o, where $\vec{r}''\cdot(\hat{r}'+\hat{r}) = 0$ but $\hat{n}\times(\hat{r}'+\hat{r}) \neq 0$ and examine the following three cases, using (B. 7) instead of (B. 5).

(1) $\vec{r}''\cdot\hat{r}' = 0$,

(2) $\vec{r}''\cdot\hat{r}' = r''\cos\gamma$ where $0 < \cos^2\gamma < 1$,

(3) $\vec{r}''\cdot\hat{r}' = \pm r''$.

In the following we will treat (B. 7) as consisting of two contributions

$$\vec{H} = \int_{\substack{\text{illuminated}\\ \text{area}}} = \int_{S_1} + \int_{S_2}$$

where S_2 contains ϕ''_o and $S_1 + S_2$ = illuminated area. We will concern ourselves only with $\int_{S_2}$ since $\int_{S_1}$ presents no problem.

CASE I

In the neighborhood of ϕ_o'' we have

$$\vec{r}'' \cdot (\hat{r}' + \hat{r}) = 0 \quad \text{and} \quad \vec{r}'' \cdot \hat{r}' = 0 \ ,$$

hence we may write (B. 7) as

$$\vec{H}_s = \int_{S_1} + \frac{H_o\, ike^{ikr'}}{2\pi r'} \int_{\phi_o''-\epsilon}^{\phi_o''+\epsilon} \int_0^{\infty} \left[(\hat{r}' \cdot \hat{n})\, \hat{p} - (\hat{r}' \cdot \hat{p})\, \hat{n} \right] \exp\left(ik \frac{r''^2}{2r'} \right) r'' \sin\alpha \, dr'' \, d\phi'' \tag{B. 8}$$

The r'' integration can be performed by an Abelian limit argument as follows

$$\int_0^{\infty} \exp\left(ik \frac{r''^2}{2r'} \right) r'' \, dr'' = \lim_{\delta \to 0} \int_0^{\infty} \exp\left[\left(\frac{ik}{2r'} - \delta \right) r''^2 \right] r'' \, dr''$$

$$= \lim_{\delta \to 0} \left[\frac{\exp\left[\left(\frac{ik}{2r'} - \delta \right) r''^2 \right]}{2\left(\frac{ik}{2r'} - \delta \right)} \Bigg|_0^{\infty} \right]$$

$$= \frac{r'}{ik} \ .$$

Thus (B. 8) becomes

$$\vec{H}_s = \int_{S_1} + \frac{H_o\, e^{ikr'}}{2\pi} \sin\alpha \int_{\phi_o''-\epsilon}^{\phi_o''+\epsilon} \left[(\hat{r}' \cdot \hat{n})\, \hat{p} - (\hat{r}' \cdot \hat{p})\, \hat{n} \right] d\phi'' \ .$$

Applying the mean value theorem, we obtain

$$\vec{H}_s = \int_{S_1} + \frac{H_o\, e^{ikr'}}{\pi} \sin\alpha \left[(\hat{r}' \cdot \hat{n})\, \hat{p} - (\hat{r}' \cdot \hat{p})\, \hat{n} \right] \epsilon$$

for $\hat{n} = \hat{n}(\phi_1'')$, $\phi_o'' - \epsilon \leq \phi_1'' \leq \phi_o'' + \epsilon$.

Thus $\vec{H}_s \approx \int_{S_1}$

where $\int_{S_1}$ can be evaluated by the method of Section II.

CASE II

In the neighborhood of ϕ_o'' we have $\vec{r''}\cdot(\hat{r'} + \hat{r}) = 0$ and $\vec{r''}\cdot\hat{r'} = r'' \cos\gamma$ where $\cos^2\gamma$ is bounded away from 0 and 1. In this case, we may write (B.7) as

$$\vec{H}_s = \int_{S_1} + \frac{H_o ike^{ikr'}}{2\pi r'} \sin\alpha \int_{\phi_o''-\epsilon}^{\phi''+\epsilon} \int_0^{\infty} \left[(\hat{r'}\cdot\hat{n})\hat{p} - (\hat{r'}\cdot\hat{p})\hat{n}\right] \exp\left[\frac{ikr''^2}{2r'}\sin^2\gamma\right] r''\, dr''\, d\phi'' \qquad (B.9)$$

Since $\sin^2\gamma$ is bounded away from zero, we proceed exactly as in Case I obtaining

$$\vec{H}_s = \int_{S_1} + \frac{H_o e^{ikr'}}{\pi \sin^2\gamma} \sin\alpha \left[(\hat{r'}\cdot\hat{n})\hat{p} - (\hat{r'}\cdot\hat{p})\hat{n}\right] \epsilon$$

for $\hat{n} = \hat{n}(\phi_1'')$, $\phi_o'' - \epsilon \leq \phi_1'' \leq \phi_o'' + \epsilon$.

Thus again we see that the contribution from the neighborhood containing ϕ_o'' vanishes with ϵ and

$$\vec{H}_s \approx \int_{S_1}$$

CASE III

In the neighborhood of ϕ_o'' we have $\vec{r''}\cdot(\hat{r'} + \hat{r}) = 0$ and $\vec{r''}\cdot\hat{r'} = \pm r''$. Thus either (a), $\vec{r''}\cdot\hat{r'} = r''$ and $\vec{r''}\cdot\hat{r} = -r''$ or (b), $\vec{r''}\cdot\hat{r'} = -r''$ and $\vec{r''}\cdot\hat{r} = r''$. In (a) we have the receiver on a cone generator and the transmitter on the extension of that generator while in (b) the transmitter is on the generator and the receiver is on the extension. These are the transition cases which we cannot handle by these techniques and must exclude from our analysis.

APPENDIX C

IDEAL CURRENT DISTRIBUTION FOR A CONICAL ANTENNA

It was pointed out in Section I that it was theoretically possible to duplicate a pattern produced by one type of antenna with another antenna of equal or greater aperture. It was pointed out there that the problems involved in attempting to instrument the current distribution required appeared to be of such complexity that a serious attempt at instrumentation would not be warranted since this is not an optimal array. In this Appendix we consider this problem of duplicating a given pattern. Specifically, for illustration, we consider the pattern produced by an ideal parabolic dish and calculate the current distribution which, if activated on a cone surface in any manner whatsoever, would make the cone yield a pattern identical with the dish pattern.

Consider a conical surface behind which a dish antenna is pivoted about the point 0. By application of Huygens Principle the field at a point **P** outside a surface S can be obtained from knowledge of the tangential field produced by the source at the surface. In this case the source is a dish and the surface a cone. The field of a dish is approximated by a plane wave; the tangential component on the cone surface will be studied.

An $\hat{i}, \hat{j}, \hat{k}$ coordinate system is considered to be affixed to the cone as in Figure C-1. A plane wave is considered to be produced from the dish with polarizations as follows in the two cases to be considered here:

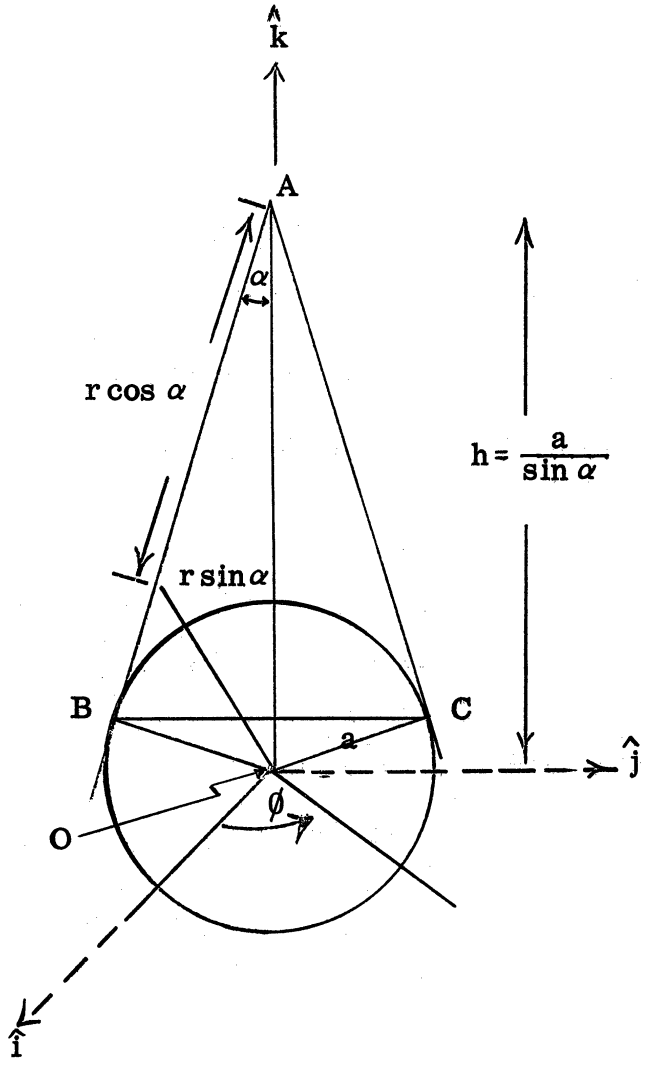

FIG. C-1

$$\vec{E}_1 = (\hat{i}\cos\beta - \hat{k}\sin\beta)\, e^{i\vec{k}\cdot\vec{r}} \tag{C.1}$$

$$\vec{E}_2 = \hat{j}\, e^{i\vec{k}\cdot\vec{r}} \tag{C.2}$$

in which the e^{iwt} time dependence is assumed. $\vec{E}_1$ lies in the y-plane and $\vec{E}_2$ is $\perp$ to the y-plane.

In each case the beam is considered to take the orientations

$$\beta = 0^o, 20^o, 40^o, 60^o, 80^o.$$

In order to graph the amplitude, phase and direction of the field, the cone is unrolled and forms a two-dimensional cone of apex angle $= 2\pi \sin\alpha$.

The tangential component of the field on the illuminated part of the cone is respectively

$$\hat{n} \times \vec{E}_1 = e^{i\vec{k}\cdot\vec{r}} \left[\hat{i}(-\cos\alpha \sin\beta \sin\phi) + \hat{j}(\sin\alpha \cos\beta + \cos\alpha \sin\beta \cos\phi) + \hat{k}(-\cos\alpha \cos\beta \sin\phi)\right] \tag{C.3}$$

$$\hat{n} \times \vec{E}_2 = e^{i\vec{k}\cdot\vec{r}} \left[\hat{i}(-\sin\alpha) + \hat{k}(\cos\alpha \cos\phi)\right] , \tag{C.4}$$

and, in spherical coordinates on the cone surface,

$$\hat{n} \times \vec{E}_1 = e^{i\vec{k}\cdot\vec{r}} \left[\hat{r}(\cos\beta \sin\phi) + \hat{\phi}(\sin\alpha \cos\beta \cos\phi + \sin\beta \cos\alpha)\right] \tag{C.5}$$

$$\hat{n} \times \vec{E}_2 = e^{i\vec{k}\cdot\vec{r}} \left[\hat{r}(-\cos\phi) + \hat{\phi}(\sin\alpha \sin\phi)\right] . \tag{C.6}$$

The amplitudes and directions of the field on the cone surface are

$$|E_1| = \sqrt{\cos^2\beta \sin^2\phi + (\sin\alpha \cos\beta \cos\phi + \sin\beta \cos\alpha)^2} \tag{C.7}$$

$$|E_2| = \sqrt{\cos^2\phi + \sin^2\alpha \sin^2\phi} \tag{C.8}$$

$$\tan\theta_1 = \frac{\sin\alpha \cos\phi + \tan\beta \cos\alpha}{\sin\phi} \tag{C.9}$$

$$\tan\theta_2 = \frac{\sin\alpha \sin\phi}{-\cos\phi} \tag{C.10}$$

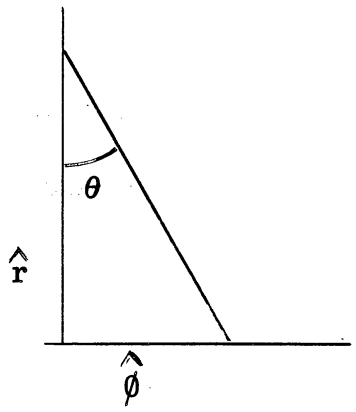

FIG. C-2

Since propagation takes place in y = const. planes, the phase in each case is given by

$$\vec{k} \cdot \vec{r} = kz \cos\beta + kx \sin\beta \qquad \text{(C.11)}$$

We are interested in the phase over the illuminated region of the cone's surface. From the figure we see that $z = h - r\cos\alpha$ and $x = r\sin\alpha\cos\phi$. Therefore, the phase angle is given by

$$\frac{2\pi}{3}\left[\frac{a}{\sin\alpha} - r\cos\alpha\cos\beta + r\sin\alpha\sin\beta\cos\phi\right] \qquad \text{(C.12)}$$

To find the minimum distance between two points along a cone generator at which the radiation is in phase we equate the phase angle above to zero and 2π, we solve for r (obtaining r_o and $r_{2\pi}$), and then subtract the values of r obtaining the distance ℓ

$$\ell = r_o - r_{2\pi} = \frac{3}{(\cos\alpha\cos\beta - \sin\alpha\sin\beta\cos\phi)} \text{ (cm.)} \qquad \text{(C.13)}$$

Equations for the direction lines

The equations for the direction lines on the cone surface may be obtained in the following manner: Consider a ξ , η coordinate system on which the unrolled cone is placed as shown in Figure C-3.

Then

$$\frac{dn}{d\xi} = \tan(\theta + \phi^1)$$

$$n = r \sin\phi^1 \frac{dn}{dr} = \sin\phi^1 \frac{dn}{d\phi^1} = r\cos\phi^1$$

$$\xi = r\cos\phi^1 \frac{d\xi}{dr} = \cos\phi^1 \frac{d\xi}{d\phi^1} = r\sin\phi^1$$

then

$$\frac{\sin\phi^1\, dr + r\cos\phi^1\, d\phi^1}{\cos\phi^1\, dr - r\sin\phi^1 d\phi^1} = \tan(\theta + \phi^1) = \frac{\tan\theta + \tan\phi^1}{1 - \tan\theta\tan\phi^1}$$

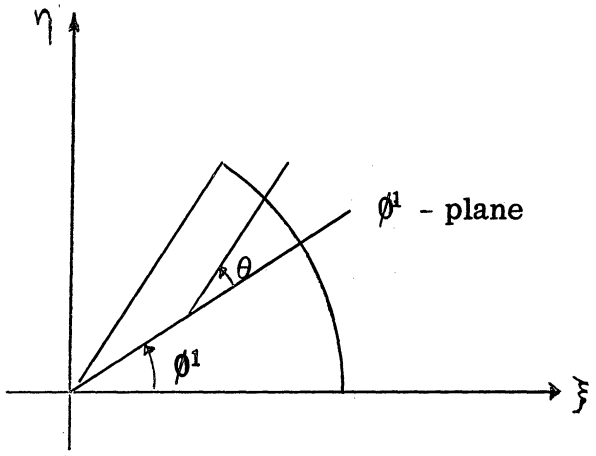

FIG. C-3

$$(\sin \phi^1\, dr + r \cos \phi^1\, d\phi^1)\,(1 - \tan\theta \tan \phi^1) - (\cos \phi^1\, dr - r \sin \phi^1\, d\phi^1)\,(\tan\theta + \tan \phi^1) = 0$$

$$-\tan\theta\, dr + r\, d\phi^1 = 0$$

but

$$d\phi^1 = \sin\alpha\, d\phi$$

$$\frac{dr}{r} = \frac{\sin\alpha\, d\phi}{\tan\theta} \qquad \text{(C.14)}$$

For the two cases considered we have

$$\theta_1: \quad r = \frac{r_o}{(\cos\phi \frac{\tan\beta}{\tan\alpha})} \qquad r_o = \text{integration const.} \qquad \text{(C.15)}$$

$$\theta_2: \quad r = r_o \csc\phi \qquad r_o = \text{integration const.} \qquad \text{(C.16)}$$

The constant r_o is a parameter which takes on all values on a generator of the cone. Due to the discontinuity of the trigonometric functions, the integrations must be performed piecewise resulting in a sign change in the r_o at the points of discontinuity.

Determination of illuminated region

We will now determine $\phi = \phi(r)$; the envelope of the illuminated region on the cone: We will first find the maximum and minimum intercept points of the beam on the cone. It can be seen from the geometry that the cylinder generators in the $y = 0$ plane intersect the cone at r_{max} and r_{min}

On $\phi = 0$ the range of r is determined by

$$r_{\substack{max \\ min}} = a\left(\frac{\sin\beta \pm \sin\alpha}{\sin\alpha \sin(\alpha+\beta)}\right) \tag{C.17}$$

ϕ is determined as a function of r by solving the equation of the intersection of the cone and cylinder. In a spherical coordinate system passing through the cone apex, the intersection equation is

$$r^2 \sin^2\alpha \sin^2\beta (1 - \cos\phi)^2 + 2r \sin\alpha \sin\beta \left[r\cos(\alpha+\beta) - h\cos\beta\right](1 - \cos\phi)$$
$$- r^2 \sin^2(\alpha+\beta) + 2rh \sin\beta \sin(\alpha+\beta) + h^2(\sin^2\alpha - \sin^2\beta) = 0$$

whose solution is (C.18)

$$\cos\phi = \frac{(r\cos\alpha - h)\cos\beta + |r - h\cos\alpha|}{r \sin\alpha \sin\beta} \tag{C.19}$$

the change of sign would occur at

$$r = h\cos\alpha$$

which is the point of maximum possible ϕ.

In order to obtain the boundary of the illuminated region on the cone we use expression (C.19)

$$\cos\phi = \frac{r\cos\alpha\cos\beta - h\cos\beta + |r - h\cos\alpha|}{r \sin\alpha \sin\beta}$$

having already obtained the range of r. For ϕ_{max} the phase is zero since the dish touches the cone at that point. Knowing the phase along the boundary of the illuminated region, we can, for given ϕ, keep laying off the distance ℓ along the generators starting at a boundary point until we attain some pre-assigned phase. The phase on the boundary is obtained from (C.12). For laying off successive curves we subtract

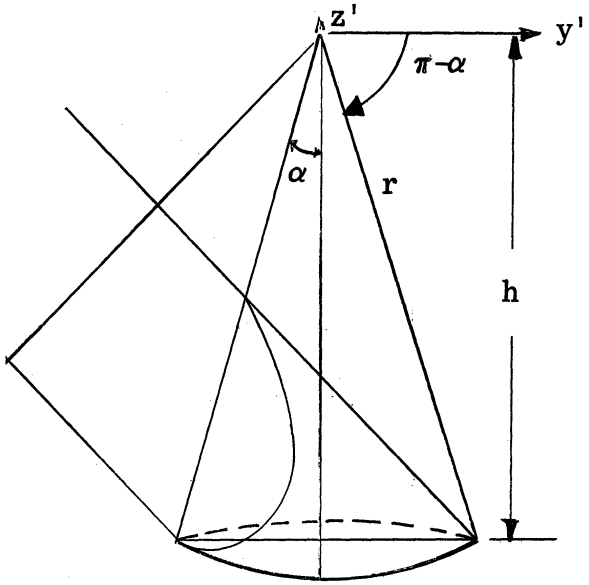

FIG. C-4

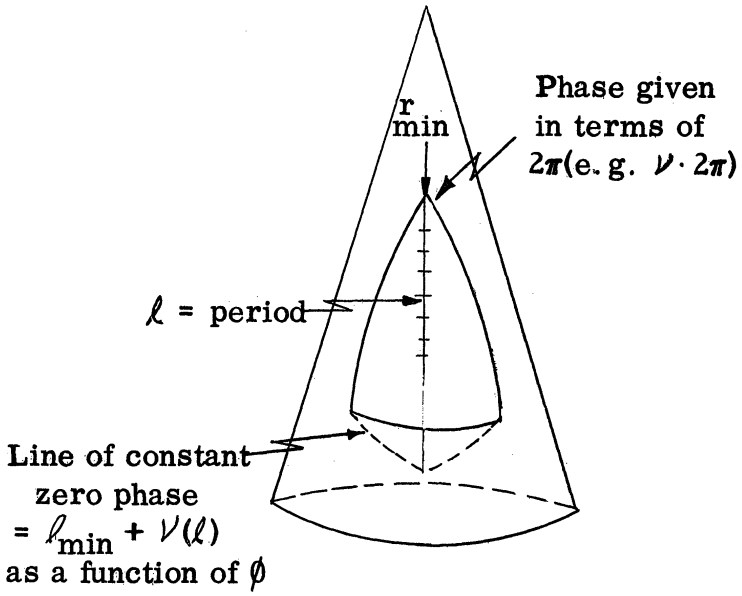

FIG. C-5

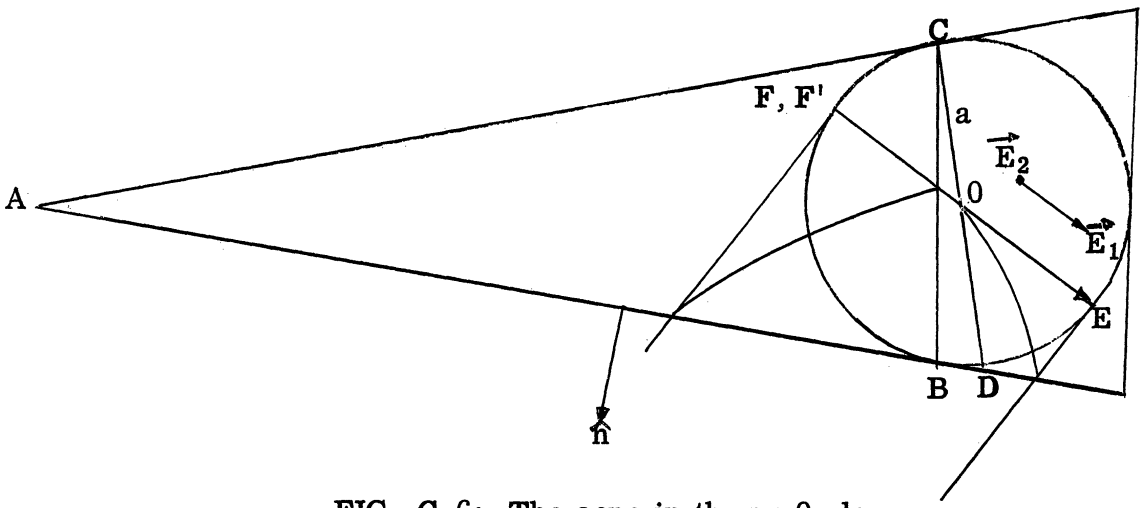

FIG. C-6: The cone in the y = 0 plane

some multiple of 2π from the line of constant zero phase where $\ell = \ell(\phi)$ is used for the distance equivalent to 2π.

Discussion of Results:

In order to see, physically, what occurs, we will consider a sphere of radius "a" equal to the radius of the dish to be inserted into the cone as shown in Figure C-6. The points of contact will constitute a circle whose two-dimensional projection is BC. The dish is focused at 0 and has a point of contact C when in the position DC and two points of contact F, F^1 when in the position EF.

The graphs in Figures C-8 through C-12 show the variation in amplitude of the tangential component of E_1 over the unrolled cone surface. The field along the $\phi=0$ generator of the cone would be small (for β small) increasing to a maximum near $\pm 90^o$ and becoming small again for 180^o. As β increases toward 90^o the amplitude will increase on the $\phi=0^o, 180^o$ surfaces and remain fairly constant on the surface near $\pm 90^o$. Therefore, for large β the amplitude is fairly constant with ϕ.

The graphs in Figures C-13 through C-17 show that the amplitude variation of the tangential component of E_2 is independent of β which is clear from Figure C-6. Figures C-18 through C-22 illustrate lines of constant phase within the illuminated region of the cone. The fact that these lines are ellipses for $\beta=0$ to 80^o, parabolas for $\beta = 80^o$, and hyperbolas for $\beta = 90^o$, can be seen by observation of Figure C-7.

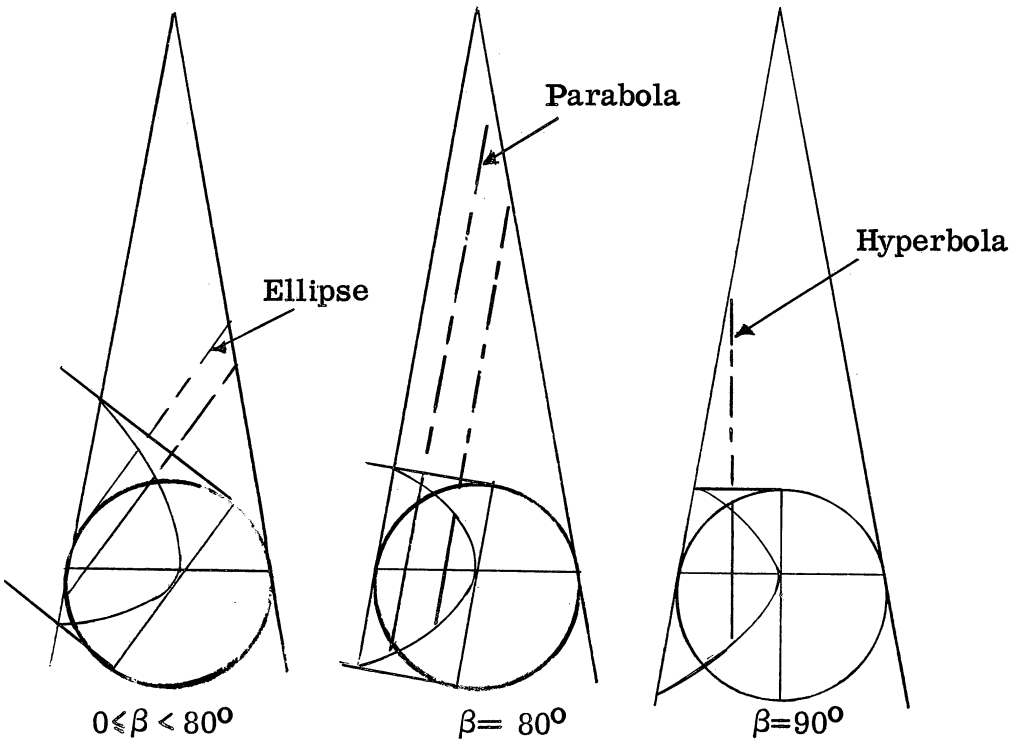

FIG. C-7

The direction of tangential E_1 is shown in Figures C-23 through C-27. It may be noted that, along the $\phi=0$ cone generator, as E_1 points more and more in the $\hat{n}(\phi=0)$ direction, the direction lines take a more acute change in direction. The direction lines would be reversed on either side of $\phi=0$ if the case $\beta=10^o$ had been calculated. In the case of $\beta=80^o$, the fact that the direction lines go along lines of constant r near $\phi=0^o$ is seen from the fact that $\vec{E}_1$ vector points along the cone near $\phi=0$; the dip near 90^o occurs since $\vec{E}_1$ is not tangent near 90^o.

The direction of tangential E_2 is shown in Figure C-28; only in the case of $\beta=0^o$ is shown since $\hat{n} \times \vec{E}_2$ is independent of β.

The discussion of this appendix is illustrated through the application of the following parameter values:

$$\alpha = 10^o$$

$$a = 20''$$

$$\lambda = 3cm.$$

The results are presented in tabular form in Tables C.1 through C.3.

TABLE C.1: $|E|$ ($\alpha = 10^{o}$) Amplitude

	$\|E_1\|$					
ϕ	$\beta = 0^{o}$	$\beta = 20^{o}$	$\beta = 40^{o}$	$\beta = 60^{o}$	$\beta = 80^{o}$	$\|E_2\|$
0^{o}	0.17363	0.500	0.766	0.940	1.000	1.000
10^{o}		0.524	0.776	0.942	1.000	0.985
20^{o}	0.37893	0.586	0.802	0.950	1.000	0.942
30^{o}		0.670	0.841	0.961	1.000	0.870
40^{o}	0.65641	0.760	0.885	0.974	0.999	0.774
50^{o}		0.845	0.928	0.986	0.998	0.656
60^{o}	0.87037	0.915	0.964	0.995	0.996	0.522
70^{o}		0.966	0.989	1.000	0.994	0.379
80^{o}	0.98527	0.995	1.000	0.998	0.990	0.244
90^{o}		0.998	0.994	0.989	0.985	0.174
100^{o}	0.98527	0.975	0.970	0.972	0.980	0.244
110^{o}		0.927	0.929	0.948	0.973	0.379
120^{o}	0.87037	0.853	0.872	0.918	0.967	0.522
130^{o}		0.756	0.803	0.884	0.960	0.656
140^{o}	0.65641	0.640	0.724	0.850	0.953	0.774
150^{o}						0.870
160^{o}	0.37893		values not needed			0.942
170^{o}						0.985
180^{o}	0.17363					1.000

TABLE C.2:
Boundary of Illuminated Region and Phase on Boundary:

$\beta = 20^{\circ}$

r in cm.	ϕ	Phase	ℓ Period for the given ϕ, in cm.
98.9	0°	63.26066 (2π)	3.464
100	16° 33'	62.805 (2π)	3.454
125	58° 2'	54.488 (2π)	3.354
150	76° 50'	46.151 (2π)	3.289
175	89° 6'	37.813 (2π)	3.245
200	98° 15'	29.475 (2π)	3.212
225	105° 30'	21.138 (2π)	3.187
250	111° 29'	12.8 (2π)	3.167
275	116° 32'	4.463 (2π)	3.1515
288.38	118° 58' = ϕ max	0	
300	37° 48'	3.875 (2π)	3.415
302.9	0°		

$\beta = 40^{\circ}$

r in cm.	ϕ	Phase	ℓ Period for the given ϕ, in cm.
179.9	0°	36.3488 (2π)	4.6672
200	49° 37'	29.475 (2π)	4.479
225	64° 38'	21.138 (2π)	4.246
250	80° 23'	12.8 (2π)	4.077
275	92° 46'	4.463 (2π)	4.005
288.38	102° 08' = ϕ max	0	
300	62° 12'	3.875 (2π)	4.291
313	0°		

TABLE C.2:
Boundary of Illuminated Region and Phase on Boundary:
(Continued)

$\beta = 60^o$

r in cm.	ϕ	Phase	ℓ Period for the given ϕ, in cm.
216.4	0^o	24.207 (2π)	8.74
225	34^o 53'	21.138 (2π)	8.129
250	66^o 22'	12.8 (2π)	6.9405
275	86^o 42'	4.463 (2π)	6.202
288.38	95^o 50' = ϕ max	0 (2π)	
300	73^o 21'	3.875 (2π)	6.676
325	0^o	12.212 (2π)	

$\beta = 80^o$

r in cm.	ϕ	Phase	ℓ Period for the given ϕ, in cm.
238.2	0^o	ka = 16.95 (2π)	
250	44^o 54'	12.8 (2π)	60.105
275	78^o 17'	4.463 (2π)	22.018
288.38	91^o 47' (ϕ max)	0	
300	76^o 23' 30"	3.875 (2π)	22.94
325	41^o 56'	12.21 (2π)	68.09
340.2	0^o		

TABLE C.3: Direction of $\vec{E}$ ($\alpha = 10^o$)

ϕ	θ_1					θ_2
	$\beta = 0^o$	$\beta = 20^o$	$\beta = 40^o$	$\beta = 60^o$	$\beta = 80^o$	
0^o	90^o	90^o	90^o	90^o	90^o	0^o
10^o		71.8^o	80.1^o	84.7^o	88.3^o	178.2^o
20^o	25.5^o	56.7^o	70.9^o	79.6^o	86.6^o	176.4^o
30^o		45.5^o	62.9^o	74.9^o	85.0^o	174.3^o
40^o	11.7^o	37.4^o	56.2^o	70.7^o	83.6^o	171.7^o
50^o		31.5^o	50.8^o	67.1^o	82.3^o	168.3^o
60^o	5.7^o	27.2^o	46.5^o	64.2^o	81.3^o	161.3^o
70^o		24.0^o	43.3^o	62.0^o	80.5^o	154.5^o
80^o	1.8^o	21.5^o	41.0^o	60.4^o	80.1^o	135.5^o
90^o		19.7^o	39.6^o	59.6^o	79.8^o	90^o
100^o	-1.8^o	18.4^o	39.0^o	59.6^o	79.9^o	44.5^o
110^o		17.7^o	39.2^o	60.3^o	80.3^o	25.5^o
120^o	-1.8^o	17.4^o	40.5^o	61.9^o	81.0^o	16.7^o
130^o						11.7^o
140^o	-11.7^o					8.3^o
150^o			values not needed			5.7^o
160^o	-25.5^o					3.6^o
170^o						1.8^o
180^o	-90^o					0^o

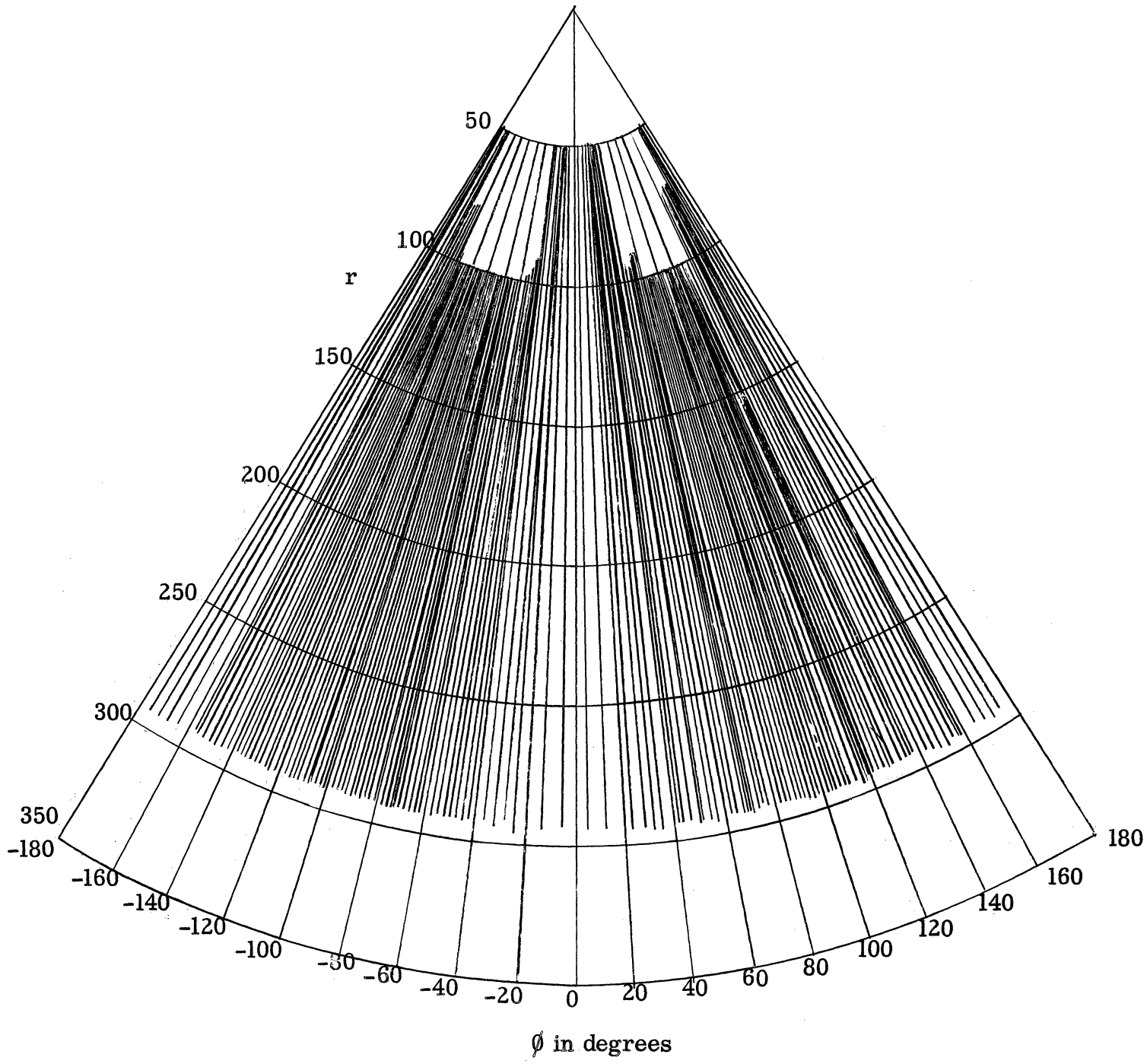

FIG. C-8 AMPLITUDE OF E_1 ON UNROLLED CONE SURFACE FOR $\beta = 0^o$

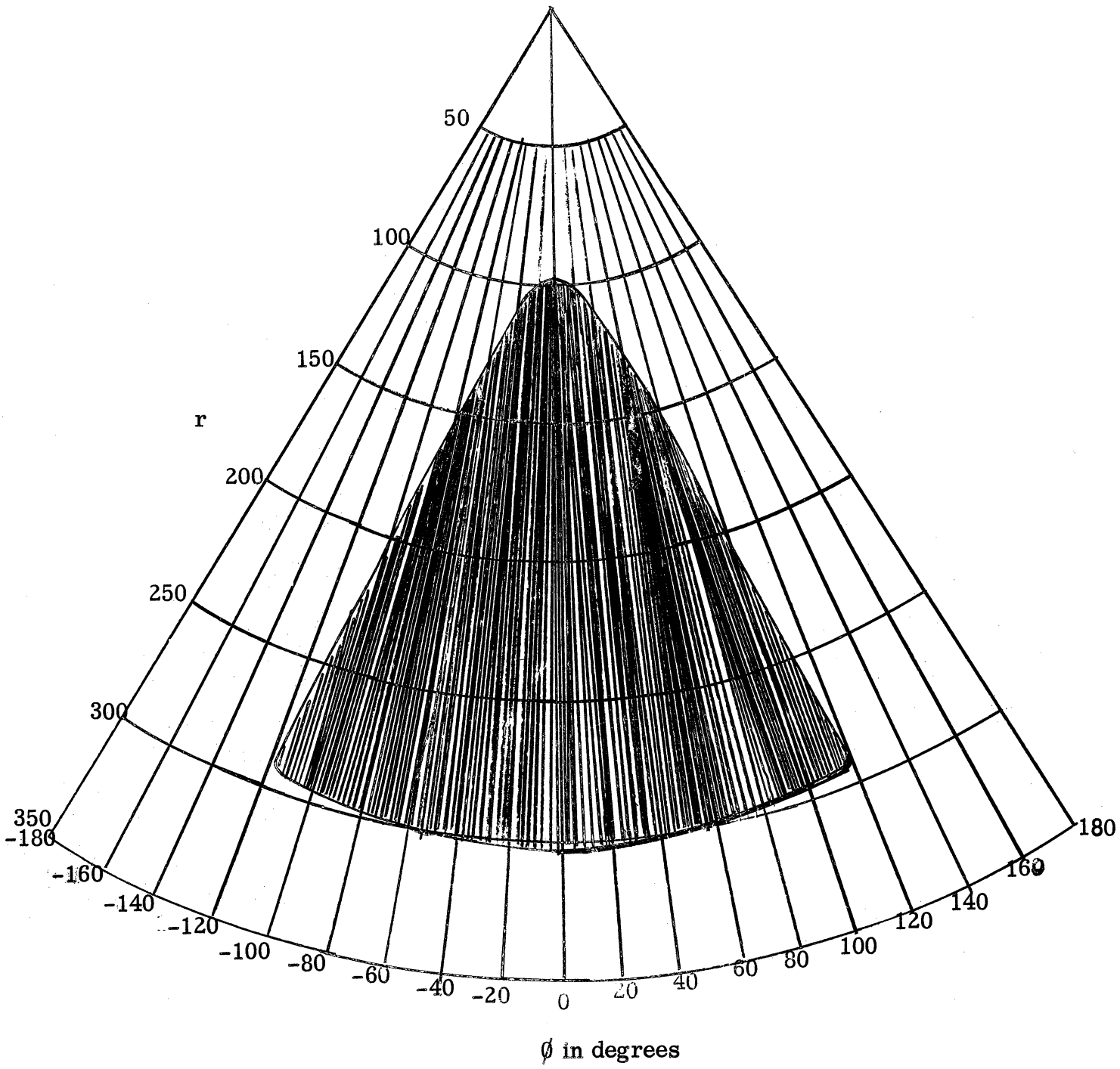

FIG. C-9 AMPLITUDE OF E_1 ON UNROLLED CONE SURFACE FOR $\beta = 20^o$

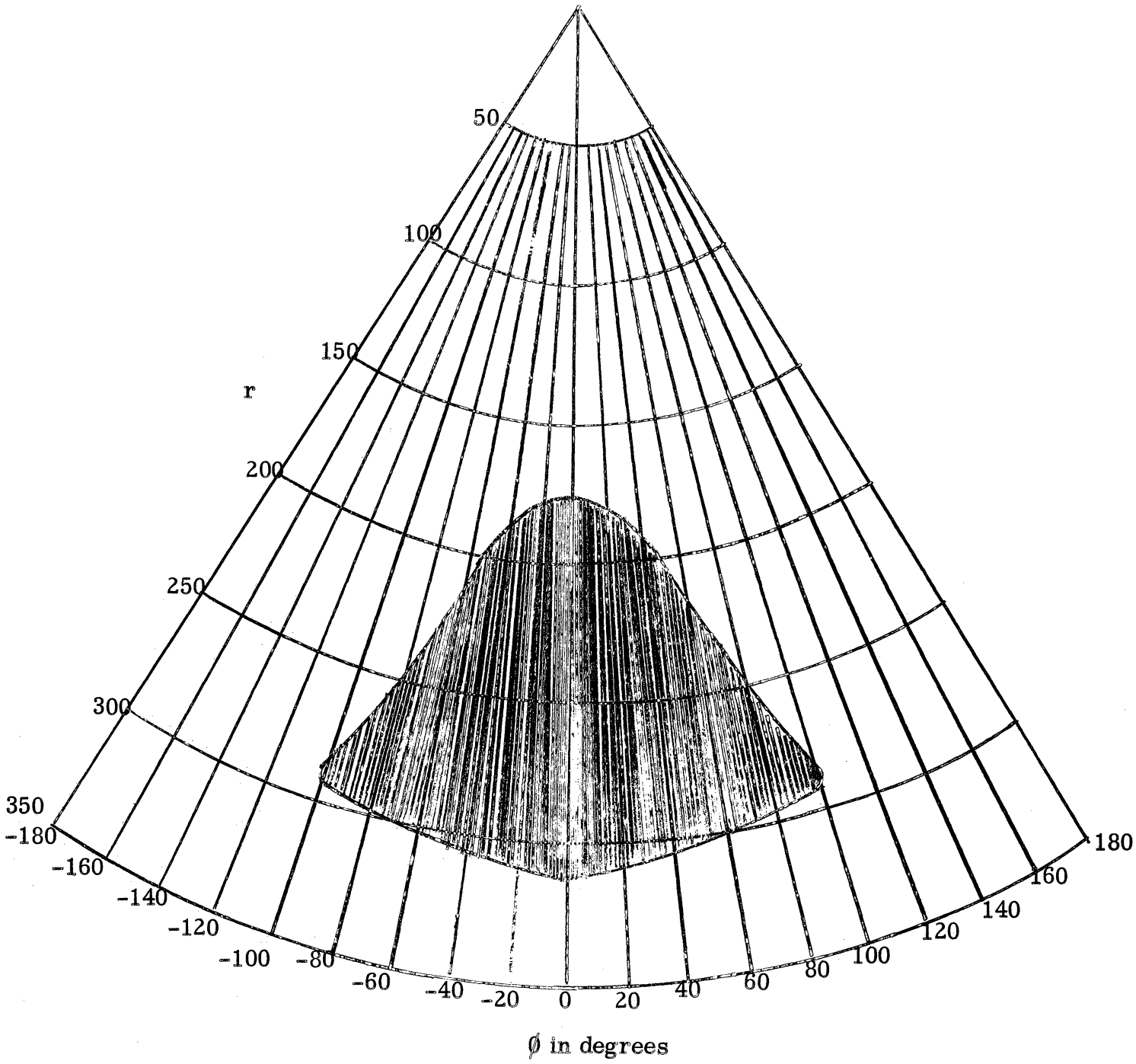

FIG. C-10 AMPLITUDE OF E_i ON UNROLLED CONE SURFACE FOR $\beta = 40^o$

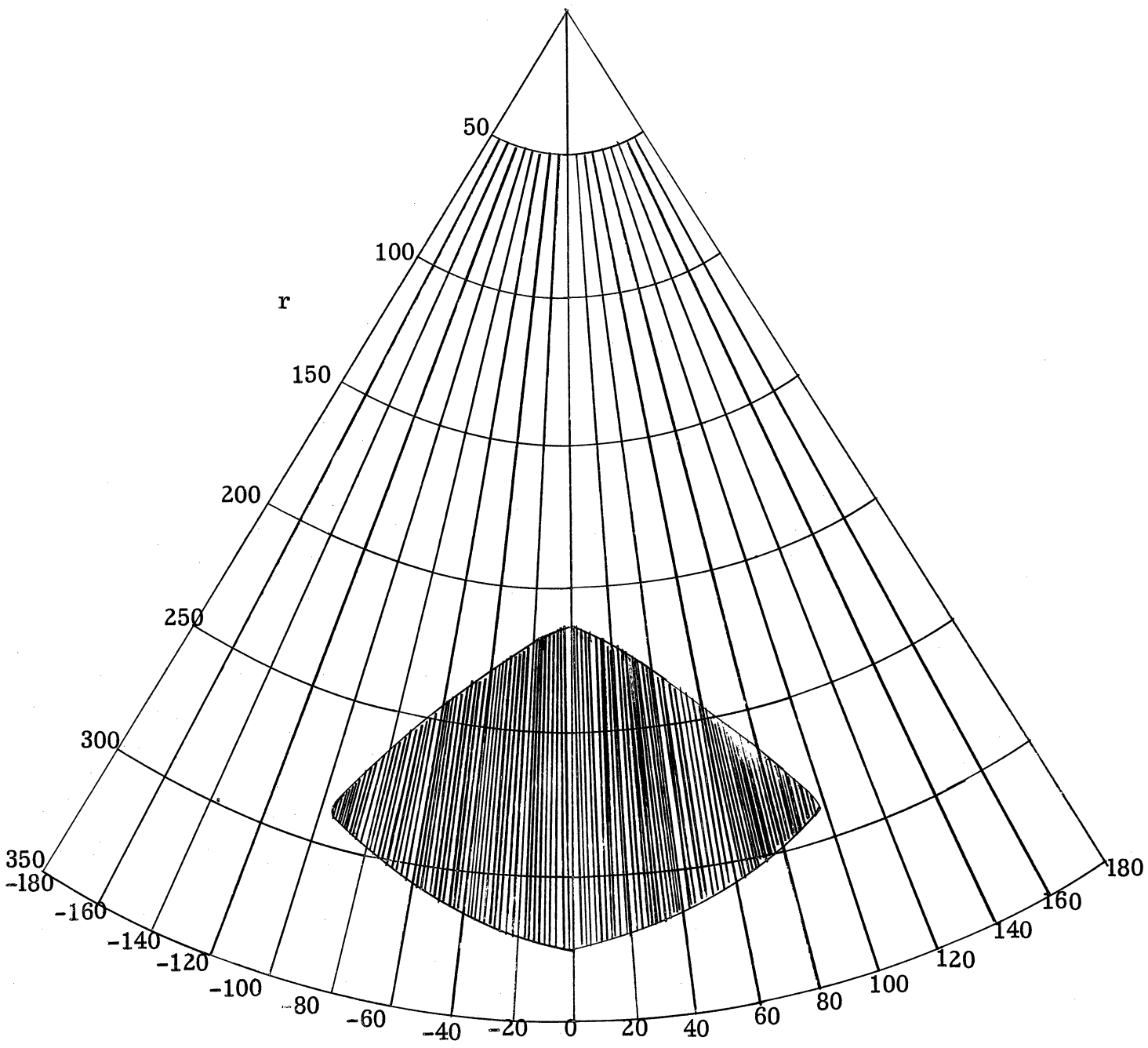

FIG. C-11 AMPLITUDE OF E_1 ON UNROLLED CONE SURFACE FOR $\beta = 60^\circ$

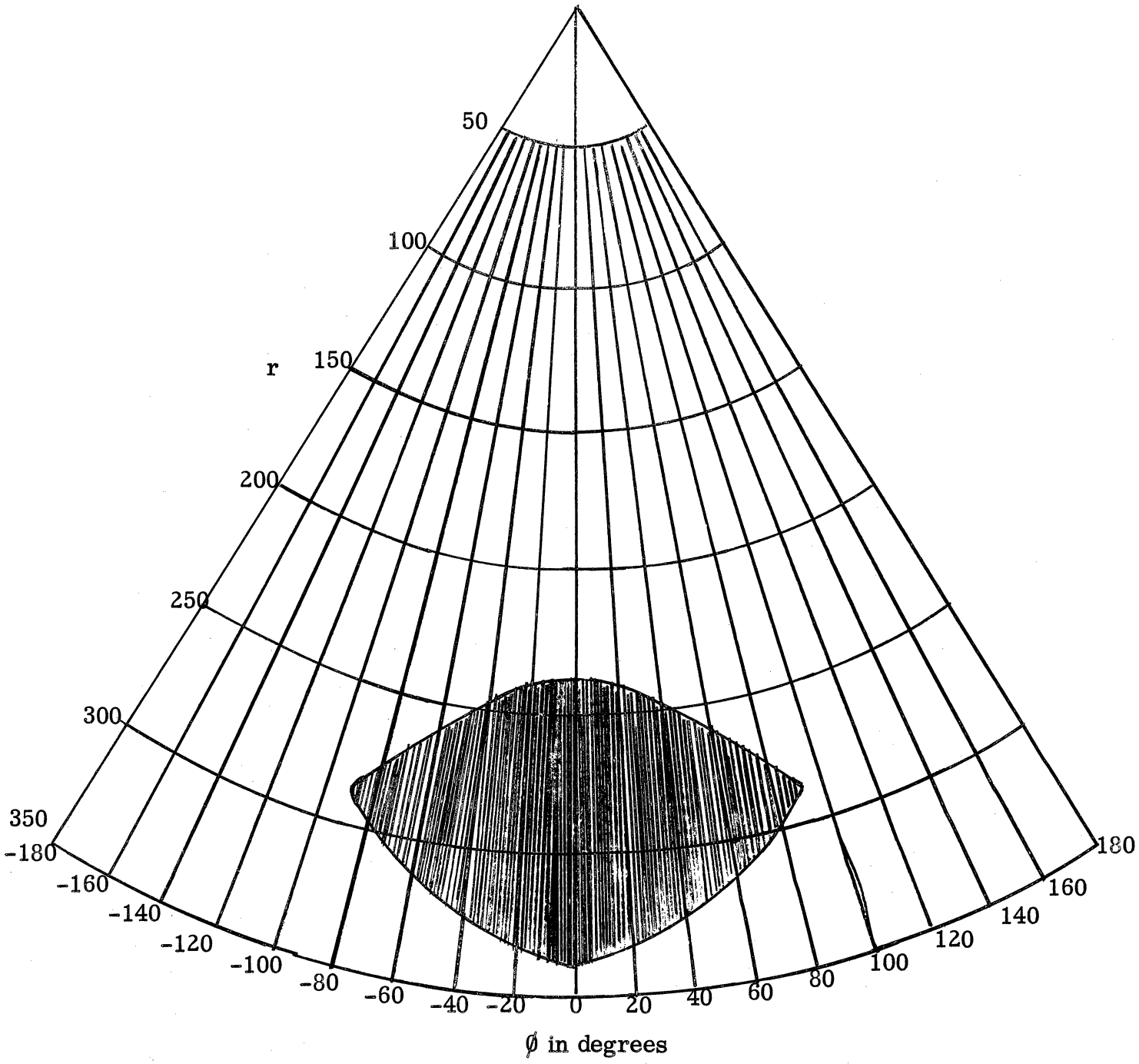

FIG. C-12 AMPLITUDE OF E_1 ON UNROLLED CONE SURFACE FOR $\beta = 80^o$

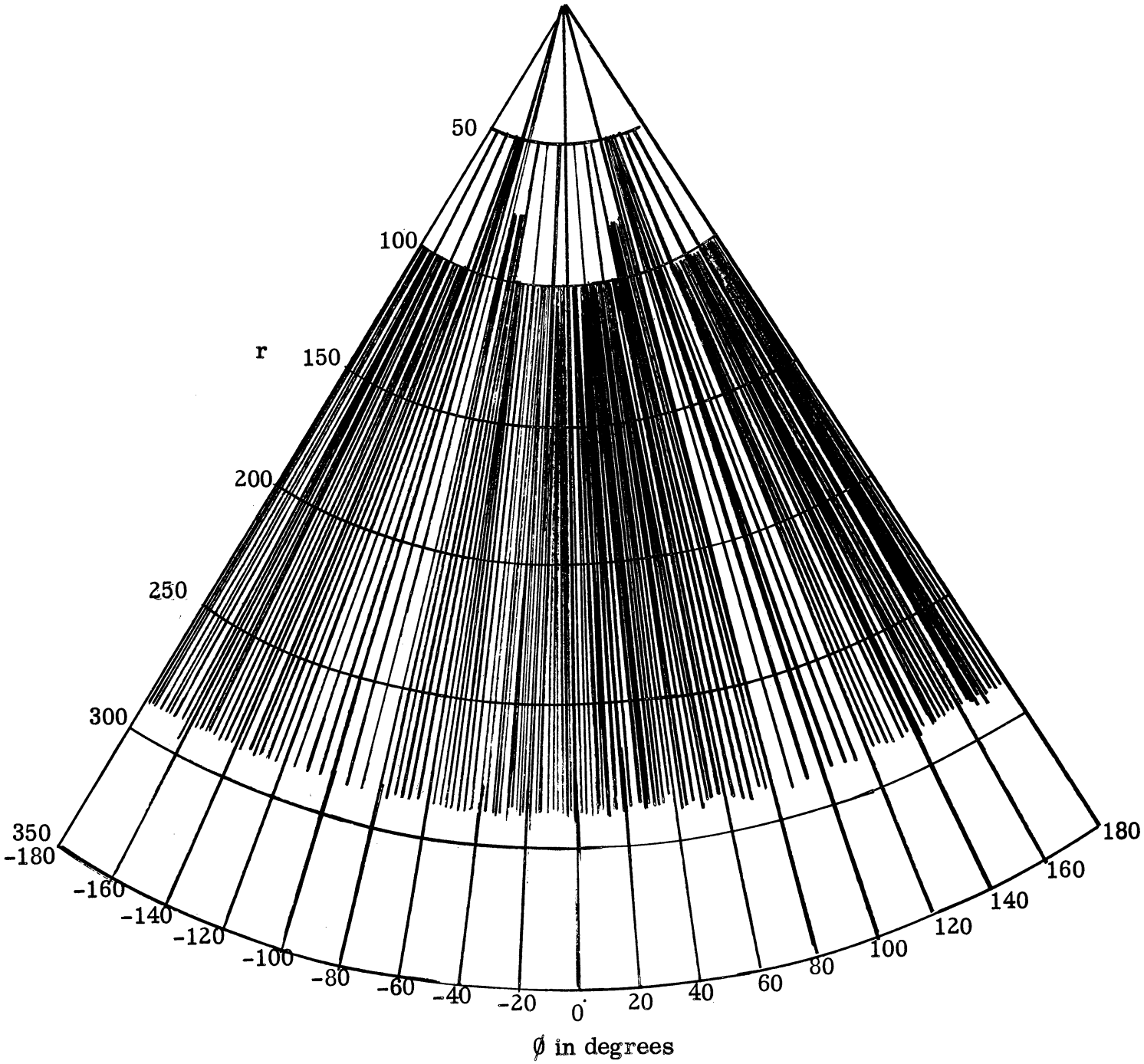

FIG. C-13 AMPLITUDE OF E_2 ON UNROLLED CONE SURFACE FOR $\beta = 0^o$

($|E_2|$ is not β-dependent therefore only the envelope of the intersection changes with β .)

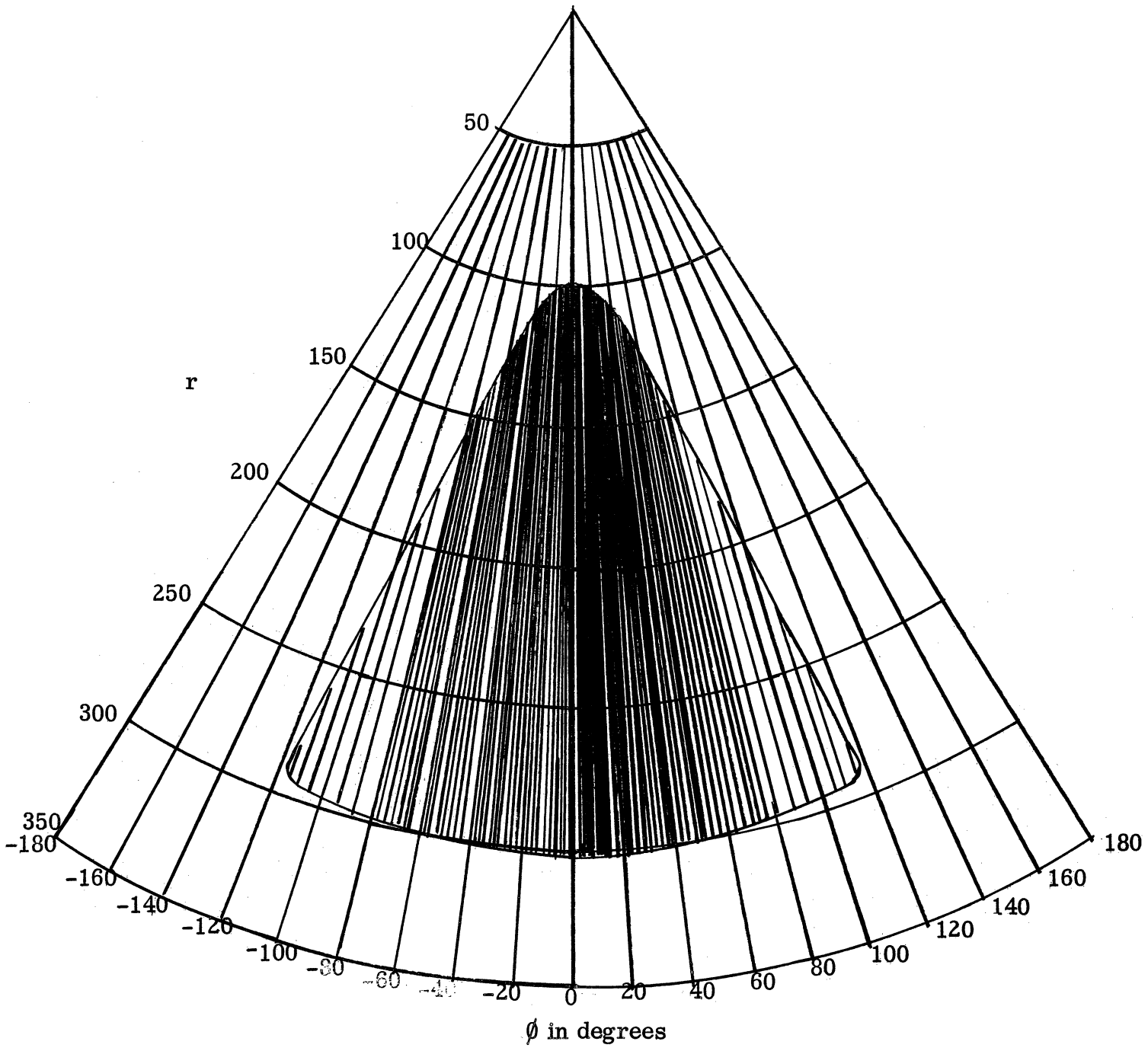

FIG. C-14 AMPLITUDE OF E_2 ON UNROLLED CONE SURFACE FOR $\beta = 20^o$

($|E_2|$ is not β-dependent therefore only the envelope of the intersection changes with β.)

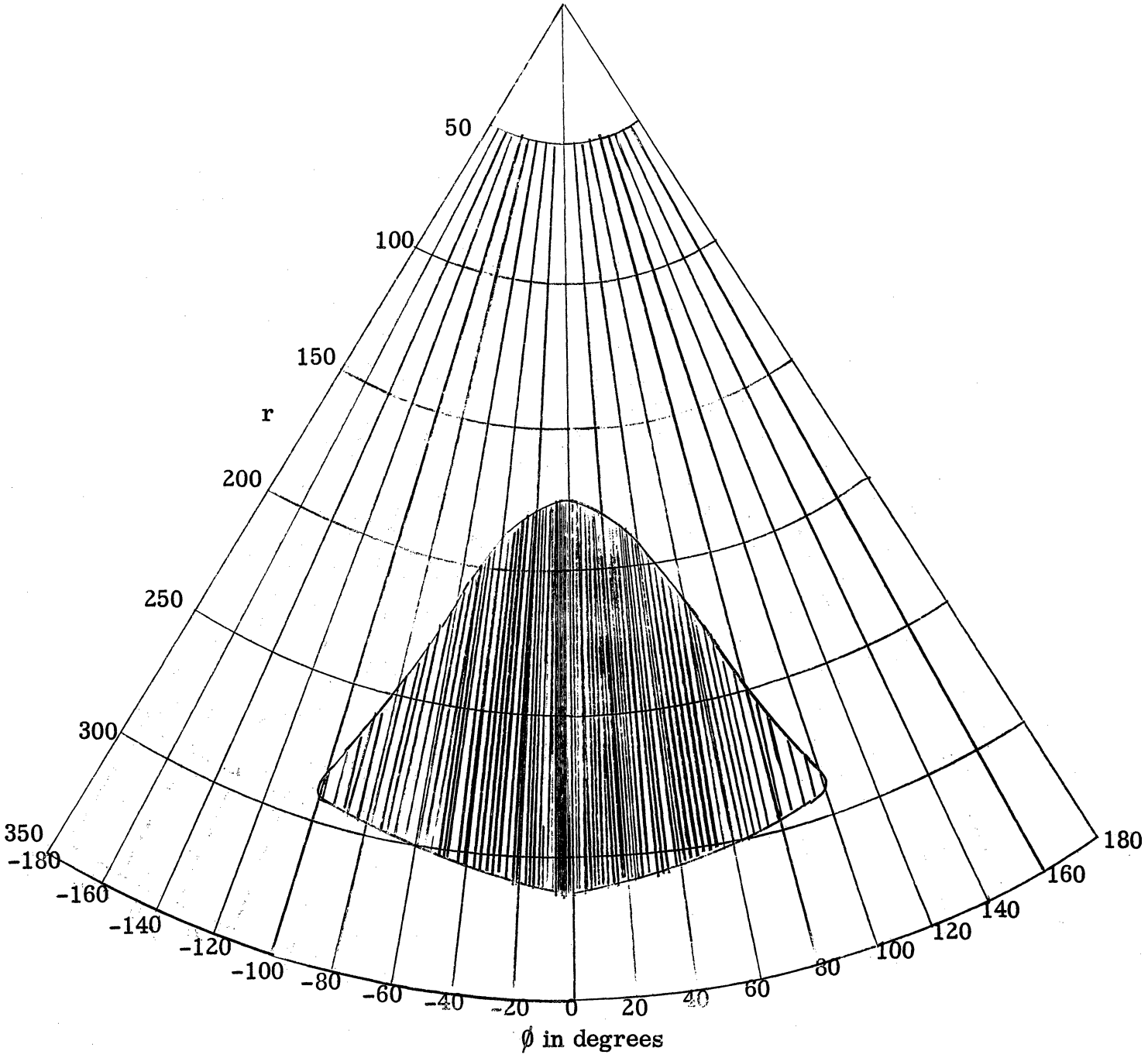

FIG. C-15 AMPLITUDE OF E_2 ON UNROLLED CONE SURFACE FOR $\beta = 40^o$

($|E_2|$ is not β-dependent therefore only the envelope of the intersection changes with β.)

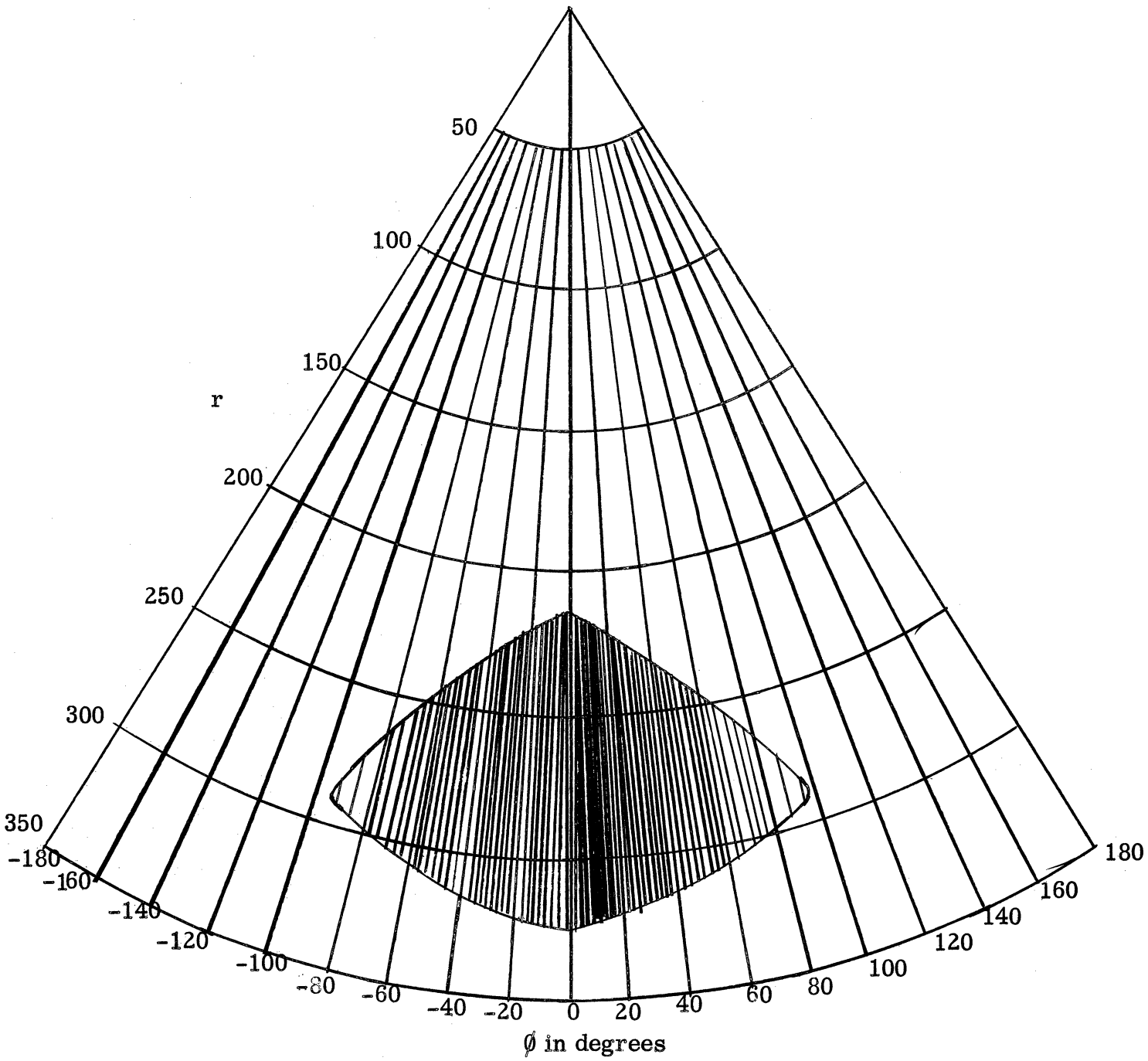

FIG. C-16 AMPLITUDE OF E_2 ON UNROLLED CONE SURFACE FOR $\beta = 60^o$

($|E_2|$ is not β-dependent therefore only the envelope of the intersection changes with β.)

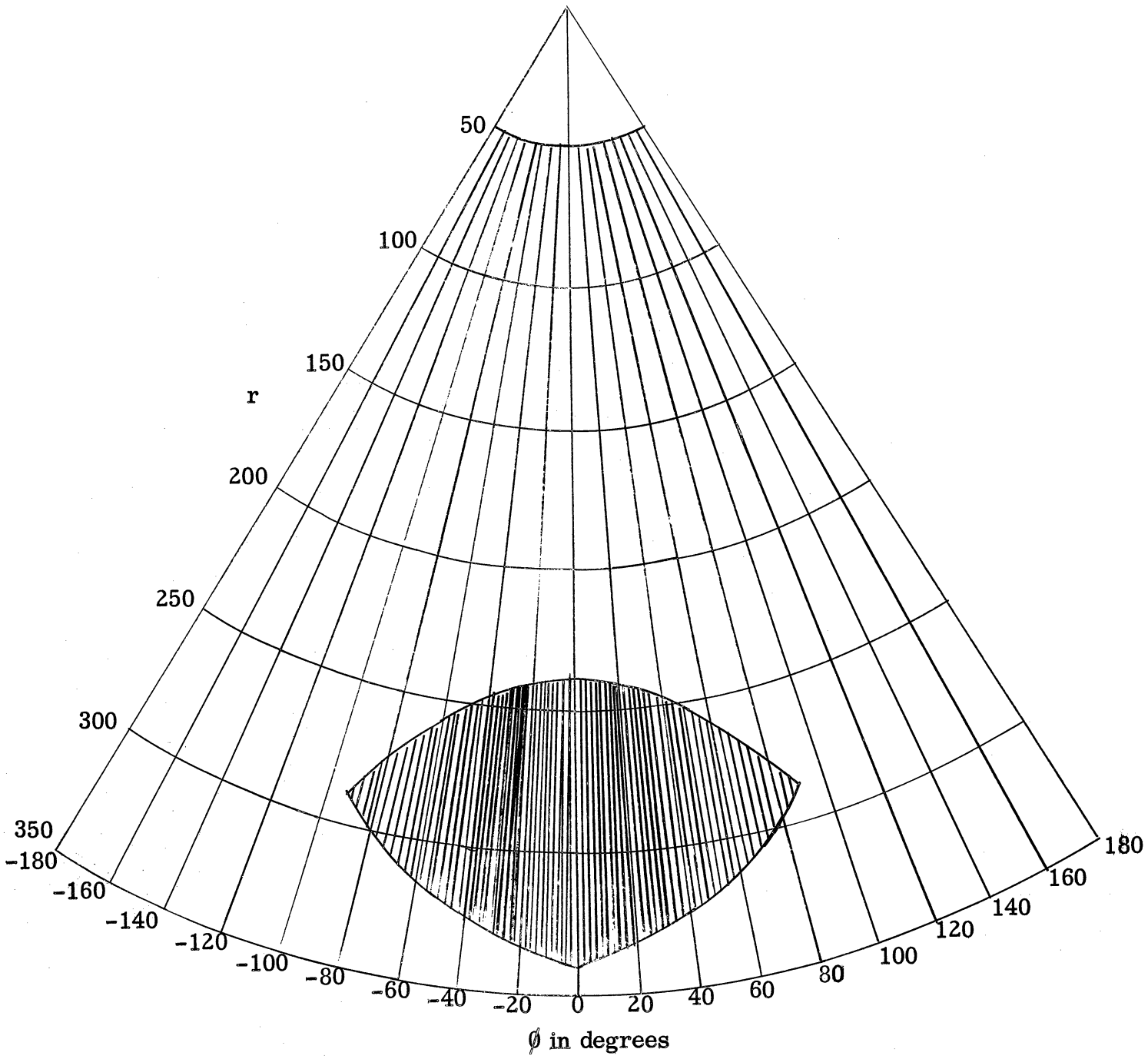

FIG. C-17 AMPLITUDE OF E_2 ON UNROLLED CONE SURFACE FOR $\beta = 30^{o}$

($|E_2|$ is not β-dependent therefore only the envelope of the intersection changes with β.)

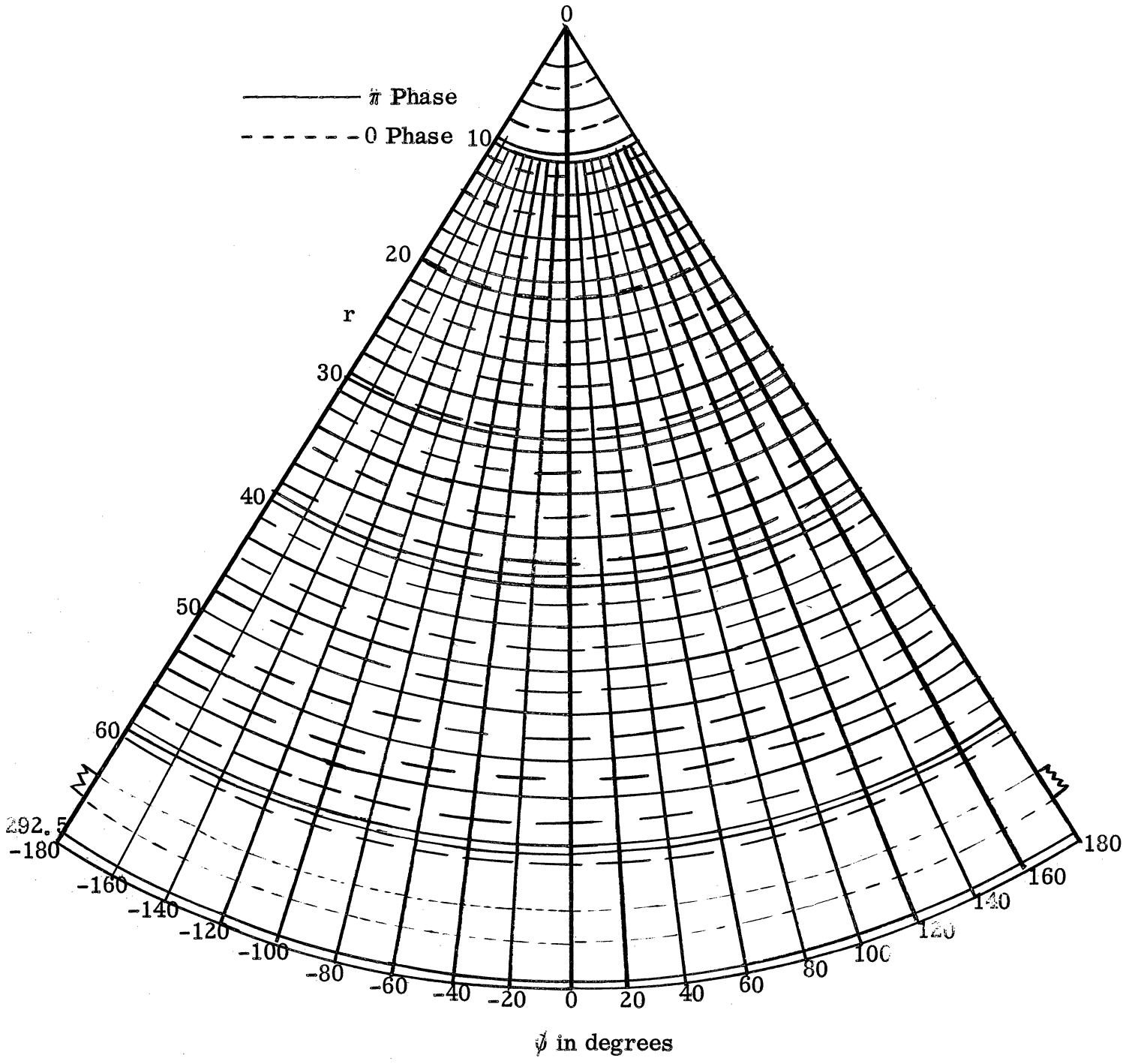

FIG. C-18 PHASE OF E ON UNROLLED CONE SURFACE FOR $\beta = 0^{o}$

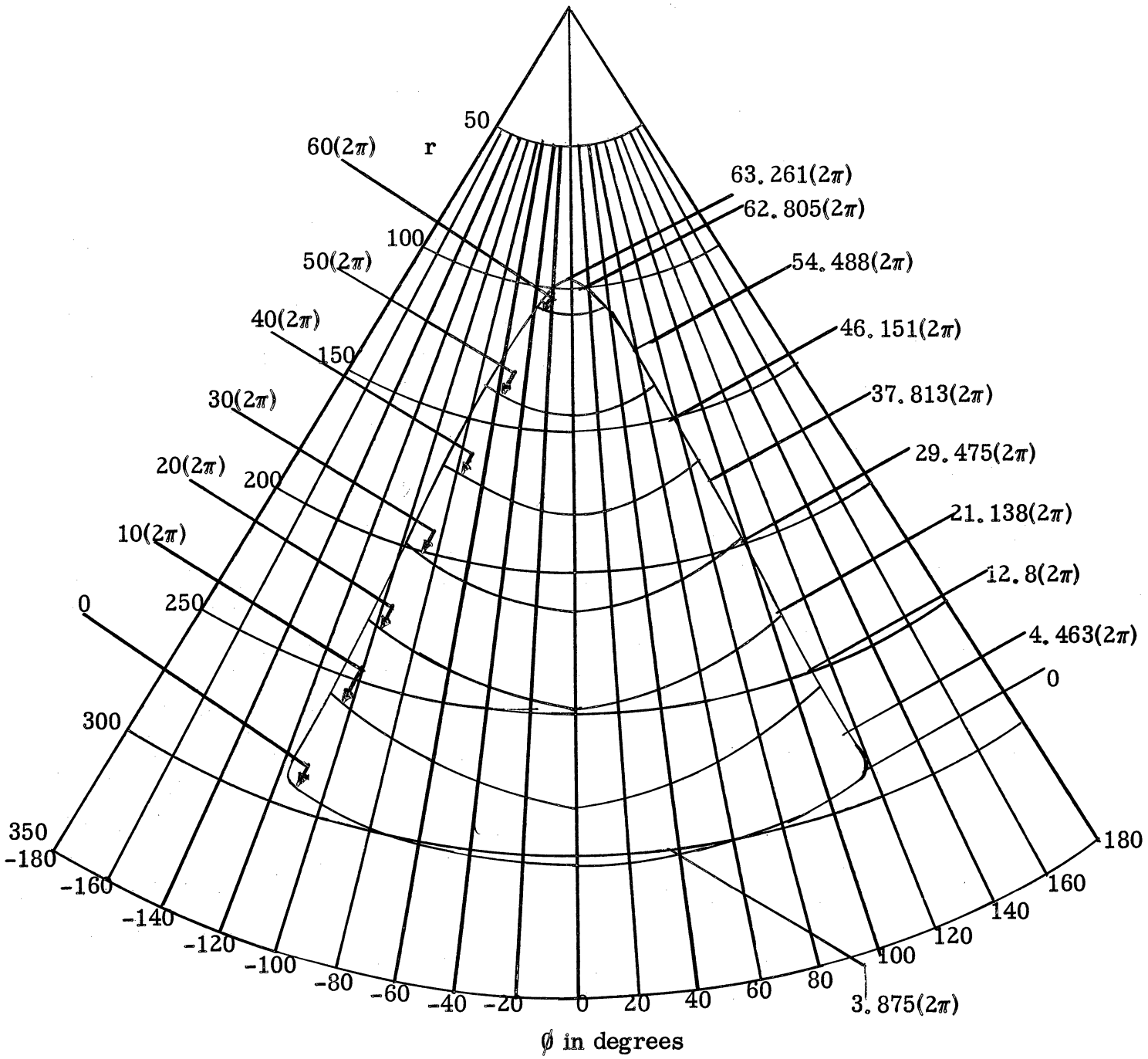

FIG. C-19 PHASE OF E ON UNROLLED CONE SURFACE FOR $\beta = 20^{o}$

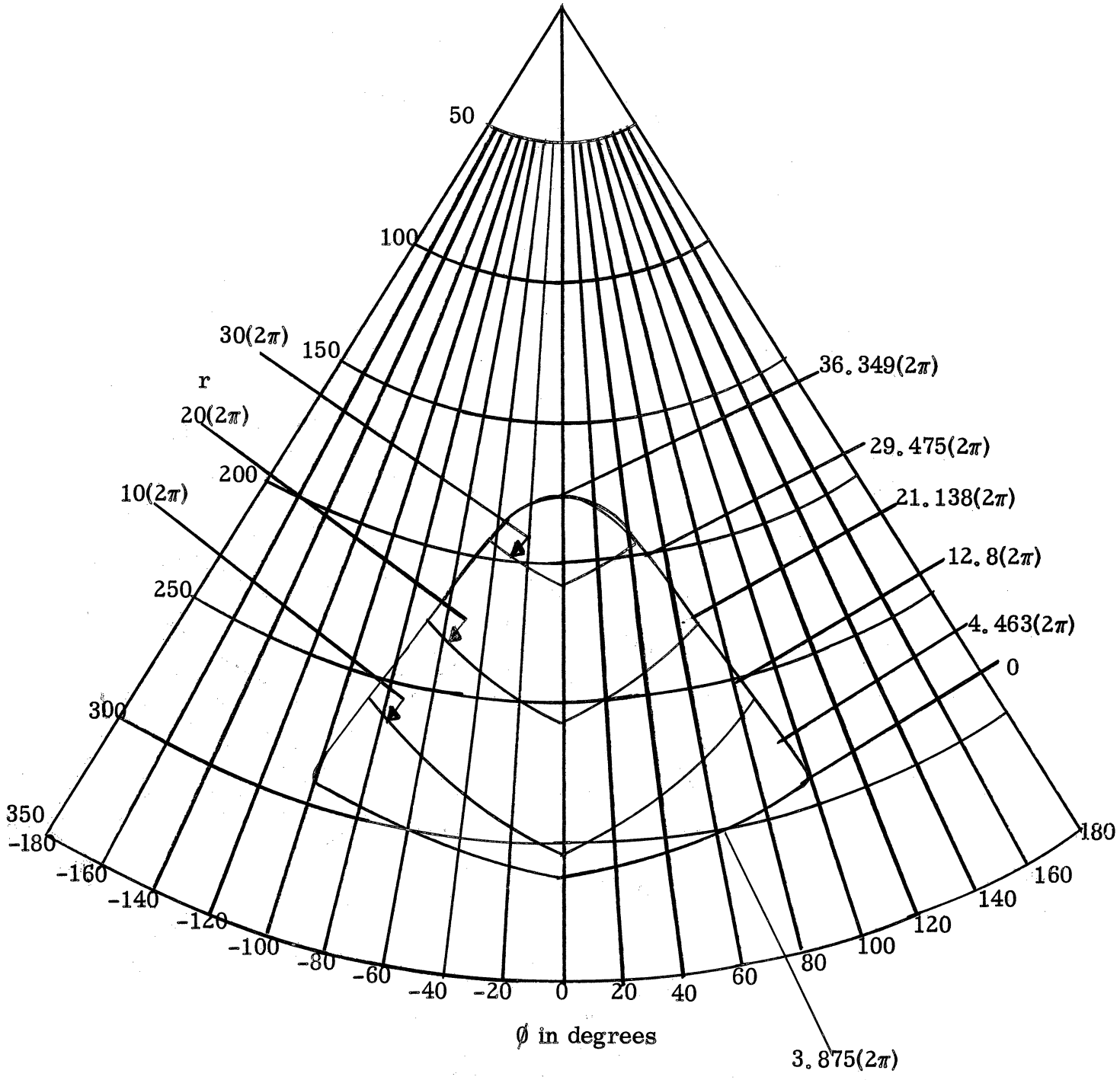

FIG. C-20 PHASE OF E ON UNROLLED CONE SURFACE FOR $\beta = 40^{o}$

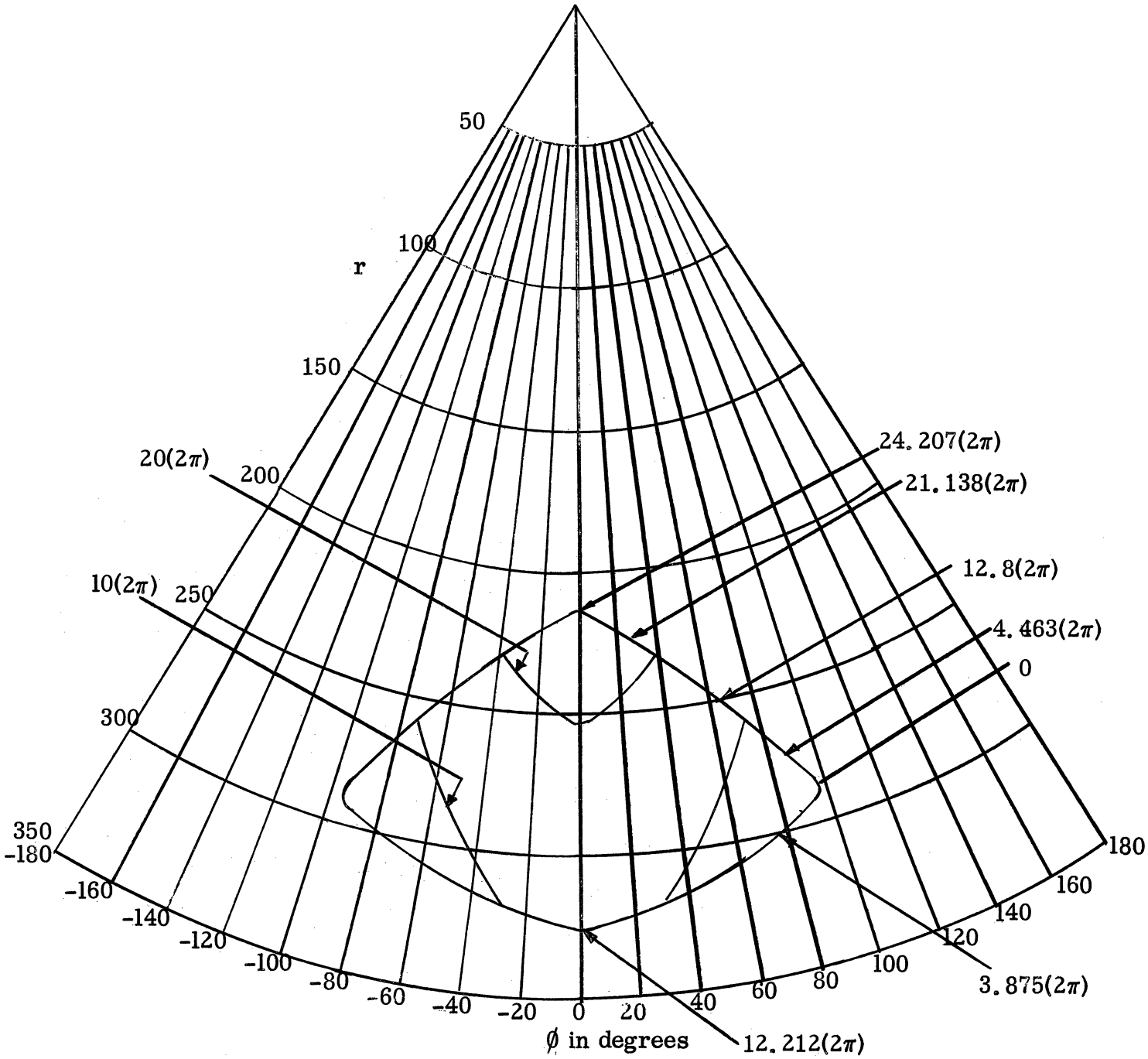

FIG. C-21 PHASE OF E ON UNROLLED CONE SURFACE FOR $\beta = 60^{o}$

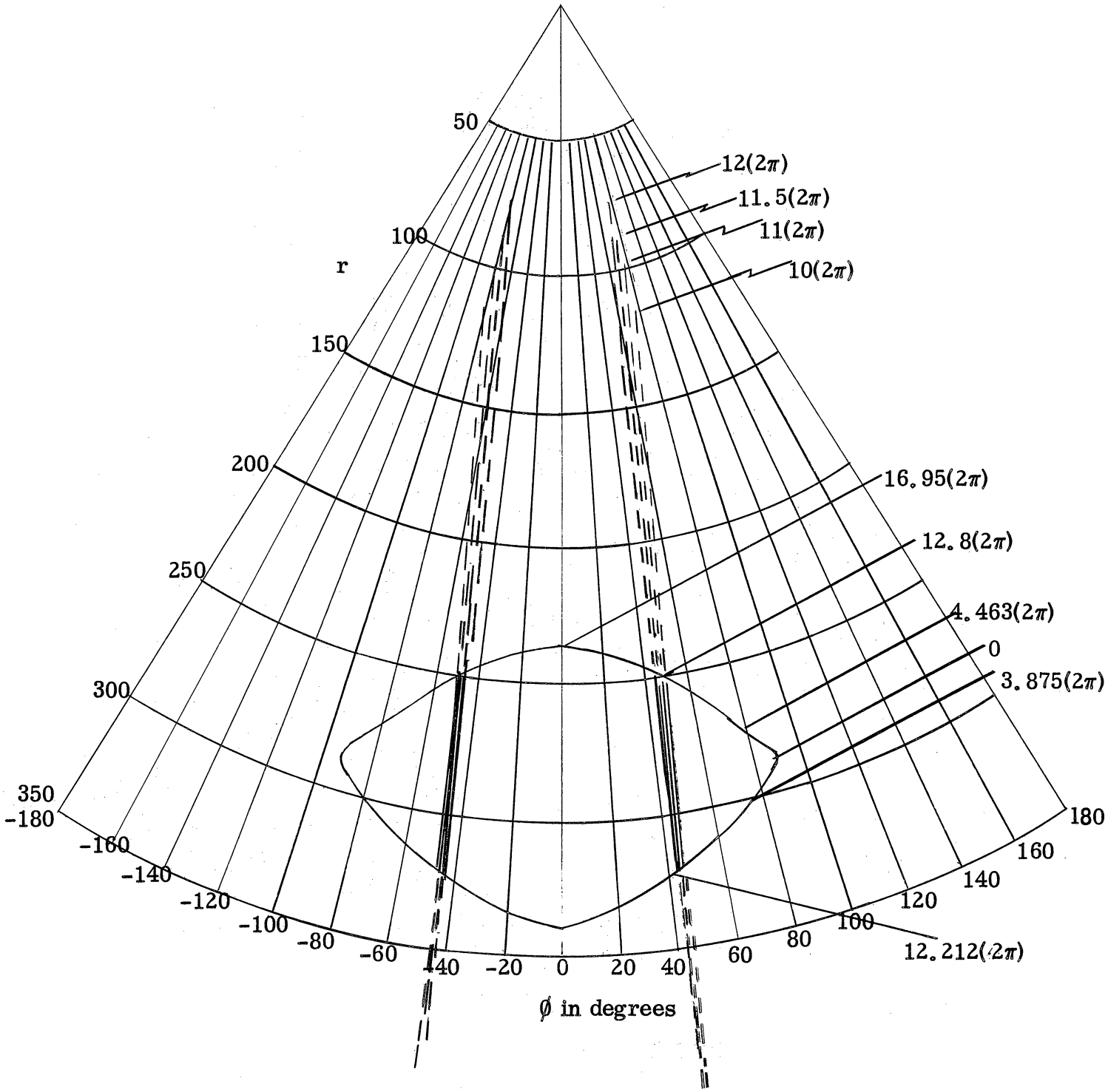

FIG. C-22 PHASE OF E ON UNROLLED CONE SURFACE FOR $\beta = 80^{o}$

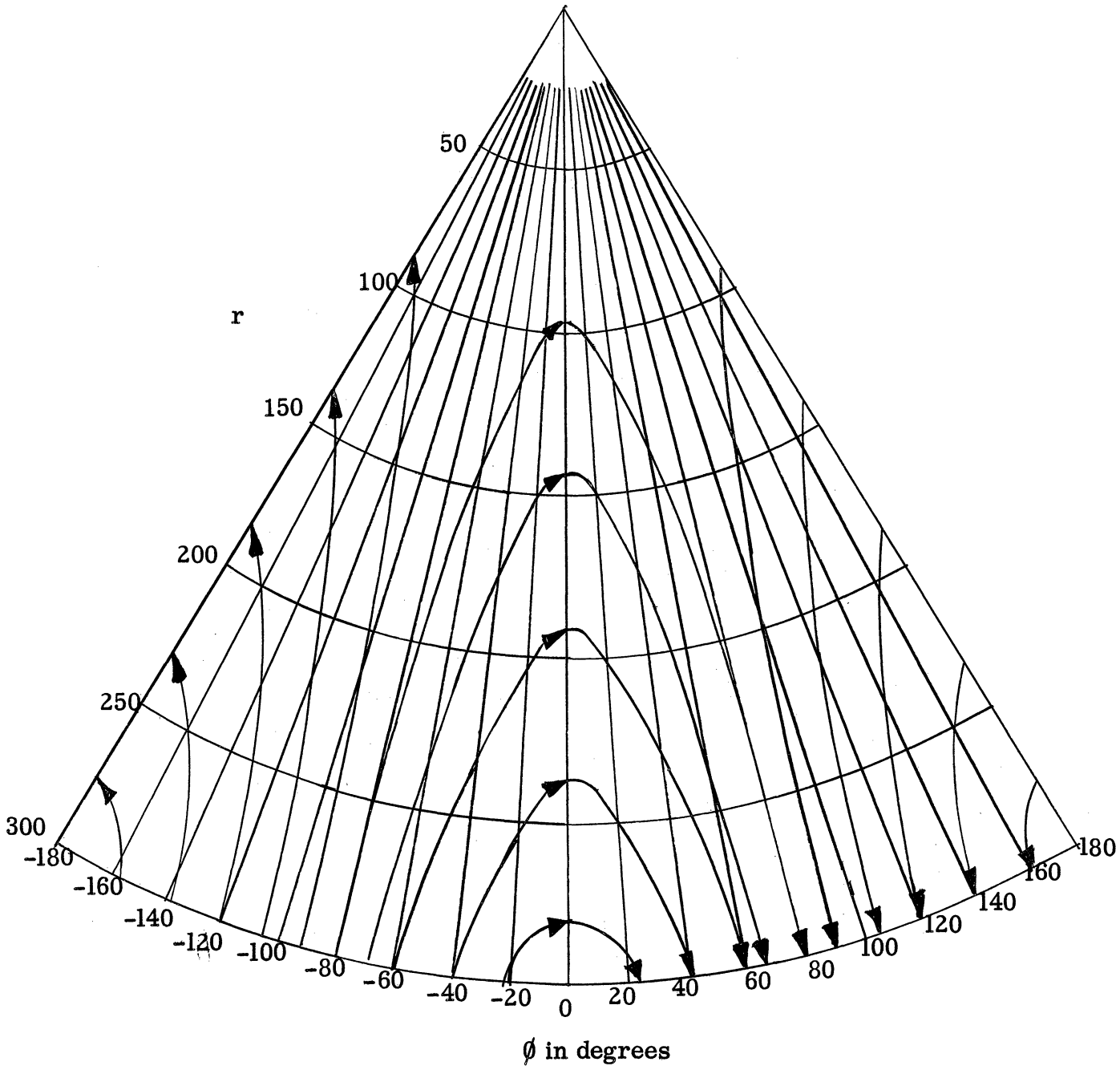

FIG. C-23 DIRECTION OF $\hat{n} \times \vec{E}_1$ ON UNROLLED CONE SURFACE FOR $\beta = 0^o$

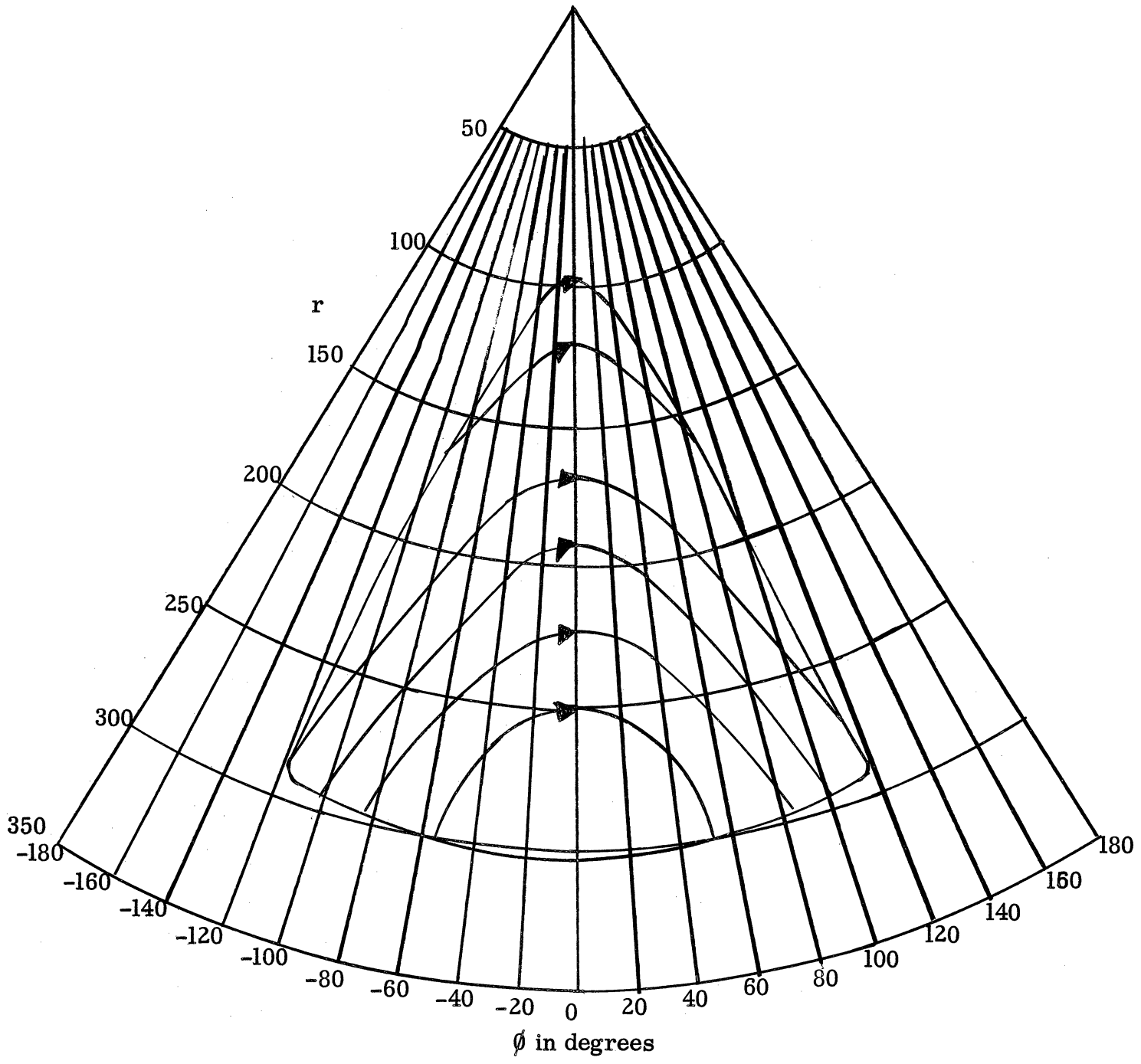

FIG. C-2.4 DIRECTION OF $\hat{n} \times \vec{E}_1$ ON UNROLLED CONE SURFACE FOR $\beta = 20^o$

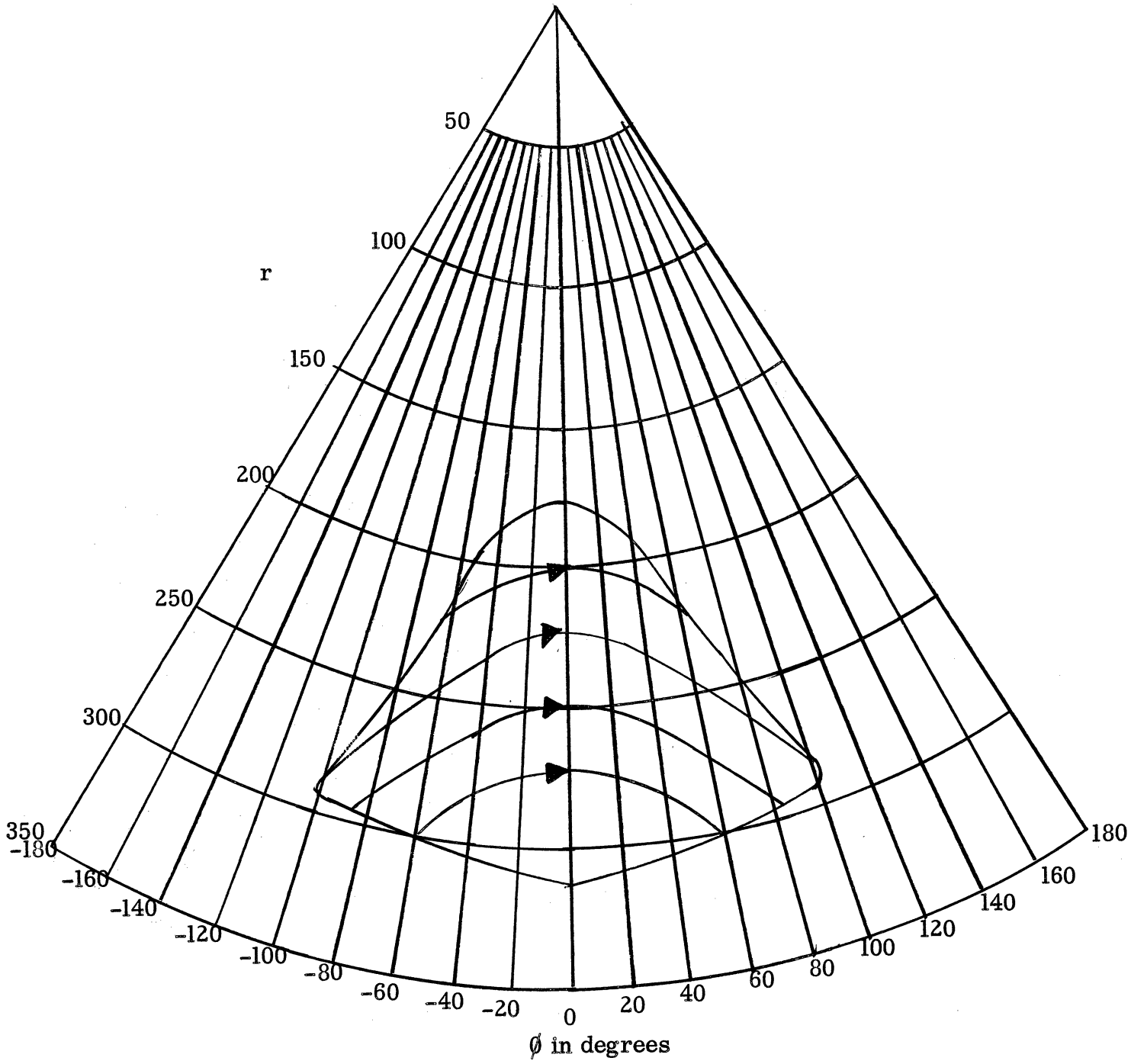

FIG. C-25 DIRECTION OF $\hat{n} \times \vec{E}_1$ ON UNROLLED CONE SURFACE FOR $\beta = 40^o$

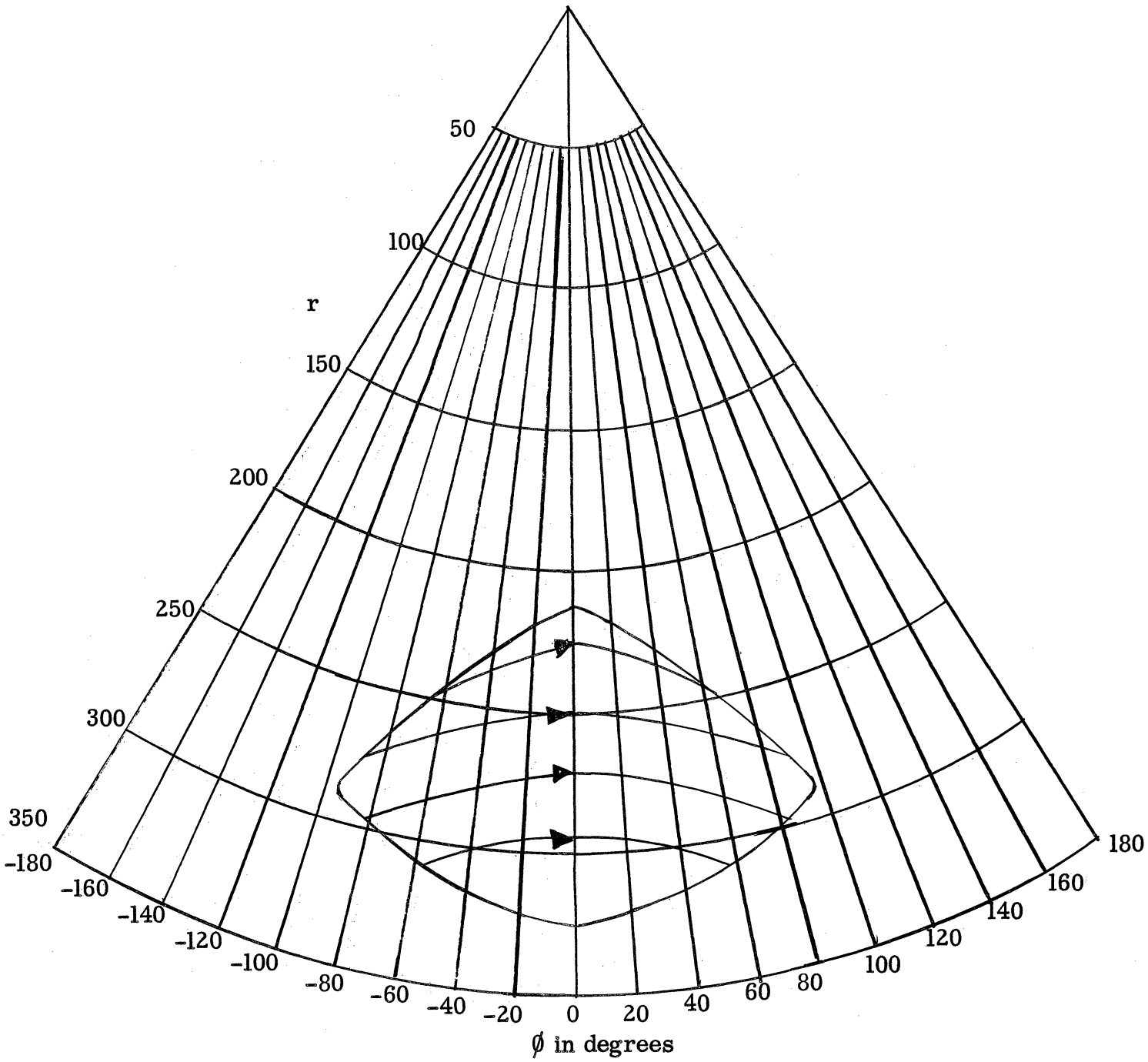

FIG. C-26 DIRECTION OF $\hat{n} \times \vec{E}_1$ ON UNROLLED CONE SURFACE FOR $\beta = 60^o$

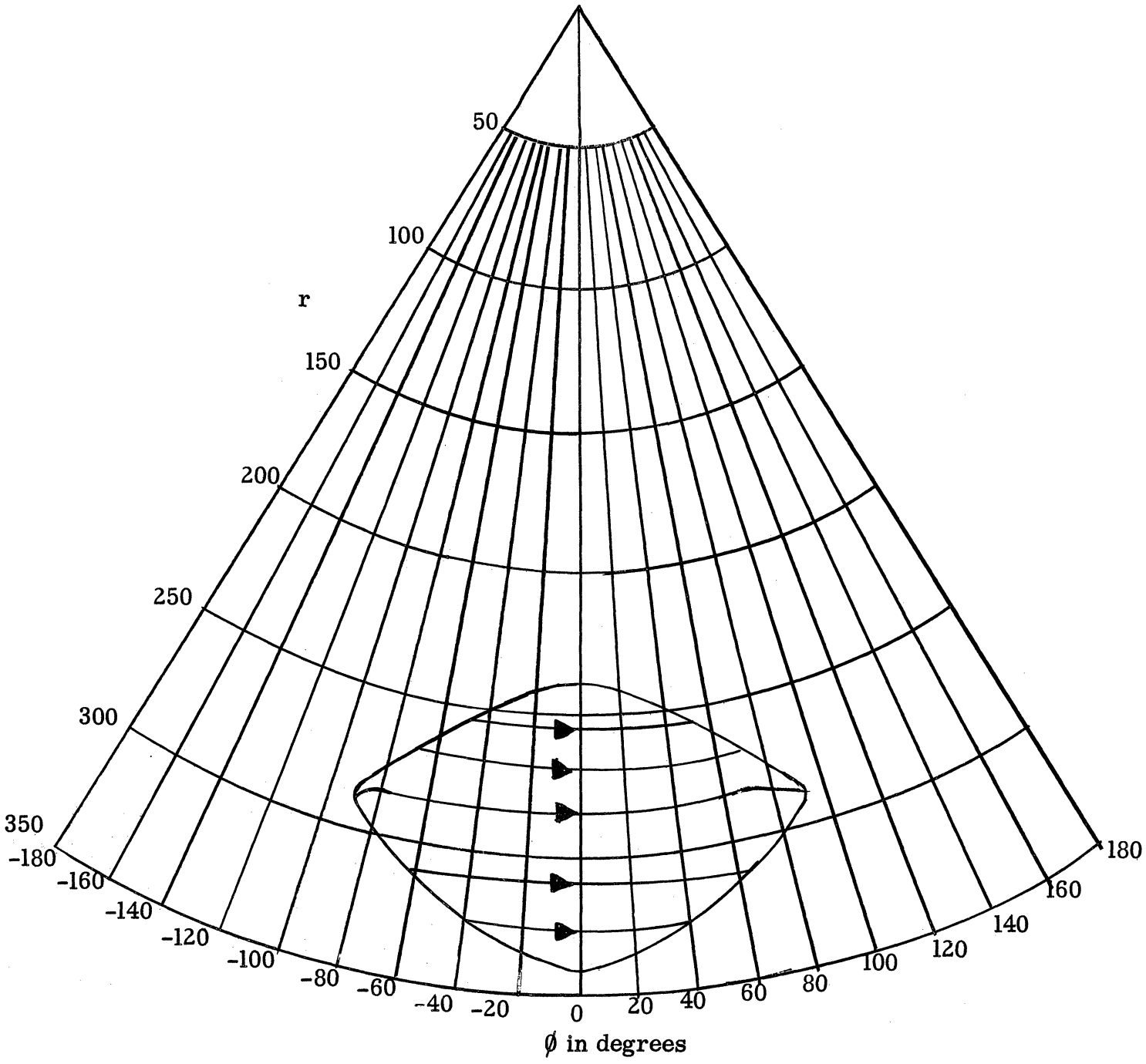

FIG. C-27 DIRECTION OF $\hat{n} \times \vec{E}_1$ ON UNROLLED CONE SURFACE FOR $\beta = 80^o$

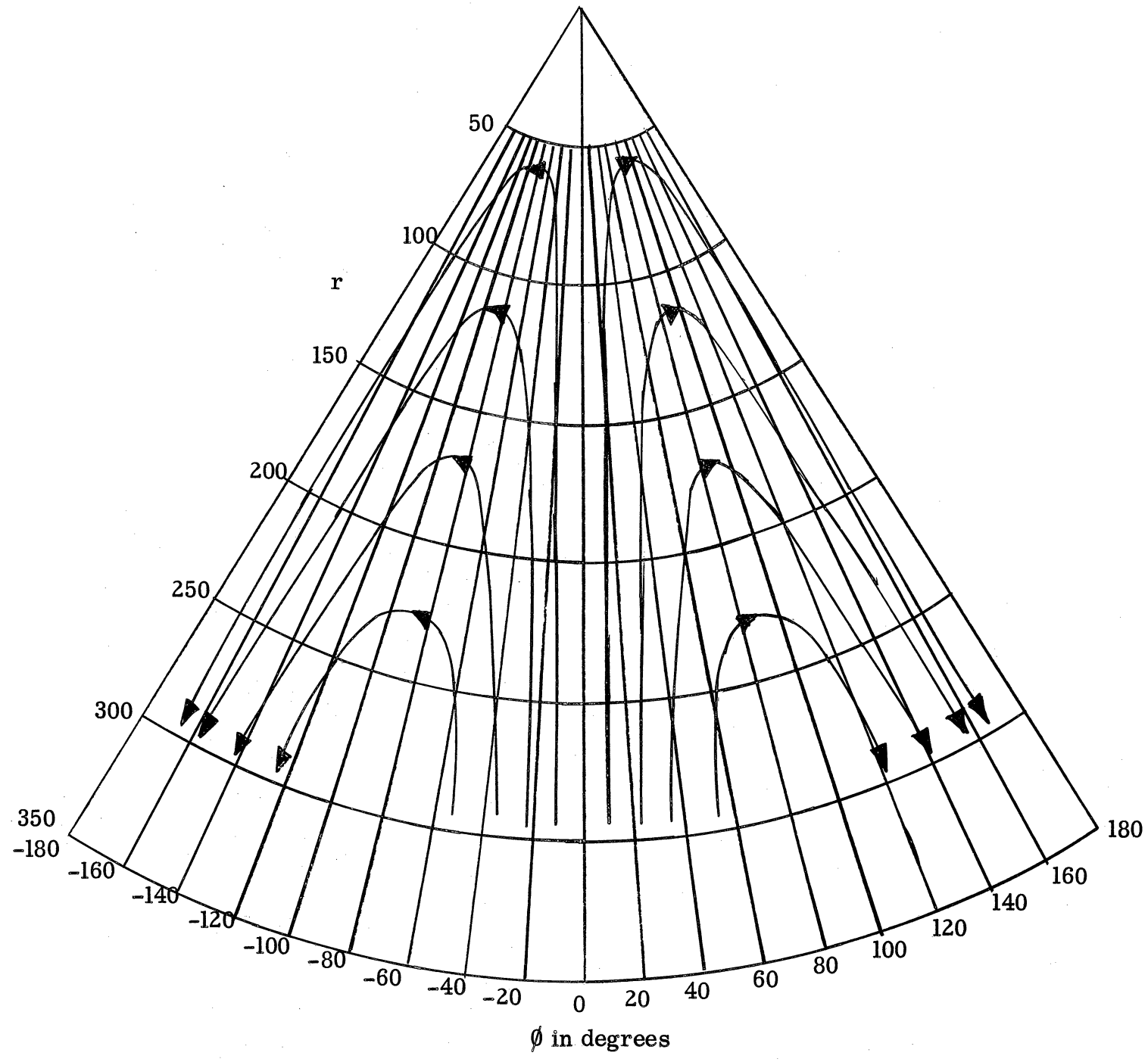

FIG. C-23 DIRECTION OF $\hat{n} \times \vec{E}_2$ ON UNROLLED CONE SURFACE FOR $\beta = 0^o$

($\hat{n} \times \vec{E}_2$ is independent of β, only the envelope of the intersection curve changes with β.)

REFERENCES

1. V. A. Fock, Journal of Physics, X, 399(1946).

2. N. A. Logan, "The Role of Fock Functions in the Theory of Diffraction by Convex Surfaces", Air Force Cambridge Research Center, Paper presented at the URSI Meeting, May 22 - 25 1957, in Washington, D. C.

3. J. B. Keller, "Diffraction by a Convex Cylinder", Transactions of the Institute of Radio Engineers, Vol. AP-4, 312(1956).

4. R. F. Goodrich, "Studies in Radar Cross Sections XXVI - Fock Theory Applied to an Infinite Cone", The University of Michigan, Report No. 2591-3-T (January 1958).

5. P. E. Mayes and W. D. James, "Pattern Synthesis With Small Radiating Slots in a Prescribed Conducting Surface", The University of Illinois, Prepared under Subcontract with The University of Michigan, Purchase Order 154216 (1957).

6. L. B. Felsen, "Field Solutions for a Class of Corrugated Wedge and Cone Surfaces", Polytechnic Institute of Brooklyn, Microwave Research Institute, Memorandum No. 32 (19 July 1957).

7. C. N. Campopiano, "Summary of Asymptotic Expansions for Bessel Functions", Polytechnic Institute of Brooklyn, Microwave Research Institute, Report No. R-582-57, PIB-502 (28 May 1957).

8. L. B. Felsen, "Radiation Patterns of Leaky and Surface Wave Distributions on a Wedge", Polytechnic Institute of Brooklyn, Microwave Research Institute, Memorandum No. 33 (23 September 1957).

9. L. B. Felsen, "Radiation of Sound From a Vibrating Wedge", Polytechnic Institute of Brooklyn, Microwave Research Institute, Report No. R-613-57, PIB-541 (11 October 1957).

10. C. N. Campopiano and L. B. Felsen, "Radiation Patterns of Two-Dimensional Leaky and Surface Wave Distributions on a Semi-Infinite Cone", Polytechnic Institute of Brooklyn, Microwave Research Institute, Memorandum No. 35 (18 November 1957).

11. K. M. Siegel, H. A. Alperin, R. R. Bonkowski, J. W. Crispin, Jr., A. L. Maffett, C. E. Schensted and I. V. Schensted, "Studies in Radar Cross Sections VIII - Theoretical Cross Sections as a Function of Separation Angle Between Transmitter and Receiver at Small Wavelengths", The University of Michigan, Report No. UMM-115 (October 1953).

REFERENCES
(cont'd)

12. Wolfgang Grobner and Nikolaus Hofreiter, "Integraltafel, Erster Teil, Unbestimmte Integrale", Springer-Verlag (1949).

13. K. M. Siegel, H. A. Alperin, J. W. Crispin, Jr., H. E. Hunter, R. E. Kleinman, W. C. Orthwein and C. E. Schensted, "Studies in Radar Cross Sections IV - Comparison Between Theory and Experiment of the Cross Section of a Cone", The University of Michigan, Report No. UMM-92 (February 1953).

14. L. B. Felsen, "Plane-Wave Scattering by Small-Angle Cones", Transactions of the Institute of Radio Engineers, Professional Group on Antennas and Propagation, Vol. AP-5 (January 1957).

15. R. F. Goodrich, A. L. Maffett, N. E. Reitlinger, C. E. Schensted and K. M. Siegel, "Studies in Radar Cross Sections XXII - Elementary Slot Radiators", The University of Michigan, Report No. 2472-13-T (November 1956).

16. R. F. Goodrich, R. E. Kleinman, A. L. Maffett, N. E. Reitlinger, C. E. Schensted and K. M. Siegel, "Radiation and Scattering from Simple Shapes II", Presented at Congres International Circuits et Antennas Hyperfréquences, Paris, France, 21 - 28 October 1957.

17. Tables of Fock Functions, Air Force Cambridge Research Center, Antenna Laboratory (to be published).